University of California Merced

Slow Progress with Quicksilver

An amalgam of research on mercury cycling, bioaccumulation, and remediation in mine-contaminated California reservoirs.

A dissertation submitted in partial satisfaction of the requirements
for the degree of Doctor of Philosophy in Environmental Systems
by
Mark Seelos

Dissertation Committee

Professor Peggy O'Day, (Chair)
Professor Marc Beutel, PE (Faculty Advisor)
Professor Sora Kim
Dr. Stephen McCord, PE

Summer 2022

The Dissertation of Mark Seelos is approved, and it is acceptable in quality and form for publication on microfilm and electronically:

_____

Professor Peggy O'Day, (Chair)

_____

Professor Marc Beutel, PE (Faculty Advisor)

_____

Professor Sora Kim

_____

Dr. Stephen McCord, PE

University of California Merced

2022

Table of Contents

Figures

Tables

Acknowledgements

In a 1675 letter to Robert Hooke, Sir Isaac Newton created academia's most overused platitude: "if I have seen further, it is by standing on the shoulders of giants." As I pull myself over the final peak of the formidable giant that is graduate school, I see dozens of more peaks before me and deduce that I must only be at the knee. Climbing giants, as it turns out, is harder than I thought. And at risk of offending the father of classical physics, I'd venture to suggest it's a larger undertaking in 2022 than it was in 1675. Every year we amass knowledge that grows the giant another foot. Alas, my dream of climbing giants has shifted to a desire to add another millimeter to its already towering height.

Like the giant, my 6-foot frame (I'm rounding up) was built with the contributions and support of others. The first foot was built by my family. I'm grateful that my parents let me choose my own path, and I wish my mom was here to see it all work out. Growing up as one of three triplets made my brothers and I choose who we are as individuals, and I'm thankful for our similarities and differences. Although I think she'd be proud, I'm not sure this is what Grandmother had in mind when she always wanted a doctor in the family. My second foot of height was built by my friends. To those with whom I've shared a summit, swapped belays, skied mountains, paddled rivers, or ridden trails – the conversation on the long drive home meant just as much to me as our adventures together. Thanks to all my supportive friends rocking a Jolly Kone jersey. My third foot of height was built by my mentors. My advisor, committee members, colleagues at the California Lake Management Society, and work mentors have provided me with invaluable support and opportunities. Marc, Peggy, Stephen, Sora, Carrie, Mark Marvin-DiPasquale – thank you for helping me find my path. My fourth foot of height comes from all the lab mates I've worked with. Byran, Edwin, Melissa, Naivy, Louis – I hope our collaboration doesn't stop here. Thank you to UAW 2865 and Student Researchers United for fighting for better pay and working conditions for my colleagues. My fifth foot of height comes from my Valley Water family. Thank you to everyone who I shared a boat or lab bench with, especially Elisabeth, Billy, Kendra, and Katie. Thanks to all my great interns over the years, especially those who contributed to projects included in this dissertation. A special thank you to Kirsten Struve, Jennifer Castillo, and Melanie Richardson, all of whom supported my academic leave of absence that enabled me to pursue a PhD. I wouldn't be writing this if not for your support. Thank you to IFTPE Local 21 for bargaining for the academic leave of absence policy. My sixth and final foot of height comes from the unwavering love and support of my partner Mareike, who believes in me more than I do. Your PhD is next!

To paraphrase Dr. Seuss, "don't cry because it's over, *smile* because it's over." Just kidding, I'd do it again (in a few years).

Introduction

Reservoirs are vital components of California's water infrastructure that allow a population of 40 million to thrive in its drought-prone climate. These engineered impoundments provide additional benefits beyond storing water for irrigation and potable supply. By containing runoff during the rainy season, reservoirs provide incidental flood protection downstream. Reservoirs can benefit the environment by storing water that maintains consistent outflow to creeks that would otherwise go dry. Reservoirs also serve recreational needs of communities by providing local opportunities for fishing, boating, picnicking, and hiking. Many of those who fish in reservoirs rely on their catch to provide themselves and their families with an inexpensive, nutritious meal. However, California's legacy of mining has contaminated fish throughout the state, putting anglers and their families at risk for mercury poisoning.

About half of reservoirs in California exceed regulatory standards for safe mercury levels in fish set by the State Water Resources Control Board. Some coastal California reservoirs are contaminated by waste material from legacy mercury mining operations. Others have received quicksilver lost to the environment during the California Gold Rush. Even seemingly pristine lakes can host fish with high mercury concentrations that result from deposition of mercury released into the atmosphere from fossil fuel combustion around the world.

Though mercury is typically present in trace concentrations in reservoir sediments, reservoirs create conditions that are conducive to the production and bioaccumulation of neurotoxic methylmercury. When inflow decreases and air temperatures rise in the springtime, reservoirs undergo thermal stratification. The warm, buoyant epilimnion floats atop the cold, dense hypolimnion, blocking off bottom waters from oxygen input from the atmosphere and photosynthesis. Aerobic bacteria consume the remaining dissolved oxygen in the hypolimnion, creating anoxic conditions in bottom waters and at the sediment-water interface. Under anoxic conditions, some anaerobic bacteria can convert inorganic mercury present in the water and sediments into methylmercury. Methylmercury is a potent neurotoxin that can cause neurological damage, cardiovascular disease, and reproductive impairment in humans and wildlife. Methylmercury is released into the water column where it concentrates in phytoplankton by millions of times its concentration in water. Methylmercury is concentrated further up the food chain in zooplankton, planktivorous fish, and predatory fish, reaching dangerously high (>0.5 ppm) concentrations in fish that are consumed by humans and wildlife.

The complexity of mercury cycling and bioaccumulation in reservoir systems presents a wide array of potential management strategies. Reservoir managers could decrease methylmercury levels in fish by limiting the microbial conversion of inorganic mercury to methylmercury, by lowering its introduction into the food web, or by controlling trophic transfer between organisms. This dissertation investigated these three

different aspects of reservoir mercury management in a series of field and laboratory studies. The overall objective of this dissertation was to investigate methods for controlling methylmercury production and bioaccumulation in reservoirs contaminated by the former New Almaden Mining District, North America's largest historical mercury mine.

Chapter 1 is a manipulated field experiment to evaluate the effects of hypolimnetic oxygenation on mercury cycling and fish tissue mercury in contaminated reservoirs. Using a 15-year dataset consisting of water quality and fish tissue measurements collected prior to and during reservoir oxygenation, I conducted statistical analyses to identify key changes in water quality and fish tissue data. Results indicated declining trends in fish mercury in two of four reservoirs, likely the result of increased primary productivity and not due to the inhibition of methylmercury production. Chapter two consists of a set of sediment slurry incubations aimed at evaluating the use of manganese oxide and activated carbon sediment amendments for mercury control through redox buffering and sorption. Manganese oxide and activated carbon amendments were equally effective in decreasing methylmercury concentrations in sediment porewater. Manganese oxide amendments were rapidly reduced to Mn^{2+}, warranting further optimization to increase longevity. Chapter three is an observational study aimed at characterizing plankton dynamics and methylmercury bioaccumulation in the pelagic food web. An increased understanding of bioaccumulation in lower-trophic level organisms is necessary when considering potential ecological mercury management options (e.g., fish stocking). Overall, results demonstrated the seasonal patterns of MeHg introduction into the pelagic food web and how complex and counteracting factors may control the magnitude of MeHg bioaccumulation. Collectively, the three chapters of this dissertation provide key information that will inform future mercury management efforts in the study reservoirs.

1 Effects of Hypolimnetic Oxygenation on Fish Tissue Mercury in Reservoirs Near the New Almaden Mining District

1.1 Abstract

Almaden, Calero, and Guadalupe reservoirs (San Jose, CA, USA) are small (< 13 million m^3) surface water reservoirs polluted by the former New Almaden Mining District, North America's most productive historical mercury (Hg) mine. Stevens Creek Reservoir (Cupertino, CA, USA) also has elevated fish Hg concentrations, but no historical mining source. We report a 15-year dataset to evaluate the effectiveness of line diffuser hypolimnetic oxygenation systems (HOSs) in reducing methylmercury (MeHg) concentrations in reservoir water and fish after four consecutive years of operation. HOSs were installed in each reservoir to increase dissolved oxygen concentrations in bottom water, thereby suppressing the activity of anaerobic bacteria (e.g., sulfate-reducing bacteria) known to produce MeHg. Before HOS operation, MeHg concentrations increased in bottom waters of all four reservoirs during periods of thermal stratification and profundal hypoxia. MeHg concentrations decreased significantly in bottom waters during HOS operation, with mean reductions of 63%-85% below pre-oxygenation concentrations. However, MeHg concentrations were unchanged or increased in surface waters. This could be the result of enhanced mixing between surface and bottom waters as a result of the line diffuser bubble plume, or continued Hg methylation occurring in the oxic water column and littoral sediments. Despite little change in whole water column MeHg concentrations, we observed modest but significant declining trends in fish tissue Hg in Guadalupe and Stevens Creek reservoirs. Results suggest that oxygenation, rather than directly lowering MeHg in water, may have mixed nutrients into surface waters, thereby enhancing primary productivity and indirectly affecting Hg bioaccumulation by diluting concentrations among more phytoplankton.

1.2 Introduction

Mercury (Hg) accumulation in reservoir fish is a major human and ecological health concern in California, affecting about half of the reservoirs in the state (SWRCB, 2017a). Reservoir impairment severity varies with Hg source (Hg mining, gold mining, atmospheric deposition); reservoir physical, chemical, and biological characteristics; and reservoir operations (Hsu-Kim et al., 2018). High Hg in fish disproportionally affects Native American tribes and subsistence fishers who depend on locally caught fish for food security (SWRCB, 2017c). The State Water Resources Control Board is currently developing the Statewide Mercury Control Program for Reservoirs to address fish Hg levels that are unsafe for consumption by humans or wildlife (SWRCB, 2017b).

A thorough understanding of Hg dynamics in reservoirs is crucial to select effective remediation strategies. Various methods have been employed to decrease MeHg production in reservoirs by buffering redox potential at the sediment-water interface. Redox buffering aims to thermodynamically disfavor methylating organisms by providing excess terminal electron acceptors for bacteria that are not known methylators

(aerobic, denitrifying, and manganese-reducing bacteria). Lake and reservoir pilot studies have used hypolimnetic addition of oxygen (Beutel et al., 2014; McCord et al., 2016) and liquid calcium nitrate (Matthews et al., 2013; Austin et al., 2016) to decrease sediment MeHg release. Manganese oxide amendments have been evaluated in experimental mesocosms, but not on a field scale (Vlassopoulos et al., 2018).

Though these methods have shown promise in reducing MeHg concentrations in bottom waters, none have been found to conclusively reduce MeHg concentrations in fish independent of other remediation actions such as sediment dredging and capping. The objective of this study was to test the efficacy of line diffuser hypolimnetic oxygenation systems (HOSs) in reducing MeHg production and bioaccumulation in contaminated reservoirs. Oxic conditions at the sediment-water interface lowered MeHg concentrations in overlying water in experimental incubations using sediments collected from water bodies in the study watershed (Duvil et al., 2018). We apply this concept at the reservoir-scale, investigating the effects of oxygen addition on MeHg production and bioaccumulation in three reservoirs located near the historical New Almaden Hg mining district south of San Jose, California and a nearby reservoir uninfluenced by mercury mining.

1.3 Site and System Description

1.3.1 Site Description

The New Almaden Mining District (San Jose, CA, USA) was North America's largest and most productive mercury mine. The Guadalupe River watershed is contaminated with Hg waste from former mining operations. Despite about $10 million USD for remediation to excavate and contain processed ore, many waste piles and miles of polluted creeks have not yet been remediated. Consequently, typical annual Guadalupe

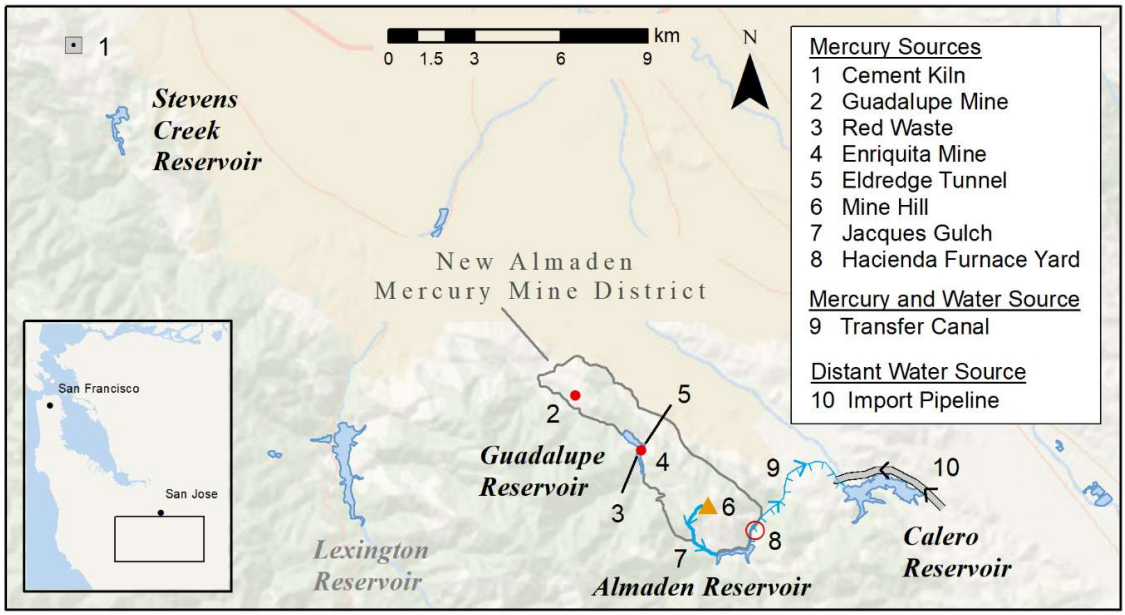

Figure 1-1: Map of study site including Almaden, Calero, Guadalupe and Stevens Creek reservoirs, historical mercury mine locations, and hydrologic connectivity between reservoirs. Mercury sources are described in Supplemental Text A1.

River Hg transport from the mining district to San Francisco Bay is 120 kg/yr (McKee et al., 2017). Almaden (AR), Calero (CR), Guadalupe (GR), and Stevens Creek (SCR) reservoirs (Santa Clara County, CA, USA) are mesotrophic to eutrophic, monomictic reservoirs constructed in the mid-1930s (Fig. 1-1, Table A1). The reservoirs are used to capture local runoff for subsequent recharge of groundwater basins used for potable supply, and for flood protection. AR and GR (Guadalupe River watershed) receive Hg mine waste from New Almaden, some of which is transported from AR to CR via Almaden-Calero Canal (Fig. 1-1) (Tetra Tech, 2005). Guadalupe and Almaden reservoirs receive water exclusively from their local watersheds. CR can receive water through a canal from AR or a pipeline from a large storage reservoir outside of the watershed fed with water from the San Joaquin/Sacramento Delta. SCR is in the Stevens Creek Watershed, where there is no known Hg mine waste. Its water source is exclusively its local watershed, and it drains to San Francisco Bay. Hg in SCR is assumed to come from a combination of geologic, local atmospheric (Rothenberg et al., 2010) and global atmospheric sources (SWRCB, 2017a). Mercury sources and fish Hg levels relative to sediment total Hg are provided in Supplemental Text A1 and S2. These different characteristics of Hg loading to the reservoirs are reflected in the relatively high sediment total Hg concentrations in AR and GR (Table 1-1).

AR, GR, and SCR receive inflow from local precipitation during the wet season (November to April) and are drawn down over 50% by volume during the dry season. These reservoirs receive little to no summer inflow. In contrast, CR, which primarily receives imported water, is maintained at a more consistent capacity year-round. All four reservoirs have bottom-release outlets that discharge hypolimnetic water throughout the year. Each reservoir exceeds regulatory thresholds for Hg concentrations in fish (SWRCB, 2017a). Hg in largemouth bass, the top predator and a sport fish, ranges from 0.75 mg/kg in SCR to 4.9 mg/kg in GR (35 cm standardized size, muscle, wet weight, Tables 1-1 and A2); GR contains among the highest fish Hg concentrations in the USA.

Reservoir	MeHg (ng/L)[a]		THg (mg/kg, dry wt)		THg (mg/kg, wet wt)		Chlorophyll *a* (ug/L)
	Epilimnion	Hypolimnion	Sediments	n	35 cm bass*	Age-1 bass (whole)	(2 m depth, dry season)
Almaden Reservoir	0.74 ± 0.1	1.86 ± 0.54	5.4[b]	1	2.8 ± 0.9	0.9 ± 0.09	3.39 ± 0.92
Calero Reservoir	0.24 ± 0.06	1.93 ± 0.52	0.42 ± 0.08[c]	18	1.1 ± 0.07	0.11 ± 0.02	8.5 ± 1.15
Guadalupe Reservoir	0.6 ± 0.12	12.05 ± 2.44	3.32 ± 0.9[c]	16	4.9 ± 1.8	0.75 ± 0.09	1.83 ± 0.2
Stevens Creek Reservoir	0.12 ± 0.03	0.76 ± 0.23	0.16 ± 0.01[d]	2	0.75 ± 0.13	0.1 ± 0.02	2.02 ± 0.48

[a] Dry season (May-October) mean. See Table S3 for details

[b] Data = 2001 [c] Data: Tetra Tech, 2005

[d] Data: 2018 *Muscle Tissue

Table 1-1: Select pre-HOS chemical characteristics of Almaden, Calero, Guadalupe and Stevens Creek reservoirs. Values are mean and 95% confidence interval; sediment THg in dry weight and fish THg in wet weight. For sediment mercury samples, n = 2 for Stevens Creek Reservoir. Dry season (May-October) water samples, n = 48-84 for methylmercury and n = 39-71 for chlorophyll a.

1.3.2 Hypolimnetic Oxygenation Systems (HOS)

Line diffuser hypolimnetic oxygenation systems (HOSs) installed in AR, CR, GR, and SCR between 2011 and 2015 each deliver around 675 kg of high-purity (> 90%) oxygen gas per day to each reservoir's hypolimnion (Fig. A1). Fine oxygen bubbles are

discharged from diffuser lines extending between 305 and 610 meters laterally on the reservoir bottoms. The systems are operated from the beginning of thermal stratification (April-May) until fall destratification (September-October). Systems were operated only intermittently from 2013-2015 due to technical challenges, but near-continuous summer operation was maintained throughout the 2016-2019 stratified periods.

1.4 Methods

1.4.1 Field Methods

Vertical profiles for temperature, dissolved oxygen (DO), oxidation reduction potential (ORP, relative to Ag/AgCl reference electrodes), chlorophyll *a*, and phycocyanin were collected bi-weekly to monthly since 2005 using regularly calibrated Hydrolab® DS5 multiparameter sondes. We used a Wildco® horizontal VanDorn trace metal sampler to collect water samples from discrete depths with ultraclean handling methods ((U.S. E.P.A., 1996). Water samples for general water chemistry and total Hg and MeHg were collected from surface (2 m depth) and profundal (1 m from sediments) waters, termed "surface" and "profundal/bottom" respectively. Additional MeHg samples were collected at the top, midpoint, and bottom of the thermocline.

Fish assemblage data and tissue samples were collected as water level permitted, from annually (2011-2013) to twice-annually (spring and summer 2016-2019). Fish were collected using a Smith Root Model-H electrofishing boat at four shoreline stations for fifteen-minute passes. Black crappie (*Pomoxis nigromaculatus*), bluegill (*Lepomis macrochirus*), and largemouth bass (*Micropterus salmoides*) from 50-350 mm were euthanized using tricaine mesylate, and frozen for later analysis. Up to 42 fish samples were collected from each reservoir per sampling event, ideally collecting each species over the entire 50-350 mm length range. However, this was not always possible.

1.4.2 Analytical Methods

Water samples were analyzed by Eurofins Scientific (Pleasanton, CA, USA). Total Hg was analyzed by EPA method 1631E (U.S. E.P.A., 2002). The method detection limit for total Hg was 0.2 ng/L. Total MeHg (unfiltered) was analyzed by EPA method 1630 (U.S. E.P.A., 1998). The method detection limit for MeHg was 0.02 ng/L. Strict quality control standards were followed for trace-level Hg and MeHg analysis, including method blanks, matrix spikes/matrix spike duplicates (acceptable range = 75-125% recovery), and ongoing precision and recovery samples (acceptable range = 75-125% recovery). Sulfate was analyzed by ion chromatography (U.S. E.P.A., 1993). Total Hg in fish tissue (whole body) and sediment were analyzed by Brooks Applied Labs (Seattle, Washington, USA) using a HNO_3/H_2SO_4 digestion, followed by EPA method 1631E (U.S. E.P.A., 2002). Frozen whole fish were defrosted and thoroughly homogenized using a clean blender prior to digestion. Fish Hg analysis followed strict quality control measures, including duplicates (acceptable relative percent difference = 30%), matrix spikes/matrix spike duplicates, and method blanks. Adequate recovery was verified using certified reference material (TORT-3). Total Hg was analyzed in fish because fish Hg is known to be nearly 100% MeHg.

1.4.3 Statistical Methods

Water quality data were evaluated by comparing dry season (May 1-September 30) measurements made prior to operation of HOS (OFF) to dry season measurements made during system operation (ON). Due to periodic shutdowns, the systems were considered ON if profundal dissolved oxygen concentrations were maintained above 2 mg/L. For data that were normally distributed, or could be normalized, Welch's t-test was used to compare between ON and OFF groups. The nonparametric Mann-Whitney test was used to compare ON and OFF groups that could not be normalized.

Due to limited fish Hg data prior to HOS operation, our evaluation consists of both before/after comparisons and trend analysis following HOS installation. We compared fish Hg data collected before and during HOS operation for each species in each reservoir. The post-HOS dataset for each species/reservoir combination consisted of the most recent samples collected in the same number and length range as the pre-HOS dataset. We length-standardized each individual fish to 100 mm by dividing its Hg concentration by its length, then multiplying by 100 mm. Monson (2009) found this averaging method to be interchangeable with the commonly used least-squares method of length-standardization. We compared pre- and post-HOS length-standardized Hg concentrations in fish using the non-parametric Mann-Whitney test because data were not normally distributed and could not be transformed to fit a normal distribution.

Trends in fish Hg concentrations can be obscured by inconsistencies between sample collection events. Fish Hg varies with collection season, fish species, and fish length. While we made considerable effort to minimize variability during sampling events, this was not always possible. Several studies have used linear regression to assess trends in fish Hg over time (e.g. Monson, 2009; Monson et al., 2011, Gandhi et al., 2014). We used a multiple regression model to isolate the trend in fish Hg from the covarying factors based on the following (Eq. 1):

$$\mathbf{Hg = \beta_1 + \beta_2(Fish\ Species) + \beta_3(Fish\ Length) + \beta_4(Fish\ Species)(Fish\ Length) + \beta_5(Collection\ Season) + \beta_6(Sample\ Date)} \qquad \textbf{(Eq. 1)}$$

The key parameter of interest is the Sample Date coefficient (β_6) because it represents the change in fish Hg with time. The model was applied to each reservoir using data collected following the onset of HOS operation.

To address uncertainty in the estimates of the Sample Date coefficients (β_6), we performed a nonparametric bootstrap analysis (r = 2000) to recalculate their 95% confidence intervals. Bootstrap analysis is a common method using resampling with replacement that can be applied to estimate confidence intervals of regression coefficients (Wu, 1986).

1.5 Results

1.5.1 Pre-Oxygenation Methylmercury Production and Fish Tissue Mercury

Each reservoir was thermally stratified annually from late spring (April-May) until early autumn (September-October). During stratification, profundal DO concentrations declined and MeHg concentrations increased. For example, in GR from

June 2011 through September 2011, surface waters warmed to around 25 ˚C and anoxic profundal waters near the sediment-water interface contained over 20 ng/L MeHg, accounting for nearly 40% of the total Hg concentration (Fig. A2). Profundal MeHg buildup varied annually in each site, fluctuating with water quality conditions, water storage, and reservoir operations. In all reservoirs prior to oxygenation, MeHg buildup in bottom water corresponded with sulfate depletion and lower redox potential. In GR for example, bottom water in late summer exhibited sulfate minima typically <10 mg/L and MeHg maxima typically > 20 ng/L when ORP was < 100 mV (Fig. 1-2). Though AR and GR contained similar total Hg concentrations in sediment (~3-5 mg/kg), average dry season MeHg concentrations prior to oxygenation in GR bottom water were an order of magnitude higher than AR (12.1 vs. 1.9 ng/L) (Table 1-1). AR and CR contained similar pre-oxygenation dry season mean MeHg concentrations in bottom water (1.9 ng/L), and SCR contained notably lower concentrations (0.8 ng/L). Pre-oxygenation dry season mean MeHg concentrations in surface water, an important source of MeHg to biota, were similar in AR and GR (0.6-0.8 ng/L), and lower in CR and SCR (< 0.3 ng/L).

Though data collected prior to oxygenation were limited, mean Hg (whole body, wet weight) in age-1 largemouth bass was around 0.8 mg/kg in AR (n = 50) and GR (n = 11), and 0.1 mg/kg in CR (n = 52) and SCR (n = 7). Hg (whole body, wet weight) in 35 cm length-standardized largemouth bass ranged from 0.75 mg/kg in SCR to 4.9 mg/kg in GR (Table 1-1). Additionally, fish Hg data were collected for bluegill, black crappie, and largemouth bass up to 350 mm (Table A2).

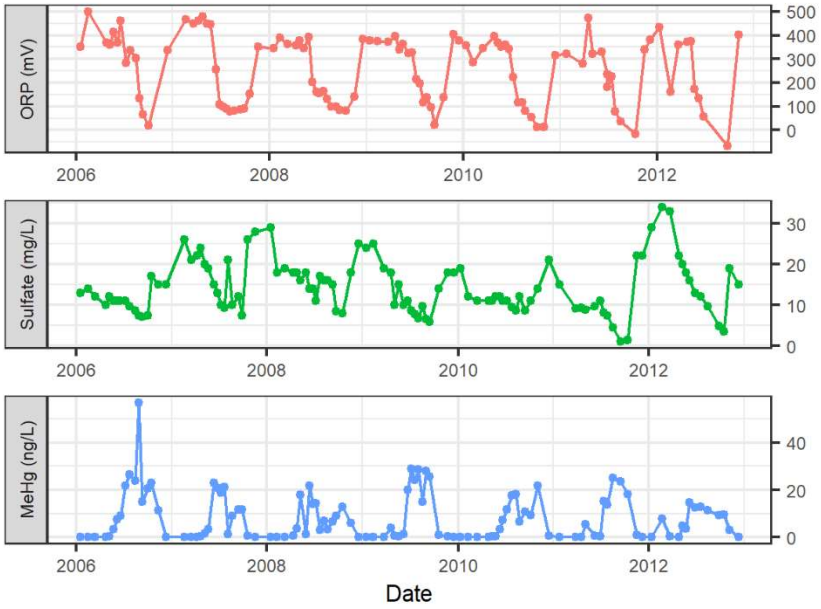

Figure 1-2: Guadalupe Reservoir oxidation reduction potential (ORP) (top), sulfate (middle) and methylmercury (MeHg) from 2006- 2012 prior to oxygenation. Measurements were taken one meter from the reservoir bottom.

1.5.2 Oxygenation System Operation

The hypolimnetic oxygenation systems were operated nearly continuously throughout the dry seasons of 2016-2019 (Fig. 1-3). DO saturation in bottom water increased significantly (Table A3, lines 41-48) in AR, GR, and SCR, from dry season

means of 5-26% in years prior to oxygenation to means of 91-123% during oxygenation (Fig. A3). When reservoir oxygenation was initiated prior to the onset of profundal hypoxia (DO < 2 mg/L), anoxia was avoided, and oxygen-rich conditions were maintained throughout the stratification period. Though the diffuser lines extend only through the deepest portions of the reservoirs, elevated DO concentrations propagated throughout the entire hypolimnion in all reservoirs except CR. For example, in June 2018, DO levels exceeded 14 mg/L throughout the hypolimnion of AR, including over 500 m away from the end of the oxygenation line diffuser (Fig. A4). DO saturation increased only modestly in CR, from a mean dry season saturation of 8.5% prior to oxygenation to 16.4% during oxygenation, with this effect limited to the immediate

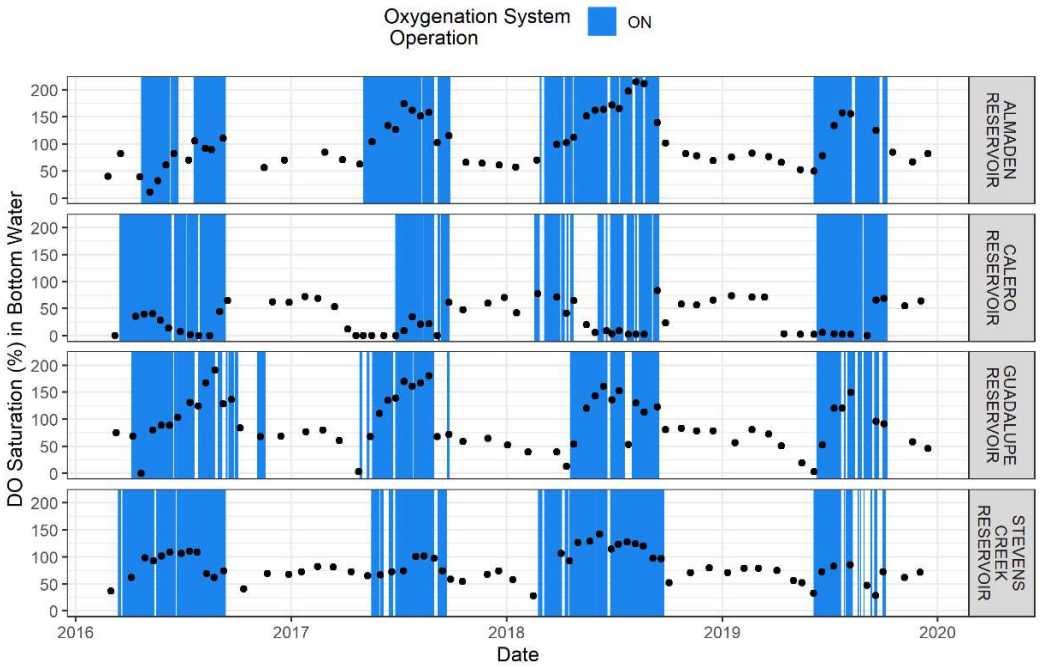

Figure 1-3: Dissolved oxygen saturation in bottom water during oxygenation system operation.

vicinity of the diffuser line (Fig. A3). Though this increase was statistically significant (Table A3, lines 43-44), the reservoir bottom experienced prolonged periods of anoxia during oxygenation (Fig. 1-3). As expected, surface water remained well-oxygenated throughout the year (mean dry season DO saturation; Table A3, lines 33-40, and Fig. A3).

1.5.3 Water Quality Results

In addition to DO, several water quality parameters of interest showed differences before and during oxygenation in bottom and surface water. Water temperatures increased significantly (Table A3, lines 105-112) in bottom water of all reservoirs except AR during oxygenation, with mean increases between 2.5 °C and 5.5 °C (Fig. A3). Surface temperature increased significantly (Table A3, lines 97-104) in CR, GR, and SCR, and nearly significantly in AR during oxygenation by about 1°C (Fig. A3). During

oxygenation, ORP unexpectedly decreased significantly in the bottom waters of AR and CR, and nearly significantly in GR (Table A3, lines 25-32) relative to previous years (Fig. A3). This effect was most pronounced in CR, where mean ORP decreased from 181 to 102 mV. In surface waters, mean ORP decreased significantly (Table A3, lines 17-24) by about 100 mV (Fig. A3). During oxygenation, mean sulfate concentrations were significantly higher in bottom waters of all reservoirs and in surface waters of all except AR (Table A3, lines 57-64; Fig. 1-4). Differences were modest, about 5 mg/L increase in CR surface and bottom waters (Fig. 1-4). Chlorophyll *a* concentration increased significantly (Table A3, lines 1-8) by 20-35% in the surface waters of all reservoirs except GR during oxygenation. This effect was most pronounced in CR, where the mean chlorophyll *a* concentration increased from 8.5 to 12.6 ug/L. Phycocyanin concentrations changed similarly, increasing by 25%-60% in the surface water of all reservoirs, with most notable increases in CR (Fig. A3).

Total Hg concentrations in bottom water were unchanged in GR but decreased significantly in AR, CR, and SCR (Table A3, lines 73-80) during oxygenation (Fig. 1-4). In SCR, total Hg concentrations in bottom water decreased from a dry season mean of 11.3 ng/L in years prior to oxygenation to 6.9 ng/L during oxygenation. Average total Hg concentrations decreased in surface waters of AR and GR (Table A3, lines 65-70). In GR, average total Hg concentrations decreased in surface waters from 13.8 to 6.6 ng/L (Table A3, lines 69-70 and Fig. 1-4).

Total MeHg decreased significantly (Table A3, lines 89-96) in the bottom waters of all reservoirs during oxygenation, with mean reductions from 63 to 85% below pre-oxygenation concentrations (Fig. 1-4). This effect was most pronounced in GR, where average concentrations decreased from 12.1 to 1.8 ng/L. However, MeHg concentrations were unchanged in surface waters, except for in SCR where concentrations increased slightly but significantly (Table A3, 81-88) from 0.12 to 0.15 ng/L (Fig. 1-4). MeHg concentrations in the mid-water column were largely unchanged in all reservoirs. Whole lake MeHg concentration, calculated as the total estimated mass of MeHg divided by the total water storage volume, increased significantly (Mann-Whitney test: $U = 414$, p-value $= 0.005$) in SCR from 0.10 ± 0.02 ng/L ($n = 37$; mean plus/minus 95% CI) prior to oxygenation to 0.17 ± 0.04 ng/L ($n = 36$) during oxygenation (Fig. A5). In GR, the whole lake MeHg concentrations decreased modestly, but significantly (Mann-Whitney test: $U = 1704$, p-value $= 0.03$) from 0.73 ± 0.16 ng/L ($n = 61$) to 0.70 ± 0.27 ng/L ($n = 45$) (Fig. A5).

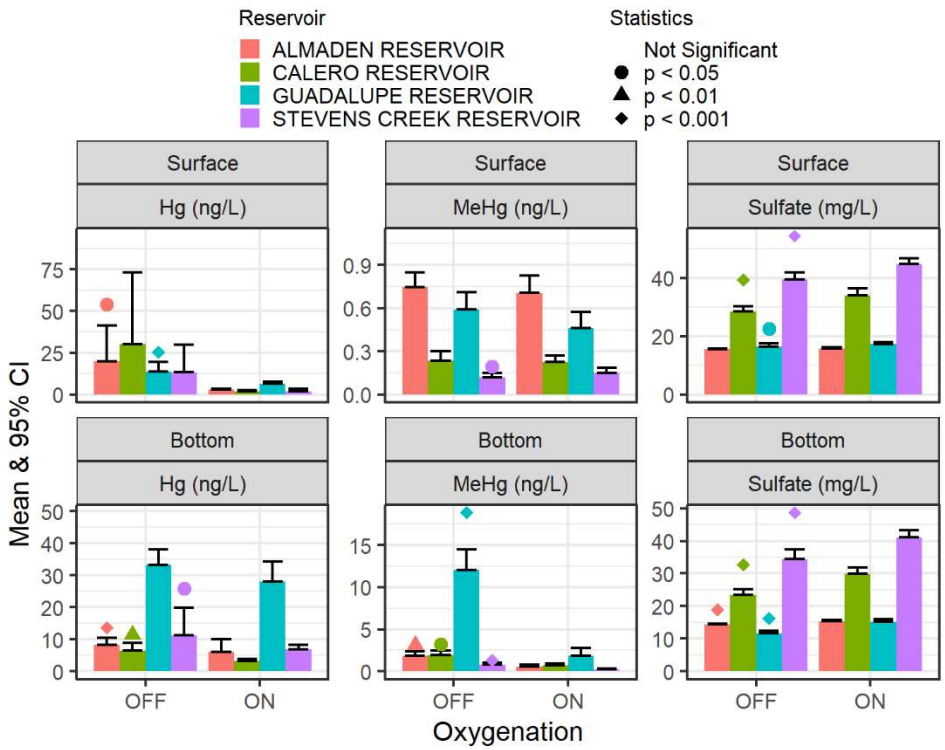

Figure 1-4: Dry season methylmercury and related analytes measured prior to (OFF) and during (ON) oxygenation. "Surface" samples were taken two meters from the surface and "Bottom" samples were taken one meter from the bottom. Symbols above the OFF bar signify a significant difference between ON and OFF. See Table A3 for statistical results.

1.5.4 Fish Tissue Mercury

We found no significant difference between pre- and post-HOS 100 mm length-standardized fish Hg concentrations, except in AR where largemouth bass Hg decreased by an average of 35%, and SCR where black crappie Hg increased by 114% (Table A4, Fig. 1-5). The Sample Date terms of the multiple regression model were significant ($p < 0.001$) and negative in GR and SCR (Table A5), indicating declining trends. To elucidate trends in fish Hg, we fit the regression models to 100 mm fish (Fig. 1-6, blue line). In GR and SCR, the bootstrapped 95% confidence intervals for the Sample Date coefficients (β_6) were comparable to the confidence intervals yielded by the multiple regression models (Table A6), confirming the declining trends. The 95% confidence intervals of the Sample Date coefficients (β_6) from both the regression and the bootstrap analysis did not overlap with zero, indicating that fish Hg in these reservoirs is declining with time. Since the beginning of HOS-operation, fish Hg has decreased in GR and SCR by 0.15 ± 0.02 mg/kg·yr and 0.02 ± 0.007 mg/kg·yr, respectively. This translates to decreases in Hg concentrations of 100 mm largemouth bass of about 55% in GR over seven years and 37% in SCR over five years of HOS operation.

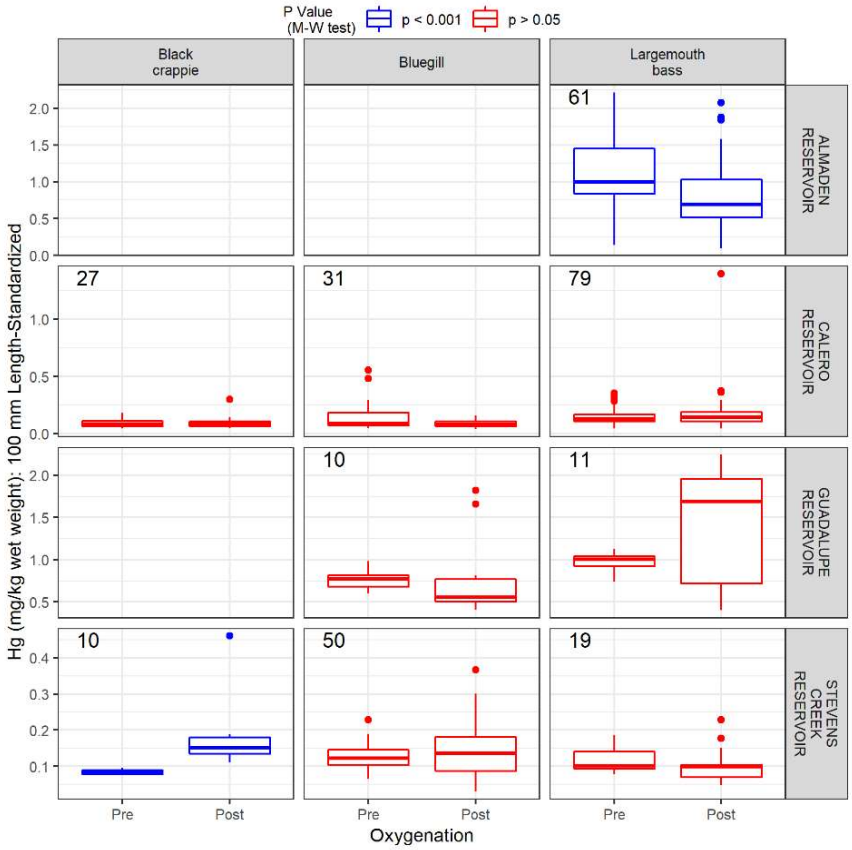

Figure 1-5: Comparison of 100 mm length-standardized fish measured pre- and post-HOS operation. Fish were length-standardized using the "averaging" method described in Monson (2009). See Table A2 for statistical results. Numbers are sample size per group.

1.6 Discussion

1.6.1 Oxygenation of Profundal Zone

Line-diffuser HOS was effective in oxygenating bottom waters in three of the four study reservoirs. DO concentrations were near or exceeded saturation throughout the profundal zone in AR, GR, and SCR. In contrast, the HOS in CR failed to overcome hypoxia (< 2 mg/L). The delivery capacity of the CR HOS (675 kg O_2/day) was designed to exceed oxygen demands of 310 kg O_2/day, estimated using water column DO depletion rates from 1999-2002 (Brown and Caldwell, 2005). The original calculation appears to have underestimated true reservoir oxygen demands, which are highest in CR due to its large sediment surface area, longer water residence time, elevated trophic status, and weaker stratification.

Several factors may account for the relatively high oxygen demand in CR. CR is the most eutrophic reservoir studied, with notably higher nutrient and phytoplankton concentrations that increased during reservoir oxygenation (Fig. A3) (Seelos, 2017). Primary productivity increases sediment oxygen demand by supplying labile organic carbon and nutrients to the profundal zone, where they stimulate microbial respiration (Beutel, 2003). It is plausible that the increased algal productivity observed in CR during

HOS operation stimulated additional oxygen demand. Additionally, the mean increase in bottom water temperature of 2.4 ˚C during HOS operation is expected to increase sediment oxygen demand by around 20% (Zison et al., 1978). Increased turbulence and DO concentration at the sediment-water interface can enhance oxygen flux into sediment, a phenomenon known as induced oxygen demand (Beutel, 2003; Gantzer et al., 2009). This is especially the case in reservoirs like Calero which has a relatively small hypolimnion thickness (i.e., high sediment area to volume ratio). In these reservoirs much of the settling organic matter deposits on the sediment where it can induce oxygen demand (Beutel, 2003). Weakly-stratified reservoirs like Calero may also experience decreased retention of added oxygen by losing added oxygen to the upper water column (Moore et al., 2015).

While HOS was generally effective in enhancing DO in bottom waters, ORP

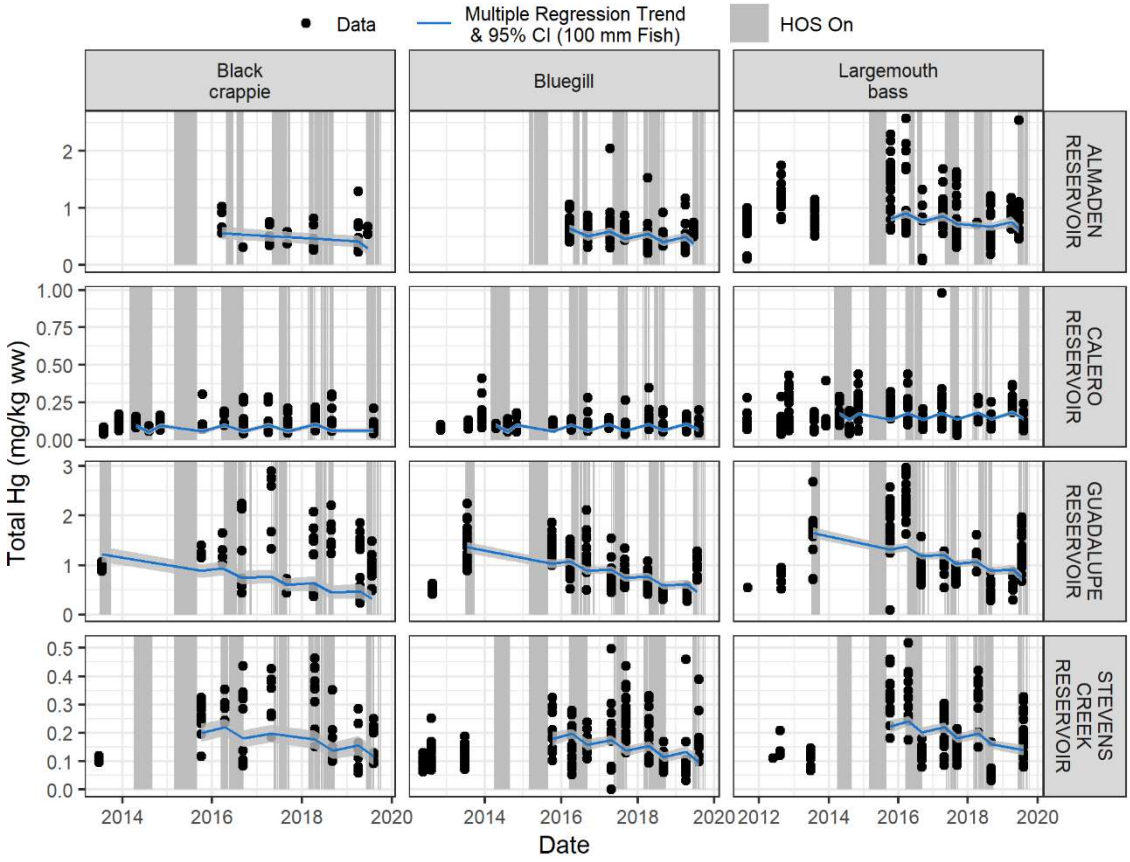

Figure 1-6: Raw Fish Hg data (black dots) and multiple regression model fitted to 100 mm fish length. Guadalupe and Stevens Creek reservoirs have significant declining trends in fish Hg since the beginning of HOS operation. (Gaps in monitoring, e.g., 2013-2015, were due to drought.)

exhibited counter-intuitive patterns. Line-diffuser HOS affected water chemistry in the profundal zone by oxidizing reduced compounds, altering microbial processes, and mixing some profundal waters throughout the water column. Surprisingly, profundal ORP either decreased or was unchanged during HOS operation. A shallow Georgia (USA) reservoir also exhibited lower ORP in surface and bottom waters during line

diffuser HOS operation (Dr. David Austin, personal communication, 6/18/2020). This phenomenon may reflect enhanced mixing at the sediment-water interface, which could induce additional oxygen demand and release of reduced compounds from the sediments into the water column (Beutel, 2003). Delayed oxidation of Mn(II), and precipitation of Fe(II) and sulfide released from sediments could create the appearance of reduced conditions and potentially give relatively low ORP readings under oxygenated conditions. This agrees with other studies showing continued release of sulfate (Duvil et al., 2018) and reduced metals from sediments under aerobic conditions (Gächter & Wehrli, 1998; Beutel et al., 2014). While our data suggests that some alteration of redox processes at the sediment-water interface did occur, these effects appear to be obscured by mixing and dilution of redox-sensitive compounds in the hypolimnetic water column caused by HOS-induced turbulence.

1.6.2 Water Quality Impacts during HOS Operation

Water quality in reservoirs generally declined after HOS operation, results that differ from other studies (Beutel and Horne, 1999; Horne et al., 2019). Line-diffuser HOS appears to have introduced profundal compounds into the upper water column through enhanced mixing at the thermocline due to turbulence associated with a rising bubble plume along the length of the diffuser line (Gantzer et al., 2009). Despite unchanged profundal total phosphorus in all reservoirs except GR during oxygenation, concentrations increased significantly in surface waters of all reservoirs (Seelos, 2017). Because these reservoirs experience little to no external loading during HOS operation, these increases are likely internal in origin. We suggest that profundal nutrients, likely including phosphate, ammonia, and Fe(II), a key cyanobacteria micro nutrient, were transported into the photic zone with rising bubble plumes. Bottom water temperature increased between 2.5 ˚C and 5.5 ˚C on average during line-diffuser HOS operation. Notable increases in chlorophyll *a* and phycocyanin during HOS operation suggest that temperature and nutrient increases stimulated algal productivity (Correll, 1999; Singh and Singh, 2015; Konopka and Brock, 1978). Elevated DO saturation in surface water during HOS operation is additional evidence of water transfer between the profundal zone and surface waters, but also may be the result of higher algal productivity.

Reservoir outlet turbidity increased in SCR during HOS operation (Fig. A6). This was probably due to sediment entrainment from turbulent mixing (Moore et al., 2015). Increased outlet temperature and turbidity present concerns when reservoirs discharge to waterways hosting salmonids, which are sensitive to these factors (Lehman et al., 2017). Though water quality may be improved during oxygenation, increases in outlet temperature and suspended sediment concentration could have negative effects in reservoir tail waters.

1.6.3 Water Column Methylmercury

Despite significant MeHg reductions in bottom waters, which averaged 63-85% across the study sites, average MeHg concentrations in the surface waters were unchanged in all reservoirs except SCR, where concentrations increased during HOS operation by 25%. MeHg in surface waters is of concern, because bioaccumulation occurs largely in the photic zone (Wu et al., 2019), and can be more pronounced in pelagic food webs (Stewart et al., 2008; Chen et al., 2014). Average water column MeHg

concentrations, estimated as the mass of MeHg in water column divided by total water storage volume, were relatively unchanged during HOS operation, except in SCR, where they increased. Because there is no inflow during HOS operation, observations suggest that HOS did not substantially reduce net MeHg production and buildup in reservoir waters. These results call into question the mechanism by which MeHg concentrations were lessened in bottom waters. It appears that the observed reductions in profundal MeHg concentrations were mainly due to dilution and mixing effects, as opposed to redox-related inhibition of methylating bacteria. In addition, MeHg production in the oxic water column and littoral sediments were likely not inhibited by HOS operation and may account for the unchanged surface water MeHg concentrations. Several studies have shown MeHg production in the oxic water column, often associated with settling particles (Eckley and Hintelmann, 2006; Achá and Hintelmann, 2012; Gascón Díez et al., 2016), and in littoral sediments (Krabbenhoft et al., 1998).

MeHg accumulates in profundal waters during periods of thermal stratification, then enters pelagic biota during fall turnover (Slotton et al., 1995; Herrin et al., 1998). Slotton et al. (1995) measured 70-200% increases in juvenile largemouth bass Hg with the seasonal entrainment of upper hypolimnion water prior to turnover in Davis Creek Reservoir, a California reservoir polluted by Hg mining that discharges from the surface. Thus, management strategies that can decrease MeHg buildup in summertime bottom waters should yield lower levels of fall bioaccumulation. However, other studies have failed to observe increased MeHg concentrations in surface waters when lakes destratify (Regnell et al., 1997; Valdes et al., 2017). In our study reservoirs prior to HOS operation, fall reservoir destratification is unlikely to control the introduction of MeHg into our study reservoir food webs. Profundal MeHg concentrations typically peaked in August at redox potentials from 0-100 mV, then declined until destratification as highly reducing conditions established (e.g. GR, Fig. 1-2). This agrees with other studies noting a "Goldilocks" zone for MeHg production, after which sulfide inhibition and demethylation prevail (Benoit et al., 1999; Beutel et al., 2020; Oremland et al., 1991). By the time the reservoirs mixed between September and October, profundal MeHg decreased notably relative to the seasonal maximum concentrations, limiting MeHg available to the upper water column (Fig. 1-2). The study reservoirs contain bottom-release outlets that discharged MeHg-rich profundal water constantly and acted to dampen MeHg buildup in bottom waters. Mass balance calculations, in which we compared over 200 discrete sampling dates collected before HOS operation during the stratified season, show that fall mixing would minimally (1-3%) increase photic zone MeHg concentrations, confirming that destratification is unlikely to control bioaccumulation in these reservoirs. HOS would be more effective in reservoirs that release water from the surface or mid-water column.

1.6.4 Mercury Reductions in Fish Tissue

Though only largemouth bass in AR contain Hg concentrations that are lower than pre-HOS data, fish Hg in GR and SCR has been declining during HOS operation despite an initial increase compared to pre-HOS (Fig. 1-6). Increases were likely due to changes in MeHg production and bioaccumulation during the peak of the California Drought of 2011-2017. Fish Hg could have increased in this period as a result of greater

MeHg production due to sulfate regeneration (Coleman Wasik, 2015; Eckley et al., 2017), temperature increases (Callister and Winfrey, 1986), or increased autochthonous carbon loading from algae blooms (Bravo et al., 2017). High water temperatures may also increase Hg bioaccumulation by altering fish metabolism and feeding patterns (Dijkstra et al., 2013).

Although this is the first study to show declining trends in fish Hg concentrations in oxygenated reservoirs, the mechanisms by which this occurred in GR and SCR remain unclear. Because surface MeHg concentrations were not significantly different during HOS operation and Hg concentrations in fish have declined in these reservoirs, bioconcentration factors have decreased. Primary productivity increased in all reservoirs during HOS operation. Higher phytoplankton and biomass could result in Hg reductions by somatic growth dilution in zooplankton (Karimi et al., 2007) and fish (Ward et al., 2010). Additionally, increased phytoplankton and cyanobacteria given constant MeHg concentration may support "bloom dilution" that reduces MeHg uptake into pelagic food webs (Pickhardt et al., 2002). Significant increases in surface water chlorophyll *a* and phycocyanin during oxygenation may have caused reductions in fish Hg by diluting MeHg concentrations in phytoplankton, and encouraging rapid, efficient growth in zooplankton and fish. Furthermore, oxygenation of the hypolimnia likely increased benthic habitat area, potentially providing benthic prey with lower MeHg concentrations than pelagic sources (Stewart et al., 2008). The similar, short aquatic food webs of GR and SCR support fewer trophic linkages, which may reduce biomagnification (Cabana and Tremblay, 1994). Shorter food webs may also respond faster to changes in water chemistry, which could be the reason we have not observed lower fish Hg in AR. In contrast, fish Hg in CR was likely unchanged due to the poor performance of its HOS.

1.7 Conclusion

We studied effects of line-diffuser HOS on MeHg production and bioaccumulation in three mercury mine polluted reservoirs (Almaden, Calero, and Guadalupe Reservoirs) and in another (Stevens Creek Reservoir). HOS was effective at oxygenating bottom waters in Almaden, Guadalupe, and Stevens Creek reservoirs. The HOS at Calero Reservoir did not increase DO concentrations in bottom waters above hypoxic levels (< 2 mg/L) due to the reservoir's greater oxygen demand and lower retention of added oxygen in its hypolimnion. Though MeHg concentrations decreased significantly in bottom waters, 63% to 85% on average, concentrations in the photic zone were unchanged (Almaden, Calero, and Guadalupe reservoirs) or increased (Stevens Creek Reservoir). This may be due to enhanced exchange of profundal MeHg into the photic zone due to turbulent mixing caused by HOS operation, and/or continued MeHg production in the water column and littoral sediments. Fish Hg did not decrease in before/after comparison of most species, but in Stevens Creek Reservoir surface water MeHg and Hg in one of three fish species sampled increased, likely due to HOS operation. During four years of HOS operation, we observed statistically significant declining trends in fish Hg in Guadalupe and Stevens Creek reservoirs. We suspect that higher phytoplankton concentrations observed during HOS operation may have led to biodilution of MeHg, contributing to the observed decreases in fish Hg.

1.8 References

Achá, D., Hintelmann, H., & Pabón, C. A. (2012). Sulfate-reducing Bacteria and Mercury Methylation in the Water Column of the Lake 658 of the Experimental Lake Area. Geomicrobiology Journal, 29(7), 667–674. https://doi.org/10.1080/01490451.2011.606289

Alpers, C. N., Hunerlach, M. P., & May, J. T. (2005). Mercury Contamination from Historical Gold Mining in California. Environmental Health, (October).

Austin, D., Scharf, R., Carroll, J., Enochs, M. (2016). Suppression of hypolimnetic methylmercury accumulation by liquid calcium nitrate amendment: redox dynamics and fate of nitrate. Lake and Reservoir Management, 32(1), 61-73.

Benoit, J. M., Mason, R. P., & Gilmour, C. C. (1999). Estimation of mercury-sulfide speciation in sediment pore waters using octanol-water partitioning and implications for availability to methylating bacteria. Environmental Toxicology and Chemistry, 18(10), 2138–2141. https://doi.org/10.1897/1551-5028(1999)018<2138:EOMSSI>2.3.CO;2

Beutel, M. W. (2003). Hypolimnetic anoxia and sediment oxygen demand in California drinking water reservoirs. Lake and Reservoir Management, 19(3), 208–221. https://doi.org/10.1080/07438140309354086

Beutel, M. W., & Horne, A. J. (1999). A review of the effects of hypolimnetic oxygenation on lake and reservoir water quality. Lake and Reservoir Management, 15(4), 285–297. https://doi.org/10.1080/07438149909354124

Beutel, M.W., Dent, S., Reed, B., Marshall, P., Gebremariam, S., Moore, B., … Shallenberger, E. (2014). Effects of hypolimnetic oxygen addition on mercury bioaccumulation in Twin Lakes, Washington, USA. Science of the Total Environment, 496,688–700. https://doi.org/10.1016/j.scitotenv.2014.06.117

Beutel, M. W., Fuhrmann, B., Herbon, G., Chow, A., Brower, S., Pasek, J. (2020). Cycling of methylmercury and other redox-sensitive compounds in the profundal zone of a hypereutrophic water supply reservoir. Hydrobiologia, in press.

Bravo, A., Bouchet, S., Tolu, J. et al. (2017). Molecular composition of organic matter controls methylmercury formation in boreal lakes. Nat Commun 8, 14255. https://doi.org/10.1038/ncomms14255

Brown and Caldwell (2005). Reservoir aeration/oxygenation study agreement.

Callister, S.M., Winfrey, M.R. (1986). Microbial methylation of mercury in upper Wisconsin river sediments. Water Air Soil Pollut 29, 453–465. https://doi.org/10.1007/BF00283450

Cabana, G., Tremblay, A., Kalff, J., & Rasmussen, J. B. (1994). Pelagic food chain structure in Ontario lakes: A determinant of mercury levels in lake trout (Salvelinus namaycush). Canadian Journal of Fisheries and Aquatic Sciences. https://doi.org/10.1139/f94-039

Chen, Celia Y et al. "Benthic and pelagic pathways of methylmercury bioaccumulation in estuarine food webs of the northeast United States." PloS one vol. 9,2 e89305. 18 Feb. 2014, doi:10.1371/journal.pone.0089305

Coleman Wasik, J. K., Engstrom, D. R., Mitchell, C. P. J., Swain, E. B., Monson, B. A., Balogh, S. J., Jeremiason, J. D., Branfireun, B. A., Kolka, R. K., and Almendinger, J. E. (2015), The effects of hydrologic fluctuation and sulfate regeneration on mercury cycling in an experimental peatland, J. Geophys. Res. Biogeosci., 120, 1697– 1715, doi:10.1002/2015JG002993.

Compeau, G. C., & Bartha, R. (1985). Sulfate-Reducing Bacteria: Principal Methylators of Mercury in Anoxic Estuarine Sediment. Applied and Environmental Microbiology, 50(2), 498–502.

Correll, D. L. (1999). Phosphorus: A rate limiting nutrient in surface waters. Poultry Science, 78(5), 674–682. https://doi.org/10.1093/ps/78.5.674

Cox, M. F. (2000). The History of Mercury Emissions from the New Almaden Mines, Santa Clara County, California.
Davison, W., Woof, C., & Rigg, E. (1982). The dynamics of iron and manganese in a seasonally anoxic lake; direct measurement of fluxes using sediment traps. Limnology and Oceanography, 27(6), 987–1003. https://doi.org/10.4319/lo.1982.27.6.0987

Dijkstra JA, Buckman KL, Ward D, Evans DW, Dionne M, et al. (2013) Experimental and Natural Warming Elevates Mercury Concentrations in Estuarine Fish. PLOS ONE 8(3): e58401. https://doi.org/10.1371/journal.pone.0058401

Driscoll, C. T., Mason, R. P., Chan, H. M., Jacob, D. J., & Pirrone, N. (2013). Mercury as a Global Pollutant: Sources, Pathways, and Effects. Environmental Science & Technology, 47(10), 4967–4983. https://doi.org/10.1021/es305071v

Duvil, R., Beutel, M., Fuhrmann, B., & Seelos, M. (2018). Effect of oxygen, nitrate and aluminum addition on methylmercury efflux from mine-impacted reservoir sediment. Water Research, 144(1), 740-751. https://doi.org/10.1016/j.watres.2018.07.071

Eckley, C. S., & Hintelmann, H. (2006). Determination of mercury methylation potentials in the water column of lakes across Canada. Science of the Total Environment, 368(1), 111–125. https://doi.org/10.1016/j.scitotenv.2005.09.042

Eckley, C. S., Luxton, T. P., Goetz, J., & McKernan, J. (2017). Water-level fluctuations influence sediment porewater chemistry and methylmercury production in a flood-control reservoir. Environmental pollution (Barking, Essex: 1987), 222, 32–41. https://doi.org/10.1016/j.envpol.2017.01.010

Eckley, C.S., Gilmour, C.C., Janssen, S., Luxton, T.P., Randall, P.M., Whalin, L., Austin, C. (2020). The assessment and remediation of mercury contaminated sites: A review of current approaches, Science of The Total Environment, 707, 136031, ISSN 0048-9697, https://doi.org/10.1016/j.scitotenv.2019.136031.

Gächter, R., & Wehrli, B. (1998). Ten years of artificial mixing and oxygenation: No effect on the internal phosphorus loading of two eutrophic lakes. Environmental Science and Technology, 32(23), 3659–3665. https://doi.org/10.1021/es980418l

Gandhi, N., Tang, R., Bhavsar, S., and Arhonditsis, G. (2014). Fish Mercury Levels Appear to Be Increasing Lately: A Report from 40 Years of Monitoring in the Province of Ontario, Canada Environmental Science & Technology 2014 48 (10), 5404-5414. DOI: 10.1021/es403651x

Gantzer, P. A., Bryant, L. D., & Little, J. C. (2009). Effect of hypolimnetic oxygenation on oxygen depletion rates in two water-supply reservoirs. Water Research, 43(6), 1700–1710. https://doi.org/10.1016/j.watres.2008.12.053

Gascón Díez, E., Loizeau, J. L., Cosio, C., Bouchet, S., Adatte, T., Amouroux, D., & Bravo, A. G. (2016). Role of Settling Particles on Mercury Methylation in the Oxic Water Column of Freshwater Systems. Environmental Science and Technology, 50(21), 11672–11679. https://doi.org/10.1021/acs.est.6b03260

Gilmour, C. C., Podar, M., Bullock, A. L., Graham, A. M., Brown, S. D., Somenahally, A. C., … Elias, D. A. (2013). Mercury methylation by novel microorganisms from new environments. Environmental Science and Technology, 47(20), 11810–11820. https://doi.org/10.1021/es403075t

Herrin, R. T., Lathrop, R. C., Gorski, P. R., & Andren, A. W. (1998). Hypolimnetic methylmercury and its uptake by plankton during fall destratification: A key entry point of mercury into lake food chains? Limnology and Oceanography, 43(7), 1476–1486. https://doi.org/10.4319/lo.1998.43.7.1476

Horne, A. J., Jung, R., Lai, H., Faisst, B., & Beutel, M. (2019). Hypolimnetic oxygenation 2: oxygen dynamics in a large reservoir with submerged down-flow contact oxygenation (Speece cone). Lake and Reservoir Management, 35(3), 323–337. https://doi.org/10.1080/10402381.2019.1648612

Hsu-Kim, H., Eckley, C.S., Achá, D. et al. Challenges and opportunities for managing aquatic mercury pollution in altered landscapes. Ambio 47, 141–169 (2018). https://doi.org/10.1007/s13280-017-1006-7

Karimi, R., Chen, C. Y., Pickhardt, P. C., Fisher, N. S., & Folt, C. L. (2007). Stoichiometric controls of mercury dilution by growth. Proceedings of the National Academy of Sciences of the United States of America, 104(18), 7477–7482. https://doi.org/10.1073/pnas.0611261104

Konopka, A., & Brock, T. D. (1978). Effect of temperature on blue-green algae (Cyanobacteria) in Lake Mendota. Applied and Environmental Microbiology, 36(4), 572–576.

Krabbenhoft, David & Gilmour, Cynthia & Benoit, Janina & Babiarz, Christopher & Andren, Anders & Hurley, James. (1998). Methyl mercury dynamics in littoral sediments of a temperate seepage lake. Canadian Journal of Fisheries and Aquatic Sciences - CAN J FISHERIES AQUAT SCI. 55. 835-844. 10.1139/cjfas-55-4-835.

Lehman, B., Huff, D., Hayes, S. & L, S. (2017) Relationships between Chinook Salmon Swimming Performance and Water Quality in the San Joaquin River, California, Transactions of the American Fisheries Society, 146:2, 349-358, DOI: 10.1080/00028487.2016.1271827

Lehnherr, Igor (2014). "Methylmercury Biogeochemistry: A Review with Special Reference to Arctic Aquatic Ecosystems." Environmental Reviews, vol. 22, no. 3, 2014, pp. 229–43, doi:10.1139/er-2013-0059.

Matthews, D. A., Babcock, D. B., Nolan, J. G., Prestigiacomo, A. R., Effler, S. W., Driscoll, C. T., … Kuhr, K. M. (2013). Whole-lake nitrate addition for control of methylmercury in mercury-contaminated Onondaga Lake, NY. Environmental Research, 125, 52–60. https://doi.org/10.1016/j.envres.2013.03.011

McCord, S. A., Beutel, M. W., Dent, S. R., & Schladow, S. G. (2016). Evaluation of mercury cycling and hypolimnetic oxygenation in mercury-impacted seasonally stratified reservoirs in the Guadalupe River watershed, California. Water Resources Research, 52(10), 7726–7743. https://doi.org/10.1002/2016WR019061

McKee, L., Bonnema, A., David, N., Davis, J. A., Franz, A., Grace, R., … Yee, D. (2017). Long-term variation in concentrations and mass loads in a semi-arid watershed influenced by historic mercury mining and urban pollutant sources. Science of The Total Environment, 605–606, 482–497. https://doi.org/10.1016/J.SCITOTENV.2017.04.203

McKee, L., Gilbreath, A., Pearce, S., Shimabuku, I. 2018. Guadalupe river mercury concentrations and loads during the large rare January 2017 storm. SFEI Contribution No. 837. San Francisco Estuary Institute: Richmond, CA.

Miklavčič, Ana & Mazej, Darja & Jaćimović, Radojko & Dizdarevic, Tatjana & Horvat, Milena. (2013). Mercury in food items from the Idrija Mercury Mine area. Environmental research. 125. 10.1016/j.envres.2013.02.008.

Monson BA (2009). Trend reversal of mercury concentrations in piscivorous fish from Minnesota lakes: 1982-2006. Environ Sci Technol. 2009;43(6):1750-1755. doi:10.1021/es8027378

Monson BA, Staples DF, Bhavsar SP, et al. (2011). Spatiotemporal trends of mercury in walleye and largemouth bass from the Laurentian Great Lakes region. Ecotoxicology. 2011;20(7):1555-1567. doi:10.1007/s10646-011-0715-0

Moore, B., Mobley, M., Little, J., Kortmann, B., Gantzer, P. (2015). Aeration and Oxygenation Methods for Stratified Lakes and Reservoirs. NALMS Lakeline.

Natural Resources Conservation Service National Water and Climate Center. Retrieved January 6, 2020 from https://www.wcc.nrcs.usda.gov/.

Nevado, JJB & Bermejo, LFG & Martin-Dolmeadios, RCR. (2003). Distribution of mercury in the aquatic environment at Almaden, Spain. Environmental Pollution. 122. 261-271.

Oremland, R. S., Culbertson, C. W., & Winfrey, M. R. (1991). Methylmercury decomposition in sediments and bacterial cultures: Involvement of methanogens and sulfate reducers in oxidative demethylation. Applied and Environmental Microbiology, 57(1), 130–137.

Pickhardt, P. C., Folt, C. L., Chen, C. Y., Klaue, B., & Blum, J. D. (2002). Algal blooms reduce the uptake of toxic methylmercury in freshwater food webs. Proceedings of the National Academy of Sciences of the United States of America, 99(7), 4419–4423. https://doi.org/10.1073/pnas.072531099

Pickhardt, P. C., & Fisher, N. S. (2007). Accumulation of inorganic and methylmercury by freshwater phytoplankton in two contrasting water bodies. Environmental Science and Technology, 41(1), 125–131. https://doi.org/10.1021/es060966w

Regnell, O., Ewald, G., & Lord, E. (1997). Factors controlling temporal variation in methyl mercury levels in sediment and water in a seasonally stratified lake. Limnology and Oceanography, 42(8), 1784–1795. https://doi.org/10.4319/lo.1997.42.8.1784

Rothenberg, S. E., McKee, L., Gilbreath, A., Yee, D., Connor, M., & Fu, X. (2010). Wet deposition of mercury within the vicinity of a cement plant before and during cement plant maintenance. Atmospheric Environment, 44(10), 1255–1262. https://doi.org/10.1016/j.atmosenv.2009.12.033

San Francisco Bay Regional Water Quality Control Board. (2008). Guadalupe river watershed mercury total maximum daily load (TMDL) project staff report.

Seelos, M., (2017). Guadalupe River watershed mercury TMDL: 2016-2017 progress report on methylmercury production and control measures. Report by the Santa Clara Valley Water District for the san Francisco Bay regional water quality control board.

Singh, S. P., & Singh, P. (2015). Effect of temperature and light on the growth of algae species: A review. Renewable and Sustainable Energy Reviews, 50, 431–444. https://doi.org/10.1016/j.rser.2015.05.024

Singleton, V. L., & Little, J. C. (2006). Designing hypolimnetic aeration and oxygenation systems-A review. Environmental Science and Technology, 40(24), 7512–7520. https://doi.org/10.1021/es060069s

Slotton, D. G., Reuter, J. E., & Goldman, C. R. (1995). Mercury uptake patterns of biota in a seasonally anoxic northern California reservoir. Water, Air, & Soil Pollution, 80, 841–850.

Sobek, S., Gudasz, C., Koehler, B., Tranvik, L. J., Bastviken, D., & Morales-Pineda, M. (2017). Temperature Dependence of Apparent Respiratory Quotients and Oxygen Penetration Depth in Contrasting Lake Sediments. Journal of Geophysical Research: Biogeosciences, 122(11), 3076–3087. https://doi.org/10.1002/2017JG003833

State Water Resources Control Board. (2017a). 2014 and 2016 California Integrated Report Clean Water Act Sections 303(d) and 305(b). Staff Report. October 3.

State Water Resources Control Board. (2017b). Draft Staff Report for Scientific Peer Review for the Amendment to the Water Quality Control Plan for Inland Surface Waters, Enclosed Bays, and Estuaries of California, Mercury Reservoir Provisions — Mercury TMDL and Implementation Program for Reservoirs Statewide Mercury Control Program for Reservoirs, (April).

State Water Resources Control Board. (2017c). Draft Staff Report Including Substitute Environmental Documentation: Part 2 of the Water Quality Control Plan for Inland Surface Waters, Enclosed Bays, and Estuaries of California — Tribal and Subsistence Fishing Beneficial Uses and Mercury Provisions.

Stewart, A. R., Saiki, M. K., Kuwabara, J. S., Alpers, C. N., Marvin-DiPasquale, M., & Krabbenhoft, D. P. (2008). Influence of plankton mercury dynamics and trophic pathways on mercury concentrations of top predator fish of a mining-impacted reservoir. Canadian Journal of Fisheries and Aquatic Sciences, 65(11), 2351–2366. https://doi.org/10.1139/F08-140

Tetra Tech (2005a). Guadalupe river watershed mercury TMDL project final conceptual model report.

U.S. E.P.A. (1993). Method 300.0, Revision 2.1: Determination of Inorganic Anions by Ion Chromatography.

U.S. E.P.A. (1998). Method 1630. Methyl mercury in water by distillation, aqueous ethylation, purge and trap, and CVAFS.

U.S. E.P.A. (2002). Method 1631, Revision E: Mercury in Water by Oxidation, Purge and Trap, and Cold Vapor Atomic Fluorescence Spectrometry.

U.S. E.P.A. (1996). Method 1669 Sampling Ambient Water for Trace Metals at EPA Water Quality Criteria Levels.

Valdes, C., Black, F. J., Stringham, B., Collins, J. N., Goodman, J. R., Saxton, H. J., … Johnson, W. P. (2017). Total Mercury and Methylmercury Response in Water, Sediment, and Biota to Destratification of the Great Salt Lake, Utah, United States. Environmental Science and Technology, 51(9), 4887–4896. https://doi.org/10.1021/acs.est.6b05790

Vlassopoulos, D., Kanematsu, M., Henry, E. A., Goin, J., Leven, A., Glaser, D., … O'Day, P. A. (2018). Manganese(iv) oxide amendments reduce methylmercury concentrations in sediment porewater. Environmental Science: Processes and Impacts, 20(12), 1746–1760. https://doi.org/10.1039/c7em00583k

Ward, D. M., Nislow, K. H., Chen, C. Y., & Folt, C. L. (2010). Rapid, Efficient Growth Reduces Mercury Concentrations in Stream-Dwelling Atlantic Salmon. Transactions of the American Fisheries Society, 139(1), 1–10. https://doi.org/10.1577/T09-032.1

Wu, C. (1986). Jackknife, Bootstrap and Other Resampling Methods in Regression Analysis. The Annals of Statistics, 14(4), 1261-1295. Retrieved June 18, 2020, from www.jstor.org/stable/2241454

Wu, P., Kainz, M. J., Bravo, A. G., Åkerblom, S., Sonesten, L., & Bishop, K. (2019). The importance of bioconcentration into the pelagic food web base for methylmercury biomagnification: A meta-analysis. Science of the Total Environment, 646, 357–367. https://doi.org/10.1016/j.scitotenv.2018.07.328

Zison, SW & Mills, WB & Deimer, D & Chen, Carl. (1978). Rates, Constants, and Kinetics Formulations in Surface Water Quality Modeling. Available from the National Technical Information Service, Springfield VA 22161 as PB-290 938, Report.

2 Evaluation of Manganese Oxide Amendments for Mercury Remediation in Contaminated Aquatic Sediments

2.1 Abstract

Aquatic sediments are important sources of toxic methylmercury (MeHg) to the environment because they support anaerobic bacteria that methylate inorganic mercury (Hg). Common Hg remediation strategies such as sediment removal or capping can be prohibitively expensive or impractical when compared to *in situ* treatment methods designed to disfavor Hg methylation and increase sorption of MeHg to solids. Using profundal sediments from a Hg-contaminated reservoir, we assessed the effectiveness of Mn(IV) oxide (MnOx) amendment in decreasing porewater and sediment Hg and MeHg concentrations relative to sediments treated with granular activated carbon (AC) and unamended controls. We conducted two sediment slurry incubation experiments (0-20 days and 0-5 days) using sediments amended with MnOx, AC, or a mixture of the two. X-ray absorption spectroscopy data showed that the MnOx amendments were rapidly reduced to Mn^{2+} over the course of the incubation. In both experiments, MnOx addition resulted in elevated oxidation-reduction potential and lower MeHg concentrations in porewater relative to unamended controls after 2-3 days. The MnOx amendment decreased porewater MeHg with similar or greater effectiveness as AC. However, sediments amended with MnOx released inorganic Hg into porewater in some experiments. Coamendment of MnOx with sorbents could curtail diffusion of MeHg from aquatic sediments and slow MnOx reduction while limiting the release of potentially problematic byproducts such as Mn^{2+} and Hg(II).

2.2 Introduction

Mercury (Hg) is a global environmental pollutant that enters aquatic systems from natural and anthropogenic sources (Driscoll et al., 2013). Ecological and human health impacts of Hg pollution mainly come from exposure to neurotoxic methylmercury (MeHg) through fish consumption (Driscoll et al., 2013). Inorganic Hg can be microbially converted to MeHg in aquatic sediments (Compeau and Bartha, 1985; Gilmour et al., 1992). Methylmercury bioaccumulates in aquatic food webs, reaching fish tissue concentrations that can exceed water concentrations by six orders of magnitude (Pickhardt and Fisher, 2007; Lehnherr, 2014). Because trace concentrations of Hg in water and sediments contribute to MeHg biomagnification, remediation strategies emphasize decreasing the production and bioaccumulation of MeHg in addition to source control (Eckley et al., 2020).

Many remediation methods for Hg have been investigated, including sediment capping, phytoremediation, sorbent amendments, and redox controls (Randall and Chattopadhyay, 2013; Chattopadhyay et al., 2012; Gilmour et al., 2013b; Matthews et al., 2013; Vlassopoulos et al., 2018; Leven et al., 2018; Beutel et al., 2020; Seelos et al., 2021). Redox buffering aims to thermodynamically disfavor MeHg formation by poising the redox state at the sediment-water interface above potentials that favor iron and sulfate reduction, two processes associated with microbial Hg methylation (Gilmour et al., 2013a). Aqueous calcium nitrate addition and reservoir oxygenation have been used in

lakes to attempt to curtail MeHg production and bioaccumulation (Matthews et al., 2013; Seelos et al., 2021). Solid phase sediment amendments have potential advantages over aqueous and gas phase additions because they can be relatively inexpensive, may require less frequent application, and combine redox buffering and adsorptive properties.

Sorbent amendments have been studied extensively for remediation of metals and organic pollutants. Many sorbents are available, including activated carbon (AC), biochar, surface functionalized substrates, and modified clays (Ghosh et al., 2011; Goñez-Rodriguez et al., 2021). Activated carbon has been applied extensively for aquatic remediation of organic contaminants and metals (Ghosh et al., 2011; Patmont et al., 2015). Gilmour et al. (2013b) found that AC amendments lowered porewater Hg and MeHg concentrations, as well as MeHg uptake by oligochaete worms in experimental microcosms using contaminated sediments. A field trial showed that a thin-layer AC cap decreased porewater Hg and MeHg in salt marsh sediments (Gilmour et al., 2018). Activated carbon amendments may reduce net Hg methylation by decreasing the bioavailability of Hg(II) to bacteria, or decrease biotic uptake by of MeHg by keeping it bound to solids (Wang et al., 1998; Bussan et al., 2016).

Amendment with reactive manganese (IV) oxide (MnOx) is a novel strategy for *in situ* Hg remediation that may decrease MeHg production and release from sediments (Vlassopoulos et al., 2018; Leven et al., 2018). Manganese oxide (ideally MnO_2(s) but often non-stoichiometric) has been studied extensively for its ability to oxidize organic contaminants (Remucal and Vogel, 2014). Manganese oxide is also used in water treatment for its ability to sorb cations and oxidize organic compounds (Islam et al., 2018; Husnian et al., 2020). Because the reduction of MnOx occurs at higher redox potentials than microbial processes associated with Hg methylation (i.e., Fe(III) or sulfate reduction), MnOx addition should thermodynamically disfavor MeHg production (Table B1). Additionally, MnOx surfaces can efficiently sorb Hg(II) and MeHg, potentially decreasing bioavailability (Thanabalasingham et al., 1985; Desauziers et al., 1997). Manganese oxide amendments have been shown to decrease MeHg concentrations in bacterial cultures, lake sediments, and sediment porewater (Vlassopoulos et al., 2018; Farrel et al., 1998; Jackson et al., 1989). However, MnOx amendments have not been employed in field settings for Hg remediation to date.

In this laboratory study, we evaluated the use of MnOx amendments for remediation of Hg-contaminated reservoir sediments compared to unamended controls and sediments amended with AC in short-term experiments (up to 20 days). Unlike past studies using MnOx amendments that primarily focused on porewater or sediments alone, our work compares the roles of sorption and redox buffering in reducing the concentrations of Hg and MeHg in porewater, and comprehensively investigates resulting changes in porewater and sediment chemistry, as well as the transformation and fate of the amendments. As opposed to our previous work using fifteen-month static incubations with a sediment-water interface, these short-term experiments were designed to examine in detail changes in porewater chemistry immediately after amendment addition that influence Hg methylation and dissolved concentrations of Hg and MeHg.

2.3 Methods

2.3.1 Sediment Incubations

We collected profundal sediment and water samples from a surface water reservoir (Guadalupe Reservoir, San Jose, CA, USA) contaminated by historical Hg (cinnabar) mining in June 2019 and November 2019 (see Text B1 and Fig. B1a-d for site description and field methods). We conducted two sediment slurry incubation experiments using the profundal sediments amended with solid phase additions (Table 2-1). Amended treatment groups included AC (granular activated carbon, Fisher Chemical, CAS: 7440-44-0), Mn (Carus Corporation Carulite® manganese oxide), or Mn+AC (1:5 mixture of AC and MnOx). Experiment 1 (E1) had longer incubation time intervals (0, 3, 10, and 20 days) than Experiment 2 (E2) (0, 0.5, 1, 2, and 5 days). Furthermore, all E2 treatment groups except C (unspiked control) contained additions of labile organic carbon and sulfate to stimulate sulfate reduction and Hg methylation (see below).

Experiment	Treatment	Amendment	Amendment Conc.	Spike	Time Steps
E1	C	NA	NA	NA	0d, 3d, 10d, 20d
	Mn	Carulite® MnO_2	5% Dry Basis		
	AC	Granular Activated Carbon	1% Dry Basis		
	Mn + AC	Carulite + Activated Carbon	5% of 5:1 Mn:AC		
E2	C	NA	NA	NA	0d, 0.5d, 1d, 2d, 5d
	C*	NA	NA	123 mg/L Acetate 181 mg/L Pyruvate 300 mg/L Sulfate	
	Mn*	Carulite® MnO_2	5% Dry Basis		
	AC*	Granular Activated Carbon	1% Dry Basis		
	Mn+AC*	Carulite + Activated Carbon	5% of 5:1 Mn:AC		

Table 2-1: Design parameters of Experiment 1 (E1) and Experiment 2 (E2). The asterisk (*) denotes DOC and sulfate addition.

2.3.2 Experiment 1

Experiment 1 (E1) used sediments collected in June 2019. We homogenized 4 kg of reservoir sediments in clean, high-density polyethylene (HDPE) buckets specific to each treatment group (C, AC, Mn, Mn+AC; Table 2-1). The control (C) treatment contained no added amendment. The Mn treatment bucket contained a Carulite addition of 5% by dry weight, a common dose for sorbent sediment amendments (Ghosh et al., 2011; Kwon et al., 2010; Sanders et al., 2018). The AC contained 1% granular activated carbon by dry weight. The lower amendment percentage in the AC treatment was intended to adjust for the higher specific surface area of the granular activated carbon compared to the Carulite®, which was estimated to be five times larger based on the manufacturers' reported values. The Mn+AC bucket contained 0.83% AC and 4.17% Carulute® by dry weight. Filtered profundal water was added to the Mn, AC, and Mn+AC groups to adjust their solids:liquid ratios to the same value as the C group. Sediment slurry mixtures from each treatment were split into triplicate sets (320 grams each) and transferred to 250 mL polypropylene copolymer centrifuge bottles (PPCO), with a separate set for each time step (0, 3, 10, and 20 days). Further details for experimental setup are given in Text B2. Each set of bottles was held in the dark at 12 ˚C for the duration of the incubation before solid/liquid separation by centrifugation at 24,000 g and 4 ˚C for twenty minutes. Supernatant solutions were removed by pipette and processed as described in Text B3. Though day 0 samples were centrifuged immediately

following amendment addition, homogenization, and bottling (~10 minutes elapsed time from amendment addition), reaction occurred during this time that caused variability in the day 0 samples between treatment groups. Baseline values for unamended sediments are best represented by day 0 of the C group.

2.3.3 Experiment 2

Procedural details of Experiment 2 (E2) were the same as E1, but with three differences. Firstly, the sediments used were collected in November 2019 when the reservoir was mixed and oxygenated throughout (Text B1). Secondly, the incubation durations were shorter, at 0, 0.5, 1, 2, and 5 days, to capture near-term patterns of Hg transformations. Thirdly, all treatments except the C group contained additions of labile organic carbon (acetate and pyruvate) and sulfate to stimulate Hg methylation and microbial activity (see Text B4 for spike preparation). These "spiked" treatments are designated with an asterisk (*). Five kg of reservoir sediments were homogenized in clean high-density polyethylene (HDPE) buckets specific to each treatment group (C, C*, AC*, Mn*, Mn+AC*). The C and C* groups contained no solid additions. Solid amendments were added to treatment groups as described for E1 to yield 5% amendment by dry weight in the Mn* and Mn+AC* groups, and 1% by dry weight in the AC* group. The organic carbon/sulfate solution (78.125 mL) was added to each bucket for the spiked treatment groups, yielding approximate sediment porewater additions of 1.5 mM acetate, 1.6 mM pyruvate, and 3.2 mM sulfate. We homogenized the mixture and transferred 320 grams of slurry for each treatment to triplicate sets of 250 mL PPCO centrifuge bottles, with a separate set for each time step (0, 0.5, 1, 2, and 5 days). Each set of bottles was incubated and treated the same as described for E1.

2.3.4 Chemical Analysis

We analyzed total Hg in water by oxidation, purge and trap, and cold vapor atomic fluorescence spectrometry (CVAFS) (U.S. E.P.A., 2002). Total Hg in sediments was analyzed by thermal decomposition, amalgamation, and atomic absorbance spectrophotometry (U.S. E.P.A., 2007a). We extracted MeHg from water samples by distillation for three hours at 125 ˚C under Hg-free nitrogen flow using polytetrafluoroethylene (PTFE) vessels. We extracted MeHg from sediments by digesting in 2 mL of 25% KOH in methanol for four hours at 60 ˚C followed by centrifugation at 1200 g and 4 ˚C for fifteen minutes (Liang et al., 1994). Sediment and water MeHg extractions were adjusted to ~pH 4.9 using a sodium acetate buffer, ethylated using sodium tetraethylborate, then analyzed using purge and trap followed by CVAFS (U.S. E.P.A., 1998). We followed strict quality control standards for low level Hg and MeHg analysis, including method blanks, matrix spikes/matrix spike duplicates (acceptable range = 75%-125% recovery), and check standards (acceptable range = 75%-125% recovery). Further details about Hg and MeHg analysis are included in Text B5 and Table B2. We analyzed anions (Cl^-, SO_4^{2-}) using ion chromatography (U.S. E.P.A., 1993)

Metals (Fe, Mn, K, Ca, Mg) were analyzed using inductively coupled plasma optical emission spectrometry (ICP-OES) (U.S. E.P.A., 1994). Total sediment Mn and Fe concentrations were determined by microwave digestion of representative aliquots (~ 20

mg) with 12 mL of aqua regia (3 parts 12 N HCl, 1 part 15.8 M HNO_3) followed by ICP-OES analysis of digestates (U.S. E.P.A., 2007b). Extraction of sediments to estimate Mn and Fe in reducible oxide phases was done by addition of 6 mL of 0.5 M hydroxylamine hydrochloride (HHCl) to 150 mg of wet sediment in PPCO centrifuge tubes (Helmhart et al., 2012). The samples were placed on an orbital shaker table for 16 hours, then the solution was extracted by centrifugation at 1200 g and 4 ˚C for 15 minutes, filtered, and analyzed by ICP-OES. To determine moisture content of the sediments, ~1 g aliquots were dried in an incubator at 104 ˚C for 24 hours, weighed, and converted to dry weight. All sediment analyte concentrations are reported as dry weight equivalents.

Dissolved Organic Carbon (DOC) in filtered porewater was analyzed using a Shimadzu® TOC-5000A total carbon analyzer (U.S. E.P.A., 2009). We estimated organic carbon content in dry sediments by loss on ignition at 550 ˚C for 4 hours. Quality assurance data for metals, DOC, and anions are included in Table B3.

2.3.5 Amendment and Sediment Manganese Characterization

Amendment surface areas were measured by the BET method. Approximately 0.5 g of amendment was weighed and degassed with an ultra-high purity nitrogen for 6 hours and the BET specific surface area was measured with a Micromeritics Tristar II PLUS. Powder XRD was conducted using a Philips X'pert MPD diffractometer equipped with an ultrafast X'Celerator detector and with a Ni-filtered Co Kα radiation source (λ=1.78 Å) operated at 50 kV and 40 mA. Samples were mounted on zero background Si holders and scanned from 4 to 80 degrees 2θ at 0.01-degree 2θ steps. Carulite® (MnOx) amendment and sediment samples were characterized using Mn K-edge X-Ray Absorption Spectroscopy (XAS) on BL 4-1 at the Stanford Synchrotron Radiation Lightsource (SSRL) with samples held in a liquid N_2 cryostat. We averaged multiple scans using SIXPack before fitting spectra using least squares linear combination fits (LCF) with standards described in Table B4 and Fig. B1 (Webb, 2005; Ravel and Newville, 2005). Further details on XAS analysis are included in Text B6.

2.4 Results

2.4.1 Reservoir Sediment Characterization

The sediments used in the two experiments were similar, with total Hg concentrations around 1.5 mg/kg, native total Mn concentrations around 1.5 g/kg, and similar organic carbon content (LOI around 10%) (Table B5). However, total Fe concentrations were over twice as high in sediments used for E2 (44.19 g/kg) compared to E1 (19.86 g/kg). Nearly all Mn (80-98%) in the sediments was extractable with HHCl while only 20-40% of Fe was HHCl-extractable, resulting in the same amount of extractable Fe in both experiments (Table B5). X-ray absorption spectra of Mn in sediments from E1 and E2 were nearly identical (Fig. B2). Although spectra could not be fit quantitatively by linear combinations of reference spectra, the native sediment Mn appears to be comprised of Mn(II) with small fractions of Mn(III) and/or Mn(IV), likely incorporated into other minerals. Sorbed Mn(II) or amorphous solids were likely extracted during the acidic HHCl digestions.

2.4.2 Amendment Characterization

X-ray absorption spectra of the Carulite© MnOx amendment were similar to the spectrum of synthetic vernadite (δ-Mn(IV)O_2) (Fig. B3). Vernadite is a disordered Mn(IV)O_2 polymorph comprised of randomly stacked octahedral sheets of MnO_6 that contain a negative structural charge due to cation vacancies (Villalobos et al., 2003). Characterization by powder XRD suggested that the MnOx amendment was disordered, with no significant peaks in the diffractogram (Fig. B4). The surface areas of the Carulite® MnOx and granular activated carbon amendments were measured at 92.27 m^2/g and 807.71 m^2/g, respectively. Total Hg concentrations in the amendments were negligible compared to the native sediment: 2.44 ± 0.37 µg/kg (mean ± SD, n=3) in the MnOx amendment and 1.48 ± 0.06 µg/kg in the AC.

2.4.3 Experiment 1

2.4.3.1 Mercury and Methylmercury in Sediment and Porewater

Day-0 samples showed notable variability between treatment groups, resulting from both natural heterogeneity of contaminated sediments and reaction of the sediments

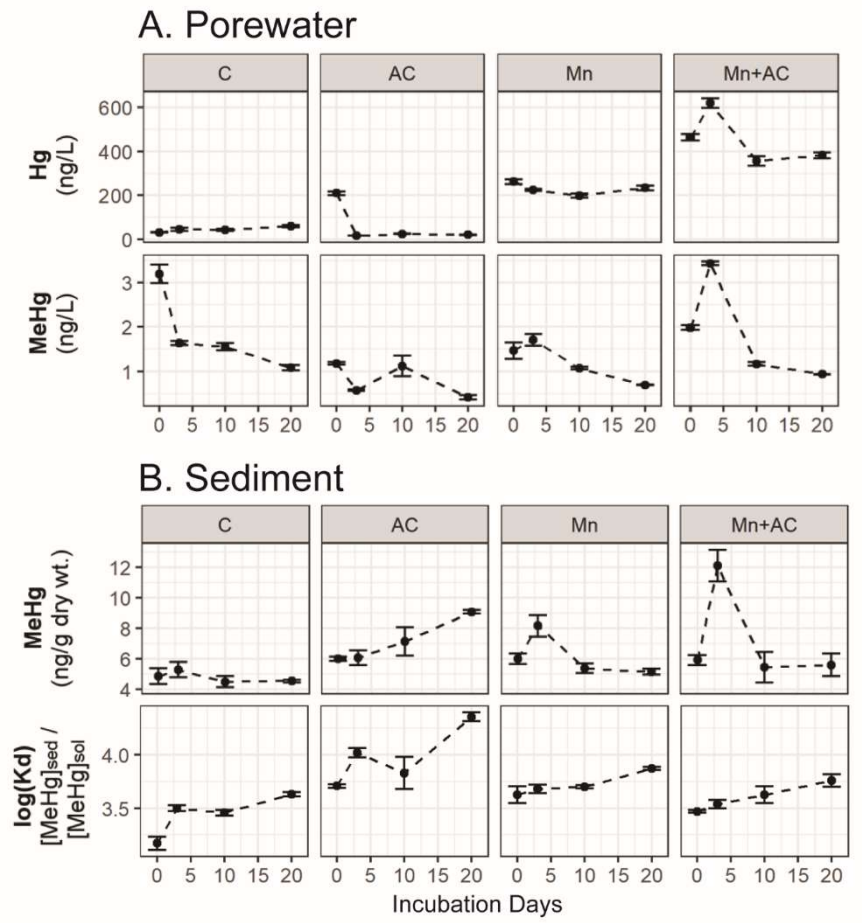

Figure 2-1: Total mercury (Hg) and methylmercury (MeHg) in filtered porewater (A) and sediment (B) of Experiment 1 (E1). Log(Kd) describes the partitioning of MeHg between the aqueous and solid phases. Error bars show standard error (sd/√n; n=3).

with the amendments during preparation of the incubations. Total Hg in porewater varied substantially between treatment groups. In the AC group, porewater total Hg decreased from about 210 ng/L at time zero to <30 ng/L after day 3 (Fig. 2-1A). Sediments amended with MnOx experienced substantial release of inorganic Hg into solution, with measured porewater concentrations up to 262 ng/L in the Mn group and 620 ng/L in the Mn+AC group compared with 60 ng/L in the control. Sediment amendment with MnOx or AC decreased porewater MeHg concentrations relative to the unamended control after 20 days of incubation, particularly in the AC treatment (Fig. 2-1A). Relatively large (1-2 ng/L) decreases in porewater MeHg occurred in the amended groups relative to the control during preparation of the incubations. MeHg concentrations in solids were generally higher in sediments amended with MnOx, and especially so for AC, compared to the C group (Fig. 2-1B). Sediment MeHg increased steadily throughout the experiment in the AC treatment, reaching 9 ng/g by day 20. Slurries amended with MnOx (Mn, Mn+AC) peaked in sediment and porewater MeHg concentrations at day 3, then declined through the remainder of the incubation period, but remained slightly higher than the C group.

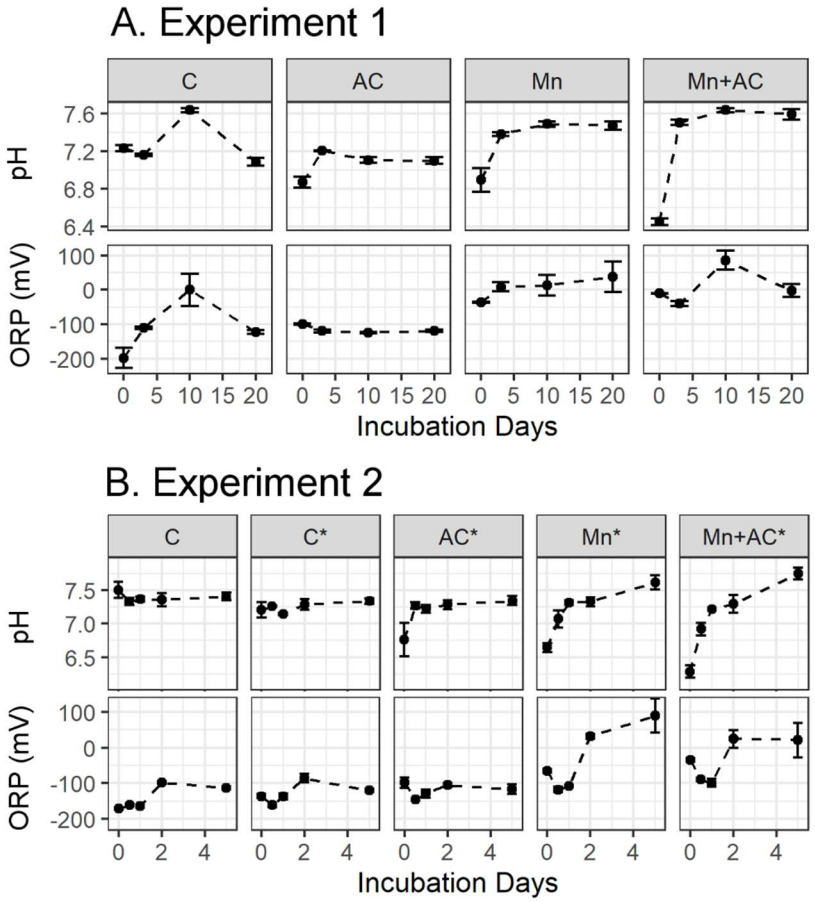

Figure 2-2: Figure 2. Oxidation-Reduction Potential (ORP) and pH in filtered porewater of Experiment 1 (A) and Experiment 2 (B).

Percent MeHg relative to total Hg ([MeHg]/[Hg]*100, %MeHg) was considerably lower in porewater of treatments containing MnOx than in the C or AC groups (Fig. B5). Percent MeHg in the whole slurry (calculation explained in Text B7) increased throughout the experiment in the AC group, but remained relatively constant in the C, Mn, and Mn+AC groups aside from a peak at day 3 in groups containing MnOx. Whole slurry %MeHg was generally higher in groups containing MnOx than in the C group. Dissolved organic carbon (DOC) in porewater was much lower in all treatment groups (<3.5 mg/L) than in the control (>9 mg/L) (Fig. B6). Oxidation-reduction potential was around -100 mV in the C and AC groups but increased above 0 mV in the Mn and Mn+AC treatments (Fig. 2-2). Porewater pH in the Mn and Mn+AC groups reached a steady state of around 7.5 after dropping below 7 initially (Fig. 2-2).

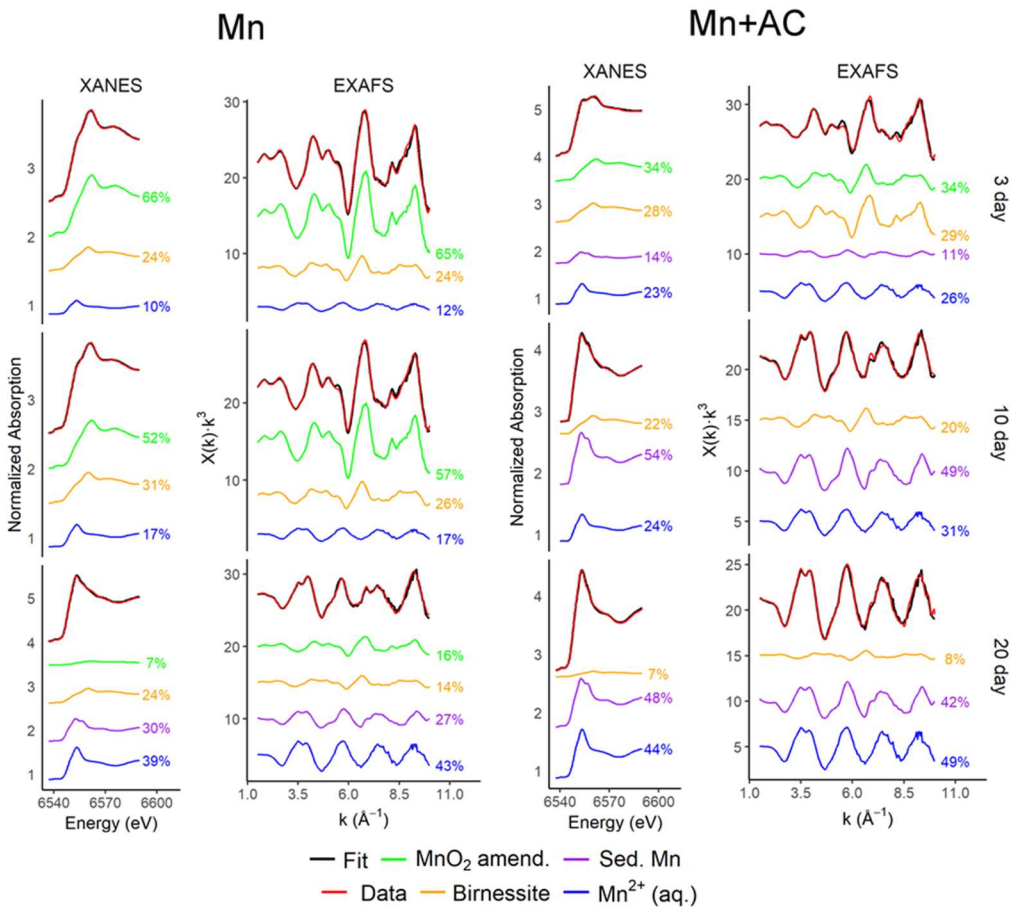

Figure 2-3: Linear combination fits of XANES (left) and EXAFS (right) spectra measured on sediments from the Mn and Mn+AC treatments of Experiment 1 after 3, 10, and 20 days of incubation. Percentages show normalized fit percentages for each compound, rounded to the nearest integer. Reference compounds used for fits are given in Fig. B1 and numerical data for fit results are reported in Table B6.

2.4.3.2 Transformation of MnOx Amendment

The MnOx amendment was progressively reduced to Mn(II) over the course of E1. Linear combination fitting of Mn reference compounds to X-Ray Absorption Near Edge Structure (XANES) and Extended X-ray Absorption Fine Structure (EXAFS) spectra measured on dry sediments from the Mn and Mn+AC groups showed decreases in the Mn(IV) amendment signal between day 3 and day 20 coupled with increases in Mn(II) species (Fig. 2-3, Table B6). The amendment signal consisted of the measured spectra of the MnOx amendment and a synthetic sodium birnessite, which has a spectrum similar but not identical to dry MnOx (Carulite® MnO_2) and vernadite (Fig. B1). We believe that hydration and cation exchange of the interlayer regions of the MnOx amendment during incubation yielded an XAS spectrum that partially resembled birnessite, which has a layered structure similar to vernadite (Villalobos et al., 2003). The products of Mn(IV) reduction retained in the solid phase are represented in the XAS spectra as variable relative fractions of Mn^{2+}(aq.) and native sediment Mn (Fig. 2-3, Table B6). In sediments with MnOx treatment, the amendment fraction decreased from ~90% at day 3 to ~30% at day 20 of the total normalized Mn signal, while the reduced Mn(II) fraction increased proportionally (Fig. 2-3). This change in the solid phase

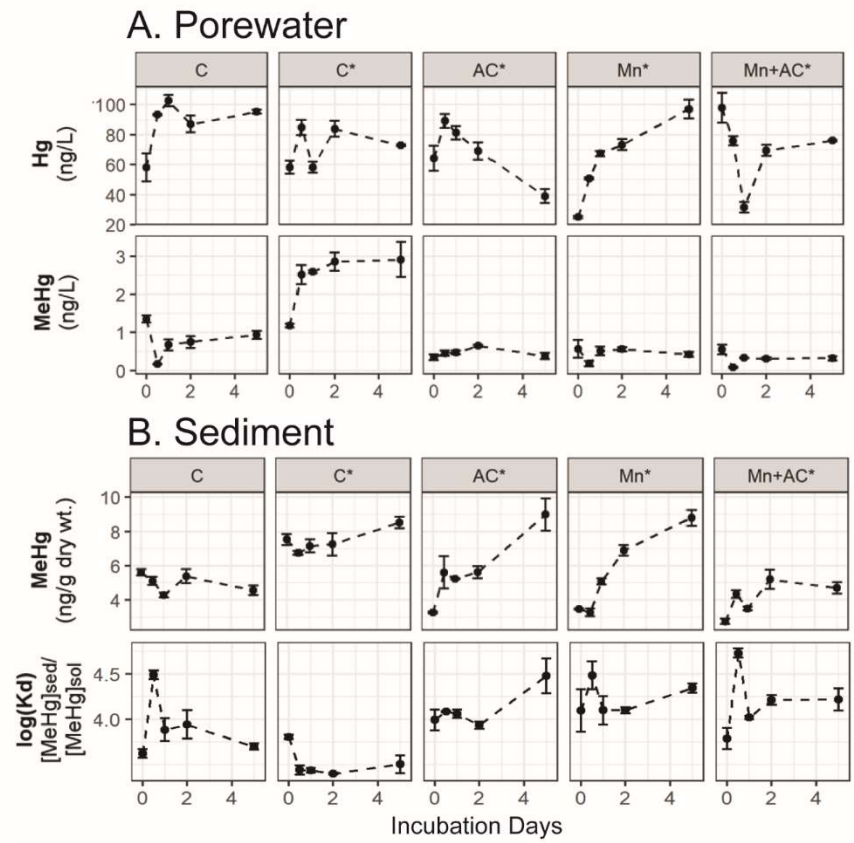

Figure 2-4: Total mercury and methylmercury in filtered porewater (A) and sediment (B) of Experiment 2 (E2); asterisk (*) indicates addition of sulfate and dissolved organic carbon (as acetic acid and Na-pyruvate). Log(Kd) describes the partitioning of methylmercury between the aqueous and solid phase. Error bars show standard error (sd/√n; n=3).

coincided with increasing concentration of dissolved Mn in porewater, up to 23 mg/L at day 20 (Fig. B6). In sediments from the Mn+AC group, the MnOx amendment signal comprised a smaller proportion of the XANES and EXAFS spectra, likely because less MnOx was added initially. The amendment signal decreased from ~63% of the spectra at day 3 to ~8% at day 20 (Fig. 2-3). Meanwhile, porewater Mn reached 15 mg/L by the end of the experiment (Fig. B6).

Experiment 2

2.4.3.3 Mercury and Methylmercury in Sediment and Porewater

In a second set of shorter incubation experiments (0-5 days) with sulfate and DOC addition, we observed stimulation of MeHg production in incubated sediments. In the control (C) group with no addition, MeHg in sediment and porewater remained relatively constant after the first 24 hours (Fig. 2-4). However, in the C* group (containing a spike of organic acids and sulfate) MeHg increased throughout the incubation period, with concentrations in sediment and porewater about 2-3 times higher than the C group. Porewater MeHg increased notably in the first 24 hours before leveling off around 3 ng/L while sediment MeHg increased steadily throughout the experiment.

Both AC and MnOx amendments decreased MeHg in porewater relative to the C* incubations (Fig. 2-4). Porewater MeHg concentrations in all amended groups (AC*, Mn*, Mn+AC*) remained around 0.5 ng/L, while porewater MeHg in the C* group exceeded 2.5 ng/L after 12 hours. However, sediment MeHg was elevated in Mn* and AC* treatments relative to the C group. In the Mn* and AC* groups, sediment MeHg concentrations were initially low, but increased throughout the incubation until becoming similar to C* at day 5 (Fig. 2-4). Sediment MeHg in the Mn+AC* group was lower than in groups amended with MnOx or AC alone and similar to C incubations, remaining below 6 ng/g for the entirety of the experiment. Total Hg exhibited contrasting patterns in the different treatment groups. Total Hg in porewater of the AC* group declined from 90 ng/L at 12 hours to 39 ng/L by day 5. In the Mn* group, total Hg increased in porewater throughout the experiment, but concentrations remained less than half of what we observed on day 3 in the Mn group of E1. In the Mn+AC* group, total Hg in porewater decreased to ~30 ng/L after 1 day before rebounding to ~80 ng/L at day 5. Percent MeHg was considerably lower in porewater of amended treatment groups (Mn*, AC*, Mn+AC*) compared to C*, but whole slurry %MeHg was similar in the C*, Mn*, and AC* groups (Fig. B5). Whole slurry percent MeHg was similar in the C and Mn+AC* groups.

2.4.3.4 Porewater Chemistry

Porewater chemistry was similar in the C* and AC* groups, and likewise in the Mn* and Mn+AC* groups. The C* group had considerably higher porewater concentrations of Mn and Fe than the C group (Fig. 2-5). The addition of organic acids in E2 resulted in differences in aqueous complexation and sorption of cations between the two experiments. Other redox-sensitive compounds likewise varied among the treatments. In the C* and AC* groups, porewater sulfate decreased throughout the experiment (Fig. 2-5). However, in groups containing MnOx, sulfate concentrations were equal to or higher than the added sulfate concentration at the end of the experiment. Iron

was removed from solution in groups containing MnOx, with no detectable Fe in porewater after 12 hours (Fig. 2-5). Oxidation-Reduction Potential was higher in the Mn* and Mn+AC* groups than in the other treatments after 1 day, indicating conditions more favorable to oxidation (Fig. 2-2). Porewater pH in the AC* group was initially low (~6.75) but increased to resemble the C* group after 12 hours of incubation (Fig. 2-2). In groups containing MnOx, pH increased from <6.75 at day 0 to near-steady state conditions of around 7.5 by day 5 (Fig. 2-2). Dissolved organic carbon remained constant in the C group, at around 15 mg/L (Fig. 2-5). In the C* and AC* groups, DOC declined throughout the experiment until it reached a similar concentration as the C group. In the Mn* and Mn+AC* treatments, DOC increased after 12 hours of incubation before nearly depleting at day 5.

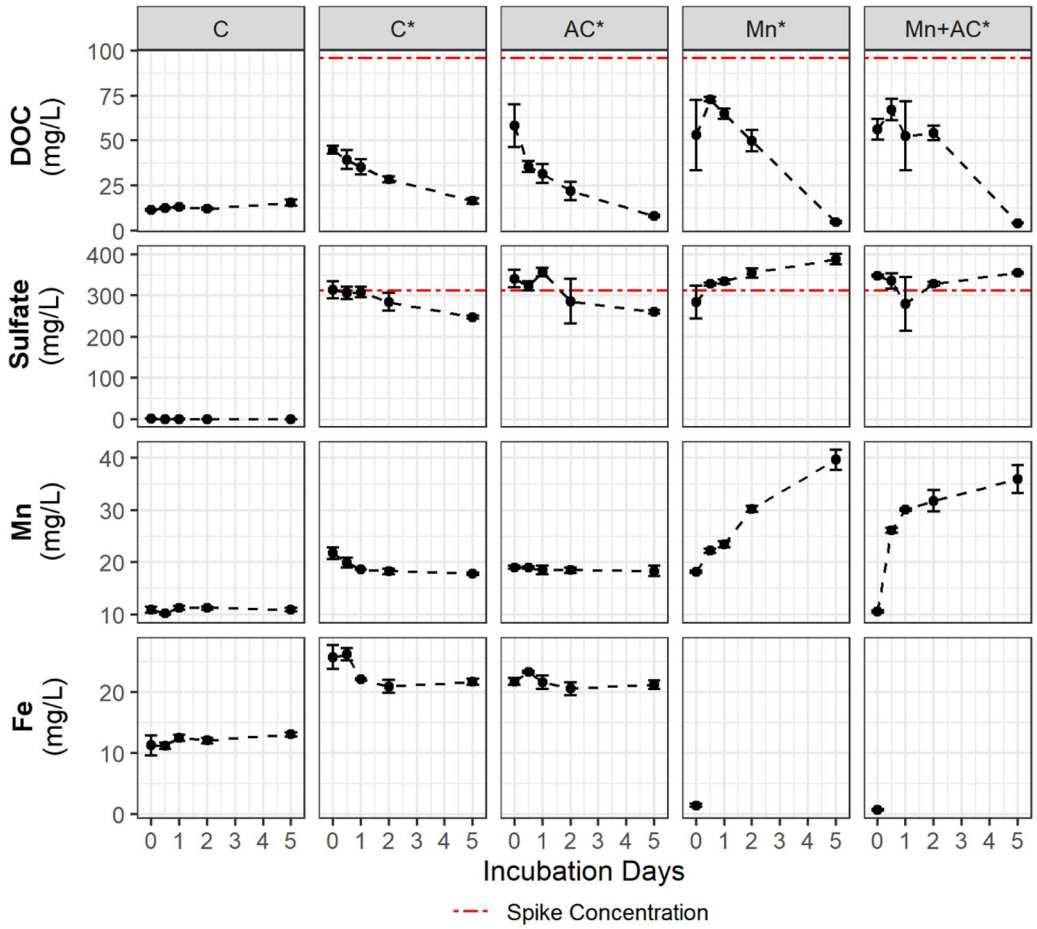

Figure 2-5: Dissolved organic carbon (DOC) and redox-sensitive analytes in filtered porewater of Experiment 2. The red line reflects the added DOC (acetate and pyruvate) and sulfate concentration in spiked treatments. Non-detect values are not shown.

2.4.3.5 Transformation of MnOx Amendment

Similar to E1, the loss of the MnOx amendment observed in Mn XAS analysis of E2 sediment spectra coincided with the appearance of Mn(II) reduction products. The amendment signal (MnOx amendment + sodium birnessite) decreased from ~90% of the

fitted spectral components at day 0 to ~40% in the Mn* group and ~60% in the Mn+AC* group at day 5 (Fig. B7, Table B7). Meanwhile, the spectral relative fraction of reduced Mn species (native sediment Mn + Mn^{2+}) increased from ~11% at day 0 to ~60% in the Mn* group and ~40% in the Mn+AC* group at day 5. We did not observe the formation of Mn(II) mineral phases in E1 or E2. Loss of the MnOx amendment signal coincided with accumulation of dissolved Mn in porewater. Porewater Mn increased throughout the experiment, reaching about 40 mg/L in the Mn* group and 35 mg/L in the Mn+AC* group at day 5, notably higher concentrations than were observed in E1 (Fig. 2-5 and Fig. B6).

2.5 Discussion

2.5.1 Effects of MnOx Amendments on MeHg and Hg Concentrations

In E1 and E2, reservoir sediments were amended with MnOx and/or AC, which influenced the sediment-porewater biogeochemistry. Both experiments showed changes in porewater chemistry that were most notable during the first 2-3 days of incubation. In groups containing MnOx, porewater had higher measured ORP and pH compared to control experiments. In groups amended with AC, ORP and pH returned to resemble control groups after day 0. The most notable changes in Hg, MeHg, and redox-sensitive species occurred during the initial perturbation.

Methylmercury concentrations in the solid phase of sediments amended with MnOx were generally similar to or greater than concentrations in the control groups. Sorption of MeHg from the aqueous phase would have a negligible effect on MeHg concentrations in solids, which are three orders of magnitude higher than MeHg concentrations in porewater. In E2, increases in sediment MeHg in MnOx-amended sediments could be attributed to Hg methylation during the first ~24 hours when ORP measurements indicated negative potentials, similar to AC treatments and controls. In E1, elevated porewater and solid phase MeHg in MnOx-amended sediments at day 3 could be the result of short-term MeHg production fueled by increased porewater Hg, sulfate, or labile DOC released through oxidation reduced compounds by MnOx. In the Mn* and Mn+AC* groups of E2, a shift to positive ORP at day 2, increasing sulfate concentrations, and the absence of Fe(II) in porewater suggest that sulfate and iron reduction were not favorable processes for the remaining time steps. Because iron and sulfate reduction are the two microbial processes most associated with net Hg methylation in aquatic systems, the inhibition of these processes should likewise disfavor MeHg formation (Gilmour et al., 2013a; Parks et al, 2013; Fuhrmann et al., 2021). Similarly in E1, high concentrations of porewater Hg and a shift to positive ORP in porewaters following day 3 indicate the establishment of oxidizing conditions.

Sediment amendment with MnOx or AC (or both) generally decreased MeHg concentrations and %MeHg in porewater, particularly in the Mn+AC* group of E2. This result agrees with previous studies that documented similar results highlighting the importance of both sorption and redox control in lowering dissolved MeHg concentrations (Gilmour et al., 2013b; Vlassopoulos et al, 2018). Porewater MeHg concentrations were similar (within 1 ng/L) regardless of the amendment used (MnOx,

AC, or both). Methylmercury partitioning from sediment to porewater can increase diffusion into overlying water, thereby enhancing accumulation in benthic biota (Wang et al., 1998; Williams et al., 2010). Thus, the decreases in porewater MeHg observed in the amendment experiments with MnOx or AC could lower the potential for MeHg bioaccumulation in aquatic systems.

2.5.2 Sediment Oxidation and Hg(II) Release by MnOx Amendment

Manganese (IV) oxides are strong oxidants with the potential to react with a wide variety of organic and inorganic compounds (Remucal and Vogel, 2014). We observed several lines of evidence suggesting oxidation of sediment and porewater species by the MnOx amendment. Iron was removed from solution in the Mn* and Mn+AC* treatments of E2, accompanied by a drop in pH at day 0 relative to the control groups (Fig. 2-2, Fig. 2-5). Iron (II) present in porewater was probably oxidized to Fe(III) by the MnOx amendment, subsequently precipitating with OH^- as ferric oxyhydroxides and initially lowering porewater pH (Schaefer et al., 2017).

Porewater sulfate increased above the added sulfate concentration in the Mn* group of E2, suggesting that sulfide (aqueous or solid phase) was oxidized by MnOx (dissolved sulfide was not measured) (Schippers and Jorgenson, 2001). We observed notable losses of DOC from porewater of sediments amended with MnOx and AC. Loss of DOC from porewater could be attributable to abiotic and/or microbial oxidation with MnOx addition, or sorption to either MnOx or AC. Dissolved organic carbon is a key constraint on Hg cycling in sediments, as it influences both microbial activity and Hg bioavailability (Ravichandran, 2004; Hsu Kim et al., 2013). Manganese oxides have been found to increase the lability of natural organic matter by oxidizing it to lower-molecular weight substrates that can be used during microbial metabolism (Sunda and Kieber, 1994; Stuckey et al., 2018). In sulfide-free environments, complexation with DOC can decrease the bioavailability of Hg(II) to methylating bacteria under equilibrium conditions (Miskimmin et al., 1992; Barkay et al., 1997; Chiasson-Gould et al., 2014). Thus, the abiotic oxidation of DOC in porewater is of particular concern because it has the potential to increase MeHg production by increasing the bioavailability of both DOC and Hg. We conducted an experiment to investigate abiotic reductive dissolution of MnOx by DOC (Text B8). Our results indicated that, while minor oxidation of DOC occurred, the primary loss mechanism of DOC was sorption to the mineral surface. Thus, decreasing DOC concentrations throughout the experiment most likely represent a mixture of microbial oxidation and sorption.

Of concern, MnOx released inorganic Hg into porewater, with 200-620 ng/L of total Hg measured in the Mn and Mn+AC groups of E1 (Fig. 2-1). However, increased concentration of dissolved Hg in either MnOx or AC amended experiments relative to controls was not observed in E2 (Fig. 2-4), which points out the variability in reactive Hg in natural sediments. $Mn(IV)O_2$ likely oxidized sulfide minerals, elemental mercury, and/or natural organic matter containing Hg, releasing Hg(II) into solution and increasing its mobility (Schippers and Jorgenson, 2001; Stuckey et al., 2018; Duvil et al., 2018; Miller et al., 2015). Increased Hg(II) and sulfate in solution could potentially stimulate MeHg production if reducing conditions are reestablished. However, oxidizing conditions with low DOC are not conducive to Hg methylation. This was evident in our experiments

by relatively little change in sediment and porewater MeHg following the establishment of oxidizing conditions despite high concentrations of inorganic Hg in porewater.

2.5.3 Fate of MnOx Amendment

Results of XAS linear combination fits of reference spectra to MnOx-amended sediment spectra suggest that the MnOx amendment reductively dissolved throughout the experiment. The major reduction product was Mn^{2+} as an aqueous or sorbed species and not as a solid phase, and Mn^{2+} concentrations in porewater increased over the course of the experiments. Most of the Mn^{2+} released by reduction of the amendment appeared to subsequently sorb to solid surfaces, which is expected for the porewater pH (Lefkowitz and Elzinga, 2015). Nonetheless, porewater Mn concentrations doubled in the Mn* and Mn+AC* groups relative to C*. Leven et al. (2018) observed the formation rhodochrosite ($MnCO_3$) in MnOx-amended sediments after 10 months of incubation. Equilibrium calculations using PhreeqC indicated that $MnCO_3$ is thermodynamically oversaturated in the Mn* group throughout E2, but we did not detect $MnCO_3$ in the XAS spectra (Text B9). This is likely due to the slow precipitation kinetics of rhodochrosite and low practical detection limit of XAS using the LCF approach (usually ~5% of the total Mn signal) (Leven et al., 2018; Jensen et al., 2002). It is probable that, in a longer-term incubation, Mn(II) reduction products would be stabilized as $MnCO_3$ in these sediments. However, in a natural system, Mn^{2+} may be lost to overlying waters by diffusion.

The MnOx amendments dissolved rapidly during our short-term incubation experiments. In environmental applications, it is important that Mn(IV) reduction occurs slowly to maintain relatively oxidized sediment-porewater conditions and avoid frequent amendment reapplication. In E1, only ~7-30% of the amendment signal remained after 20 days of reaction, and in E2 just 40-60% of the amendment signal remained after 5 days (Fig. 2-3, Fig. B7). In 15-month mesocosm experiments using pyrolusite, Leven et al. (2018) observed an amendment loss of only 27% after four months of incubation. However, our MnOx amendments were rapidly reduced to Mn(II). This is probably due to their high surface area and disordered structure that promotes rapid dissolution compared to a crystalline material, and because the slurry experiments of this study had much greater solid-water contact compared to the mesocosm experiments that employed a static sediment-water interface (see Vlassopoulos et al., 2018 for experimental details). To avoid rapid depletion of added MnOx, proper dosing should be calculated so that the amendment's oxidative capacity exceeds the reducing ability of the sediments. Prior to application, sediments should be characterized for major oxidizable species such as reactive sulfide, ferrous iron, and labile organic carbon.

2.6 Engineering Implications

Managing MeHg in water bodies is challenging because trace (ng/L) concentrations in water can result in high (mg/kg) concentrations in fish. Current remediation approaches such as sediment removal, capping, and reservoir oxygenation can be prohibitively expensive or impractical in many systems. Sediment amendment with MnOx is a potentially promising strategy for Hg remediation in aquatic systems that should theoretically decrease MeHg production and release to porewater through redox buffering and sorption.

Addition of MnOx to reduced lacustrine sediments raised ORP and lowered MeHg in porewater relative to the control groups. Lowering porewater MeHg concentrations could decrease the diffusion of MeHg into overlying water, which may result in lower bioaccumulation of MeHg in aquatic ecosystems. Decreases in porewater MeHg were similar in magnitude to the AC groups and other studies that used sorbent amendments (Gilmour et al., 2013b; Gilmour et al., 2018). Despite decreases in porewater, MeHg concentrations in the solid phase of sediments amended with MnOx were generally similar to or greater than MeHg concentrations in the control groups. Methylmercury production may have occurred during the initial period of incubation before sediments evolved to higher ORP. We observed some concerning effects of MnOx addition that should be noted. The MnOx amendment oxidized sulfide and Fe(II) to forms that could later be used for metabolism by Hg-methylating bacteria if redox potential dropped to levels that favor Hg methylation. MnOx amendments caused notable release of inorganic Hg into porewater in E1, likely through oxidative dissolution of Hg(II) complexes, Hg-containing sulfides, and/or elemental Hg. Finally, the high surface contact of MnOx with reduced sediments in the slurry incubations caused reductive dissolution of the amendment that occurred too quickly for practical application in environmental settings.

Prior to application in a field setting, further development is needed to slow the reduction of the MnOx amendment and stabilize Mn^{2+} in sediments. If reduction cannot be slowed, frequent reapplication may be needed to maintain the oxidizing conditions represented in our experiments. Crystalline MnOx with a lower specific surface area (e.g. pyrolusite) or AC coated with Mn(IV) may support slower rates of reduction to Mn(II). Coamendment of MnOx with AC or other sorbents could also help sorb Mn^{2+} released through reduction of MnOx. Adding MnOx to reduced aquatic sediments quickly consumed the oxidative capacity of the amendment, limiting its longevity and possibly delaying the establishment of oxidizing steady state conditions. Thus, sediment amendment with MnOx may not be appropriate for highly reduced systems. Instead of mixing the MnOx into surface sediments, a better application in lacustrine environments that experience seasonal hypoxia could be a reactive cap that overlays the sediment, buffering the redox state at the sediment-water interface while minimizing the surface contact between the amendment and reduced sediments. Vlassopoulos et al. (2018) showed that reactive caps consisting of MnOx and quartz sand were more effective at decreasing MeHg in overlying water than MnOx mixed into surface sediments. Because dissolved Mn can cause aesthetic problems that complicate drinking water treatment, MnOx addition is not recommended in drinking water reservoirs (Tobiason et al., 2013). Lentic ecosystems are generally better suited for solid phase amendments than fluvial systems, as amendments could be transported downstream with high flows. In riverine systems that experience oxic-suboxic cycling in surface sediments, solid phase amendments could be incorporated into erosion control features or geotextiles that may prevent amendment mobilization. MnOx amendment to oxic or moderately reduced sediments, or during more oxic cycles, may yield more effective redox buffering than amendment to consistently reduced systems, which could lead to greater inhibition of Hg methylation. One obvious drawback of sediment amendment with MnOx is the potential for oxidative dissolution of Hg(II) compounds like HgS. Coamendment of MnOx with a sorbent (e.g., AC) may help mitigate potential release of Hg(II) into overlying water.

2.7 References

Barkay, T., Gillman, M., & Turner, R. R. (1997). Effects of dissolved organic carbon and salinity on bioavailability of mercury. *APPLIED AND ENVIRONMENTAL MICROBIOLOGY*, *63*(11), 4267–4271. https://doi.org/10.1128/AEM.63.11.4267-4271.1997

Beutel, M., Dent, S., Reed, B., Marshall, P., Gebremariam, S., Moore, B., Cross, B., Gantzer, P., & Shallenberger, E. (2014). Effects of hypolimnetic oxygen addition on mercury bioaccumulation in Twin Lakes, Washington, USA. *SCIENCE OF THE TOTAL ENVIRONMENT*, *496*(11th International Conference on Mercury as a Global Pollutant), 688–700. https://doi.org/10.1016/j.scitotenv.2014.06.117

Beutel, M., Fuhrmann, B., Herbon, G., Chow, A., Brower, S., & Pasek, J. (2020). Cycling of methylmercury and other redox-sensitive compounds in the profundal zone of a hypereutrophic water supply reservoir. *HYDROBIOLOGIA*, *847*(21), 4425–4446. https://doi.org/10.1007/s10750-020-04192-3

Bussan, D. D., Sessums, R. F., & Cizdziel, J. V. (2016). Activated Carbon and Biochar Reduce Mercury Methylation Potentials in Aquatic Sediments. *BULLETIN OF ENVIRONMENTAL CONTAMINATION AND TOXICOLOGY*, *96*(4), 536–539. https://doi.org/10.1007/s00128-016-1734-6

Chattopadhyay, S., Fimmen, R. L., Yates, B. J., Lal, V., & Randall, P. (2012). PHYTOREMEDIATION OF MERCURY- AND METHYL MERCURY-CONTAMINATED SEDIMENTS BY WATER HYACINTH (EICHHORNIA CRASSIPES). *INTERNATIONAL JOURNAL OF PHYTOREMEDIATION*, *14*(2), 142–161. https://doi.org/10.1080/15226514.2010.525557

Chiasson-Gould, S. A., Blais, J. M., & Poulain, A. J. (2014). Dissolved Organic Matter Kinetically Controls Mercury Bioavailability to Bacteria. *Environmental Science & Technology*, *48*(6), 3153–3161. https://doi.org/10.1021/es4038484

COMPEAU, G. C., & BARTHA, R. (1985). SULFATE-REDUCING BACTERIA - PRINCIPAL METHYLATORS OF MERCURY IN ANOXIC ESTUARINE SEDIMENT. *APPLIED AND ENVIRONMENTAL MICROBIOLOGY*, *50*(2), 498–502. https://doi.org/10.1128/AEM.50.2.498-502.1985

Desauziers, V., Castre, N., & LeCloirec, P. (1997). Sorption of methylmercury by clays and mineral oxides. *ENVIRONMENTAL TECHNOLOGY*, *18*(10), 1009–1018. https://doi.org/10.1080/09593331808616620

Driscoll, C. T., Mason, R. P., Chan, H. M., Jacob, D. J., & Pirrone, N. (2013). Mercury as a Global Pollutant: Sources, Pathways, and Effects. *Environmental Science & Technology*, *47*(10), 4967–4983. https://doi.org/10.1021/es305071v

Duvil, R., Beutel, M. W., Fuhrmann, B., & Seelos, M. (2018). Effect of oxygen, nitrate and aluminum addition on methylmercury efflux from mine-impacted reservoir sediment. *Water Research*, *144*, 740–751. https://doi.org/10.1016/j.watres.2018.07.071

Eckley, C. S., Gilmour, C. C., Janssen, S., Luxton, T. P., Randall, P. M., Whalin, L., & Austin, C. (2020). The assessment and remediation of mercury contaminated sites: A review of current approaches. *SCIENCE OF THE TOTAL ENVIRONMENT*, *707*. https://doi.org/10.1016/j.scitotenv.2019.136031

Farrell, R. E., Huang, P. M., & Germida, J. J. (1998). Biomethylation of mercury(II) adsorbed on mineral colloids common in freshwater sediments. *APPLIED ORGANOMETALLIC CHEMISTRY*, *12*(8–9), 613–620. https://doi.org/10.1002/(SICI)1099-0739(199808/09)12:8/9<613::AID-AOC769>3.0.CO;2-7

Fuhrmann, B. C., Beutel, M. W., O'Day, P. A., Tran, C., Funk, A., Brower, S., Pasek, J., & Seelos, M. (2021). Effects of mercury, organic carbon, and microbial inhibition on methylmercury cycling at the profundal sediment-water interface of a sulfate-rich hypereutrophic reservoir. *Environmental Pollution*, *268*. https://doi.org/10.1016/j.envpol.2020.115853

Ghosh, U., Luthy, R. G., Cornelissen, G., Werner, D., & Menzie, C. A. (2011). In-situ Sorbent Amendments: A New Direction in Contaminated Sediment Management. *ENVIRONMENTAL SCIENCE & TECHNOLOGY*, *45*(4), 1163–1168. https://doi.org/10.1021/es102694h

Gilmour, C. C., Podar, M., Bullock, A. L., Graham, A. M., Brown, S. D., Somenahally, A. C., Johs, A., Hurt, R. A., Bailey, K. L., & Elias, D. A. (2013a). Mercury Methylation by Novel Microorganisms from New Environments. *ENVIRONMENTAL SCIENCE & TECHNOLOGY*, *47*(20), 11810–11820. https://doi.org/10.1021/es403075t

Gilmour, C. C., Riedel, G. S., Riedel, G., Kwon, S., Landis, R., Brown, S. S., Menzie, C. A., & Ghosh, U. (2013b). Activated Carbon Mitigates Mercury and Methylmercury Bioavailability in Contaminated Sediments. *ENVIRONMENTAL SCIENCE & TECHNOLOGY*, *47*(22), 13001–13010. https://doi.org/10.1021/es4021074

Gilmour, C., Bell, T., Soren, A., Riedel, G., Riedel, G., Kopec, D., Bodaly, D., & Ghosh, U. (2018). Activated carbon thin-layer placement as an in situ mercury remediation

tool in a Penobscot River salt marsh. *SCIENCE OF THE TOTAL ENVIRONMENT*, *621*, 839–848. https://doi.org/10.1016/j.scitotenv.2017.11.050

Gonez-Rodriguez, L., Johs, A., Lowe, K. A., Carter, K. E., Loffler, F. E., & Mayes, M. A. (2021). Evaluation of engineered sorbents for the sorption of mercury from contaminated bank soils: a column study. *ENVIRONMENTAL SCIENCE AND POLLUTION RESEARCH*, *28*(18), 22651–22663. https://doi.org/10.1007/s11356-020-12073-4

Helmhart, M., O'Day, P. A., Garcia-Guinea, J., Serrano, S., & Garrido, F. (2012). Arsenic, Copper, and Zinc Leaching through Preferential Flow in Mining-Impacted Soils. *SOIL SCIENCE SOCIETY OF AMERICA JOURNAL*, *76*(2), 449–462. https://doi.org/10.2136/sssaj2011.0269

Hsu-Kim, H., Kucharzyk, K. H., Zhang, T., & Deshusses, M. A. (2013). Mechanisms regulating mercury bioavailability for methylating microorganisms in the aquatic environment: A critical review. *Environmental Science and Technology*, *47*(6), 2441–2456. https://doi.org/10.1021/es304370g

Husnain, S. M., Asim, U., Yaqub, A., Shahzad, F., & Abbas, N. (2020). Recent trends of MnO2-derived adsorbents for water treatment: a review. *NEW JOURNAL OF CHEMISTRY*, *44*(16), 6096–6120. https://doi.org/10.1039/c9nj06392g

Islam, M. A., Morton, D. W., Johnson, B. B., Mainali, B., & Angove, M. J. (2018). Manganese oxides and their application to metal ion and contaminant removal from wastewater. *JOURNAL OF WATER PROCESS ENGINEERING*, *26*, 264–280. https://doi.org/10.1016/j.jwpe.2018.10.018

Jackson, T.A. (1989). The Influence of Clay Minerals, Oxides, and Humic Matter on the Methylation and Demethylation of Mercury by Micro-organisms in Freshwater Sediments. *Applied Organometallic Chemistry*, 3(1), 1–30, doi:10.1002/aoc.590030103.

Jensen, D. L., Boddum, J. K., Tjell, J. C., & Christensen, T. H. (2002). The solubility of rhodochrosite (MnCO3) and siderite (FeCO3) in anaerobic aquatic environments. *APPLIED GEOCHEMISTRY*, *17*(4), 503–511. https://doi.org/10.1016/S0883-2927(01)00118-4

Kwon, S., Thomas, J., Reed, B. E., Levine, L., Magar, V. S., Farrar, D., Bridges, T. S., & Ghosh, U. (2010). EVALUATION OF SORBENT AMENDMENTS FOR IN SITU REMEDIATION OF METAL-CONTAMINATED SEDIMENTS. *ENVIRONMENTAL TOXICOLOGY AND CHEMISTRY*, *29*(9), 1883–1892. https://doi.org/10.1002/etc.249

Lefkowitz, J. P., & Elzinga, E. J. (2015). Impacts of Aqueous Mn(II) on the Sorption of Zn(II) by Hexagonal Birnessite. *ENVIRONMENTAL SCIENCE & TECHNOLOGY*, *49*(8), 4886–4893. https://doi.org/10.1021/es506019j

Lehnherr, I. (2014). Methylmercury biogeochemistry: a review with special reference to Arctic aquatic ecosystems. *Environmental Reviews*, *22*(3), 229–243. https://doi.org/10.1139/er-2013-0059

Leven, A., Vlassopoulos, D., Kanematsu, M., Goin, J., & O'Day, P. A. (2018). Characterization of manganese oxide amendments for in situ remediation of mercury-contaminated sediments. *ENVIRONMENTAL SCIENCE-PROCESSES & IMPACTS*, *20*(12), 1761–1773. https://doi.org/10.1039/c7em00576h

LIANG, L., BLOOM, N. S., & HORVAT, M. (1994). SIMULTANEOUS DETERMINATION OF MERCURY SPECIATION IN BIOLOGICAL-MATERIALS BY GC/CVAFS AFTER ETHYLATION AND ROOM-TEMPERATURE PRECOLLECTION. *CLINICAL CHEMISTRY*, *40*(4), 602–607.

Matthews, D. A., Babcock, D. B., Nolan, J. G., Prestigiacomo, A. R., Effler, S. W., Driscoll, C. T., Todorova, S. G., & Kuhr, K. M. (2013). Whole-lake nitrate addition for control of methylmercury in mercury-contaminated Onondaga Lake, NY. *ENVIRONMENTAL RESEARCH*, *125*(10th International Conference on Mercury as a Global Pollutant), 52–60. https://doi.org/10.1016/j.envres.2013.03.011

Miller, C. L., Watson, D. B., Lester, B. P., Howe, J. Y., Phillips, D. H., He, F., Liang, L. Y., & Pierce, E. M. (2015). Formation of Soluble Mercury Oxide Coatings: Transformation of Elemental Mercury in Soils. *ENVIRONMENTAL SCIENCE & TECHNOLOGY*, *49*(20), 12105–12111. https://doi.org/10.1021/acs.est.5b00263

MISKIMMIN, B. M., RUDD, J. W. M., & KELLY, C. A. (1992). INFLUENCE OF DISSOLVED ORGANIC-CARBON, PH, AND MICROBIAL RESPIRATION RATES ON MERCURY METHYLATION AND DEMETHYLATION IN LAKE WATER. *CANADIAN JOURNAL OF FISHERIES AND AQUATIC SCIENCES*, *49*(1), 17–22. https://doi.org/10.1139/f92-002

Parks, J. M., Johs, A., Podar, M., Bridou, R., Hurt, R. A., Smith, S. D., Tomanicek, S. J., Qian, Y., Brown, S. D., Brandt, C. C., Palumbo, A. V, Smith, J. C., Wall, J. D., Elias, D. A., & Liang, L. Y. (2013). The Genetic Basis for Bacterial Mercury Methylation. *SCIENCE*, *339*(6125), 1332–1335. https://doi.org/10.1126/science.1230667

Patmont, C. R., Ghosh, U., LaRosa, P., Menzie, C. A., Luthy, R. G., Greenberg, M. S., Cornelissen, G., Eek, E., Collins, J., Hull, J., Hjartland, T., Glaza, E., Bleiler, J., & Quadrini, J. (2015). In Situ Sediment Treatment Using Activated Carbon: A Demonstrated Sediment Cleanup Technology. *INTEGRATED ENVIRONMENTAL*

ASSESSMENT AND MANAGEMENT, *11*(2), 195–207. https://doi.org/10.1002/ieam.1589

Pickhardt, P. C., & Fisher, N. S. (2007). Accumulation of inorganic and methylmercury by freshwater phytoplankton in two contrasting water bodies. *ENVIRONMENTAL SCIENCE & TECHNOLOGY*, *41*(1), 125–131. https://doi.org/10.1021/es060966w

Randall, P. M., & Chattopadhyay, S. (2013). Mercury contaminated sediment sites-An evaluation of remedial options. *ENVIRONMENTAL RESEARCH*, *125*(10th International Conference on Mercury as a Global Pollutant), 131–149. https://doi.org/10.1016/j.envres.2013.01.007

Ravel, B., & Newville, M. (2005). ATHENA, ARTEMIS, HEPHAESTUS: data analysis for X-ray absorption spectroscopy using IFEFFIT. *JOURNAL OF SYNCHROTRON RADIATION*, *12*, 537–541. https://doi.org/10.1107/S0909049505012719

Ravichandran, M. (2004). Interactions between mercury and dissolved organic matter - A review. *Chemosphere*, *55*(3), 319–331. https://doi.org/10.1016/j.chemosphere.2003.11.011

Remucal, C. K., & Ginder-Vogel, M. (2014). A critical review of the reactivity of manganese oxides with organic contaminants. *ENVIRONMENTAL SCIENCE-PROCESSES & IMPACTS*, *16*(6), 1247–1266. https://doi.org/10.1039/c3em00703k

Sanders, J. P., Andrade, N. A., Menzie, C. A., Amos, C. B., Gilmour, C. C., Henry, E. A., Brown, S. S., & Ghosh, U. (2018). Persistent reductions in the bioavailability of PCBs at a tidally inundated Phragmites australis marsh amended with activated carbon. *ENVIRONMENTAL TOXICOLOGY AND CHEMISTRY*, *37*(9), 2496–2505. https://doi.org/10.1002/etc.4186

Schaefer, M. V, Handler, R. M., & Scherer, M. M. (2017). Fe(II) reduction of pyrolusite (beta-MnO2) and secondary mineral evolution. *GEOCHEMICAL TRANSACTIONS*, *18*. https://doi.org/10.1186/s12932-017-0045-0

Schippers, A., & Jorgensen, B. B. (2001). Oxidation of pyrite and iron sulfide by manganese dioxide in marine sediments. *GEOCHIMICA ET COSMOCHIMICA ACTA*, *65*(6), 915–922. https://doi.org/10.1016/S0016-7037(00)00589-5

Seelos, M., Beutel, M., Austin, C. M., Wilkinson, E., & Leal, C. (2021). Effects of hypolimnetic oxygenation on fish tissue mercury in reservoirs near the new Almaden Mining District, California, USA. *Environmental Pollution*, *268*. https://doi.org/10.1016/j.envpol.2020.115759

Stuckey, J. W., Goodwin, C., Wang, J., Kaplan, L. A., Vidal-Esquivel, P., Beebe, T. P., & Sparks, D. L. (2018). Impacts of hydrous manganese oxide on the retention and

lability of dissolved organic matter. *GEOCHEMICAL TRANSACTIONS*, *19*. https://doi.org/10.1186/s12932-018-0051-x

SUNDA, W. G., & KIEBER, D. J. (1994). OXIDATION OF HUMIC SUBSTANCES BY MANGANESE OXIDES YIELDS LOW-MOLECULAR-WEIGHT ORGANIC SUBSTRATES. *NATURE*, *367*(6458), 62–64. https://doi.org/10.1038/367062a0

THANABALASINGAM, P., & PICKERING, W. F. (1985). SORPTION OF MERCURY(II) BY MANGANESE(IV) OXIDE. *ENVIRONMENTAL POLLUTION SERIES B-CHEMICAL AND PHYSICAL*, *10*(2), 115–128. https://doi.org/10.1016/0143-148X(85)90009-6

Tobiason, J. E., Bazilio, A., Goodwill, J., Mai, X. Y., & Nguyen, C. (2016). Manganese Removal from Drinking Water Sources. *CURRENT POLLUTION REPORTS*, *2*(3), 168–177. https://doi.org/10.1007/s40726-016-0036-2

U.S. E.P.A. Method 1631, Revision E: Mercury in Water by Oxidation, Purge and Trap, and Cold Vapor Atomic Fluorescence Spectrometry, 2002.

U.S. E.P.A. Method 7473: Mercury in Solids and Solution by Thermal Decomposition, Amalgamation, and Atomic Absorption Spectrophotometry, 2007a.

U.S. E.P.A. Method 1630. Methyl mercury in water by distillation, aqueous ethylation, purge and trap, and CVAFS, 1998.

U.S. E.P.A. Method 300.0, Revision 2.1: Determination of Inorganic Anions by Ion Chromatography, 1993.

U.S. E.P.A. Method 200.7: Determination of Metals and Trace Elements in Water and Wastes by Inductively Coupled Plasma-Atomic Emission Spectrometry, 1994.

U.S. E.P.A. Method 3051A: Microwave-Assisted Acid Digestion of Sediments, Sludges, Soils, and Oils, 2007b.

U.S. E.P.A. Method 415.3, Rev. 1.2: Determination of Total Organic Carbon and Specific UV Absorbance at 254 nm in Source Water and Drinking Water, 2009.

Villalobos, M., Toner, B., Bargar, J., & Sposito, G. (2003). Characterization of the manganese oxide produced by Pseudomonas putida strain MnB1. *GEOCHIMICA ET COSMOCHIMICA ACTA*, *67*(14), 2649–2662. https://doi.org/10.1016/S0016-7037(03)00217-5

Vlassopoulos, D., Kanematsu, M., Henry, E. A., Goin, J., Leven, A., Glaser, D., Brown, S. S., & O'Day, P. A. (2018). Manganese(iv) oxide amendments reduce methylmercury concentrations in sediment porewater. *ENVIRONMENTAL*

SCIENCE-PROCESSES & IMPACTS, *20*(12), 1746–1760. https://doi.org/10.1039/c7em00583k

Wang, W. X., Stupakoff, I., Gagnon, C., & Fisher, N. S. (1998). Bioavailability of inorganic and methylmercury to a marine deposit feeding polychaete. *ENVIRONMENTAL SCIENCE & TECHNOLOGY*, *32*(17), 2564–2571. https://doi.org/10.1021/es971034i

Webb, S. M. (2005). SIXpack: a graphical user interface for XAS analysis using IFEFFIT. *PHYSICA SCRIPTA*, *T115*, 1011–1014.

Williams, J. J., Dutton, J., Chen, C. Y., & Fisher, N. S. (2010). METAL (As, Cd, Hg, and CH3Hg) BIOACCUMULATION FROM WATER AND FOOD BY THE BENTHIC AMPHIPOD LEPTOCHEIRUS PLUMULOSUS. *ENVIRONMENTAL TOXICOLOGY AND CHEMISTRY*, *29*(8), 1755–1761. https://doi.org/10.1002/etc.207

3 Plankton Population Dynamics and Methylmercury Bioaccumulation in the Pelagic Food Web of Mine-Impacted Surface Water Reservoirs

3.1 Abstract

Thermal stratification of reservoirs can lead to anaerobic conditions that facilitate the microbial conversion of mercury (Hg) to neurotoxic and bioaccumulative methylmercury (MeHg). But MeHg production is just the first step in a complex set of processes that affect MeHg in fish. Of particular relevance is uptake into suspended particulate matter (SPM) and zooplankton at the base of the pelagic food web. We assessed plankton dynamics and Hg uptake into the pelagic food web of four Hg-impaired California water reservoirs. Combining water chemistry, plankton taxonomy, and stable carbon (C) and nitrogen (N) isotope values of SPM and zooplankton samples, we investigated differences among the reservoirs that may contribute to differing patterns in MeHg bioaccumulation. Methylmercury accumulated in SPM during the spring and summer seasons. Percent MeHg (MeHg/Hg*100%) in SPM was negatively associated with δ15N values, suggesting that "fresh" algal biomass could support the production and bioaccumulation of MeHg. Zooplankton δ13C values were correlated with SPM δ13C values in the epilimnion, suggesting that zooplankton primarily feed in surface waters. However, zooplankton MeHg was poorly associated with MeHg in SPM. Our results demonstrate seasonal patterns in biological MeHg uptake and how multiple data sources can help constrain the drivers of MeHg bioaccumulation.

3.2 Introduction

Mercury (Hg) is a pollutant of concern in lakes and reservoirs, particularly in systems that experience oxic-anoxic cycling at the sediment-water interface or in the water column (Branfireun et al., 2020). Natural or anthropogenic Hg in the atmosphere can be deposited in catchments through wet or dry deposition (Driscoll et al., 2013). This atmospheric Hg, along with Hg present in soils from geologic and mining sources, can be transported into aquatic systems with runoff (Hsu-Kim et al., 2018). Under reducing conditions, anaerobic microorganisms convert inorganic Hg into neurotoxic methylmercury (MeHg), which bioaccumulates in aquatic ecosystems (Bigham et al., 2016). Methylmercury concentrates in suspended particulate matter (SPM), which serves as the main source of MeHg to the pelagic food web (Ogorek et al., 2021). Further accumulating in zooplankton and their predators through dietary intake, MeHg concentrations in fish can exceed aqueous concentrations by 7 orders of magnitude (Ogorek et al., 2021). Ingestion of fish contaminated with MeHg can cause a range of neurological, reproductive, and cardiovascular defects in humans (Young-Seoub et al., 2012). Bioaccumulation of MeHg can cause behavioral, neurochemical, hormonal, and reproductive changes in mammals, birds, and fish (Scheuhammer et al., 2007). Thus, the production and bioaccumulation of MeHg in lakes and reservoirs presents great risks to human and ecological health.

Despite the widely accepted conceptual model of MeHg diffusion into the water column followed by concentration in SPM and accumulation in the pelagic food web, the drivers that determine the degree of MeHg bioaccumulation are poorly understood. A survey of Hg concentrations in freshwater fish throughout the western United States and Canada showed that fish Hg was not correlated with sediment Hg, and only weakly corelated with sediment MeHg (Eagles-Smith et al., 2016). A 2019 meta-analysis of 32 journal articles representing 22 sites worldwide showed that water column MeHg concentrations did not predict MeHg concentrations in biota (Wu et al., 2019). These surprising results are due to the multitude of chemical, biological, and ecological processes that govern MeHg uptake and bioaccumulation.

The production and bioaccumulation of MeHg in aquatic systems is affected by numerous biological and chemical factors, many of which appear contradictory. For example, eutrophic systems with abundant nutrients, dissolved organic matter (DOM), and oxic-anoxic cycling can support high rates of net MeHg production (Bravo et al., 2017; Herrero Ortega et al., 2017; Eckley et al., 2017). On the other hand, phytoplankton biomass can attenuate MeHg bioconcentration into the food web through "bloom dilution" and promote rapid, efficient growth in fish and zooplankton that can further dilute MeHg in biota (Pickhardt et al., 2002; Karimi et al., 2007; Ward et al., 2010). Dissolved organic matter also plays a dual role in MeHg production and bioaccumulation, serving to stimulate microbial metabolism that enhances Hg methylation, while also decreasing the bioavailability of inorganic Hg(II) to methylating microbes, promoting MeHg photodegradation, and attenuating uptake of MeHg into the food web (Ravichandran et al., 2004; Graham et al., 2013; Chiasson-Gould et al., 2014; Qian et al., 2014; Luengen et al., 2012). Ecosystem structure can affect the degree of MeHg bioaccumulation. Many studies show elevated MeHg bioaccumulation with increased food web length (Cabana et al., 1994; Ouédraogo et al., 2015; Thomas et al., 2016). Uptake of MeHg can vary considerably among different algal species, highlighting the importance of algal assemblages in controlling MeHg bioconcentration in pelagic food webs (Lee and Fisher, 2016). Finally, the diets and grazing strategies of fish and zooplankton can influence their MeHg concentration. Grazing depth and diet (e.g., bacteria vs. algae) can influence MeHg concentrations in zooplankton (Hannides et al., 2013; Kainz et al., 2005). Pelagic fish commonly contain significantly higher MeHg concentrations than their benthic counterparts (Matthews et al., 2005; Ouédraogo et al., 2015; Duffil Helsnig et al., 2018). Foraging strategy may change over a species' lifecycle or because of an ecosystem perturbation, causing differences in MeHg bioaccumulation over time (Di Bennedito at al., 2013; Eagles-Smith et al., 2008).

Stable isotope values of carbon (C) and nitrogen (N) in SPM and zooplankton are valuable tools that can help ascertain the processes that drive differences in MeHg bioaccumulation between ecosystems. Carbon isotope values of SPM can elucidate the origin (i.e., autochthonous vs. allochthonous) of the detritus that forms the base of the planktonic food web, a factor that is known to affect MeHg production and bioaccumulation (Wang and Druffel, 2001; Bravo et al., 2017). Nitrogen isotopes of SPM can help identify the source of N to primary producers, an important aspect of energy flow in aquatic systems (Wada, 1967). Relationships between C and N isotopes of SPM

and zooplankton can help identify trophic linkages that facilitate the trophic transfer of MeHg to higher level organisms (Stewart et al., 2008). Finally, N isotopes in zooplankton composites can identify relative abundance of predatory and grazer zooplankton species, which can affect the degree of MeHg bioaccumulation that occurs in the planktonic food web (Post, 2002).

Patterns of MeHg bioaccumulation can be site-specific, necessitating focused studies in polluted systems to identify major drivers. In this field study, we assessed factors governing the uptake of Hg and MeHg into SPM and zooplankton in four Hg-impaired surface water reservoirs over four seasons from 2019 to 2021. We focused on uptake into the base of the pelagic food web because this is known to be the key step that controls MeHg concentration in fish (Lehnherr, 2014; Wu et al., 2019; Ogorek et al., 2021). Combining water chemistry data, algal and zooplankton taxonomic composition, and stable C and N isotope values of SPM and zooplankton samples, we investigated key differences between the reservoirs that may contribute to discrepancies in Hg and MeHg bioaccumulation. Specifically, our research questions were: (1) what are the chemical and biological similarities and differences between the study reservoirs? (2) does the abundance or structure of phytoplankton and zooplankton populations affect the degree of MeHg uptake into the food web? and (3) what factors contribute to enhanced MeHg uptake in SPM or zooplankton? Our study shed light on some of the ways that plankton dynamics affect MeHg bioaccumulation, showing the seasonal patterns of MeHg uptake, and the importance of the composition of SMP and zooplankton grazing patterns

3.3 Site Description and Methods

3.3.1 Site Description

Almaden (AR), Calero (CR), and Guadalupe (GR) reservoirs are small, mesotrophic water storage reservoirs located in the upper Guadalupe River Watershed (San Jose, CA, USA), draining to south San Francisco (SF) Bay (Fig. 3-1). Almaden Reservoir and GR are contaminated by Hg-laden runoff from the former New Almaden Mining District, North America's largest and most productive historical Hg mining district. Despite extensive remediation projects to contain and remove contaminated sediments, the New Almaden Mining District remains a major source of Hg (120 kg/yr) to the SF Bay (McKee et al., 2017). Calero Reservoir is in an adjacent subwatershed but has received contaminated water and sediments from AR through the Almaden-Calero Canal (Fig. 3-1). Stevens Creek Reservoir (SCR) has no known Hg mines in its watershed. The Hg source to SCR is assumed to be a combination of local and global atmospheric deposition (Rothenberg et al., 2010). All four reservoirs primarily receive inflow during California's wet season (October – April), but CR's capacity is maintained year-round through water imports from the Sacramento-San Joaquin Delta. Stored water is used for direct poTable Cupply (CR only), groundwater recharge, and flood control. The variable characteristics of local geology, land use, water source, and reservoir management are reflected in the range of Hg concentrations and primary productivity of each reservoir (Table C1).

Fish in each reservoir exceed regulatory targets for Hg (SFBRWQCB, 2008). Total mercury in muscle tissue of 35-cm length-standardized largemouth bass ranges

from 0.75 mg/kg (wet weight) in SCR to 4.9 mg/kg in GR (Seelos et al., 2021). Valley Water (San Jose, CA) installed line-diffuser hypolimnetic oxygenation systems (HOSs) in each reservoir to increase dissolved oxygen (DO) concentrations at the sediment-water interface and curtail Hg methylation (McCord et al., 2016). Hg concentrations in fish have declined significantly in GR and SCR since HOS (Seelos et al., 2021). The HOSs were operated intermittently during the study period (Fig. C1).

3.3.2 Field Methods

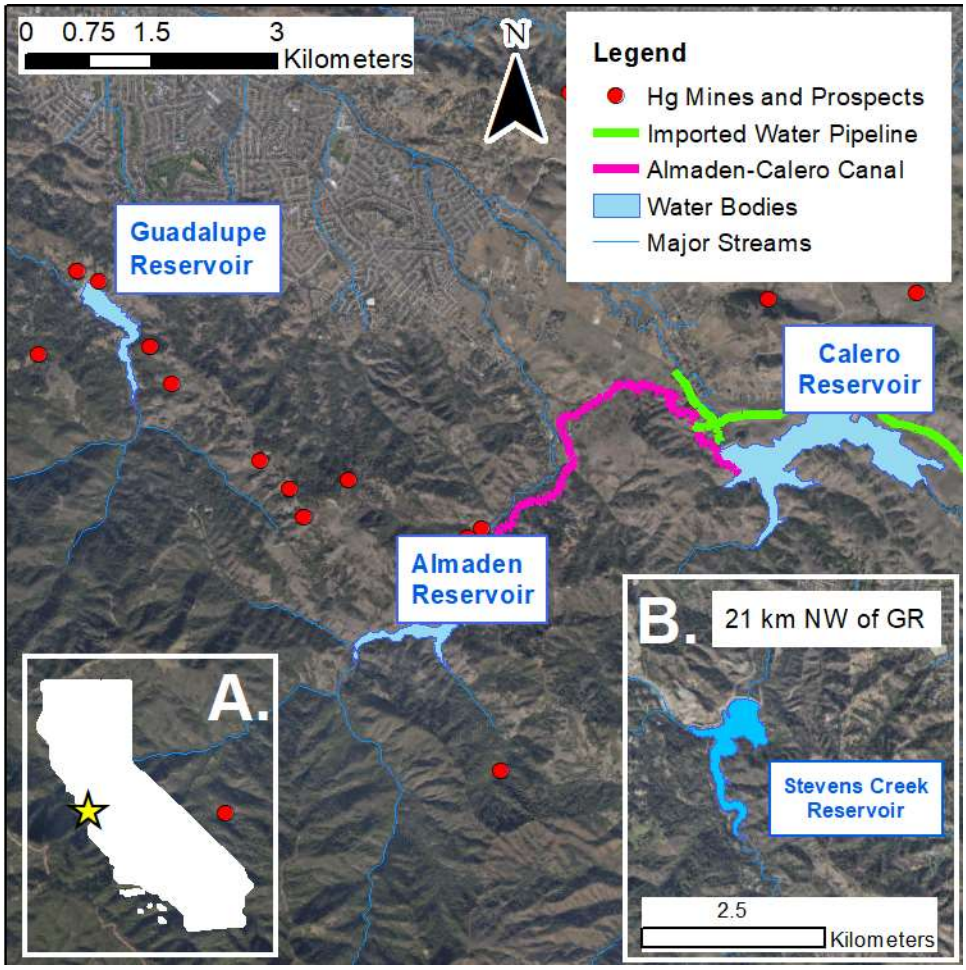

Figure 3-1: Map of upper the upper Guadalupe River Watershed hydrologic system, including Almaden Reservoir (AR), Calero Reservoir (CR), Guadalupe Reservoir (GR), major streams, canals, and pipelines. Inset A shows the site location in the state of California. Inset B shows Stevens Creek Reservoir (SCR), located 12 kilometers northwest of GR.

We completed four seasonal monitoring events (Summer 2019, Winter 2020, Fall 2020, Spring 2021) in each reservoir to capture the seasonal and interannual variability in food web structure and Hg dynamics. Data were collected at the deepest portions of the reservoir, above the bottom-release outlet structures, to target the pelagic food web. In addition, Valley Water collected water quality profiles at these locations on a monthly to bi-monthly basis (with monitoring gaps in 2020 due to the COVID-19 pandemic).

3.3.2.1 Water Sampling

Using Hydrolab DS5 sondes, we measured vertical profiles of temperature, DO, pH, oxidation-reduction potential (ORP), specific conductivity, chlorophyll *a*, and phycocyanin from the reservoir surface to the bottom at ≤ 1 m sampling interval. Grab samples were collected at discrete depths using a Wildco ® horizontal Van Dorn trace metal sampler and dispensed using ultraclean handling methods (USEPA, 1996). Surface (1-2 m depth) and bottom (1-7 m from bottom) water samples were poured into proper containers for analysis of total Hg, total MeHg, sulfate, and ammonia. 500 mL of surface and bottom water were collected into acid-washed Teflon bottles for later filtration and filter-passing MeHg analysis (FP MeHg). Three additional samples were taken between the surface and bottom samples and analyzed for MeHg. 125 mL water samples were collected at the surface, middle, and bottom depths and dispensed into amber glass bottles for analysis of algal taxonomy. An additional 4 L of water was collected at each depth for the isolation of SPM. The reservoir storage volume and thermal structure of each reservoir varied at each sample collection, providing a range of chemical and biological conditions (Fig. C2). Water samples were placed on ice and transported to the laboratory for analysis.

3.3.2.2 Zooplankton Sampling

Zooplankton samples were collected using an 80-µm nylon plankton net with a 0.5 m diameter opening (Aquatic Research Instruments). For taxonomic analysis, we collected a single vertical tow from 6-12 m depth (depending on reservoir stage) and washed all contents into a glass jar using deionized water. The sample depth was recorded for use in zooplankton density calculations. Several additional vertical tows were made at the same sampling depth as the taxonomy sample to collect sufficient zooplankton biomass for Hg, MeHg, and stable isotope analysis. The zooplankton taxonomy and biomass samples were held on ice until transport to the laboratory for processing and analysis.

3.3.3 Sample Processing

3.3.3.1 Water Samples

Immediately upon arrival at the laboratory, FP MeHg samples were filtered using sterile polystyrene filtration apparatuses and 0.45 µm polyethersulfone filters, then decanted into 250 mL fluorinated polyethylene bottles. Samples to be analyzed for Hg, MeHg, and FP MeHg were preserved with 0.5% 12 N HCl. Ammonia samples were preserved to pH <2 with H_2SO_4. Sulfate samples were unfiltered and unpreserved. All water samples were kept refrigerated (4 °C) until analysis.

3.3.3.2 Algae and SPM Samples

Microscope slides were prepared for analysis of algal taxonomy on the day of collection. A 1:100 dilution of 1% Lugol's iodine was added to water samples designated for algal taxonomy. Thirty-two mL of each sample were filtered onto a membrane filter grid (Metricel Grid: 47 mm, 0.45 um). Using clean forceps, each filter was placed sample-side down on a glass microscope cover slip. A thin layer of clear pre-polymerized 2-hydroxypropyl methacrylate (HPMA) mounting resin was spread on top of the filtered

algae membrane and cured at ≥ 35 °C. Mounted slides were labeled and stored in a slide box until taxonomic analysis.

SPM in water samples was concentrated on filters for analysis of Hg, MeHg, total suspended solids (TSS), and stable isotopes of C and N. For each SPM sample, four liters of reservoir water were prefiltered using a 150-um mesh to remove course particulates. Using a glass filtration apparatus, SPM was concentrated onto 0.45 µm glass fiber filters by pouring a known volume (~500 mL) of water through the filter until it clogged. The first subsample, used for analysis of TSS and stable C and N isotopes, was immediately transferred to an incubator and dried at 60 °C until a constant mass was obtained. TSS concentration was measured gravimetrically as the filter mass change divided by the volume of water filtered. TSS was measured using a low temperature because the filter SPM was subsequently encapsulated for stable isotope analysis (see below). Two additional subsamples were produced for analysis of Hg and MeHg, with the SPM mass on the filter calculated as the volume of water poured through the filter multiplied by the TSS. Using forceps, concentrated SPM samples for Hg and MeHg analysis were placed into acid-washed amber glass vials and frozen.

Following gravimetric analysis, the filters used for determination of TSS were placed in a desiccator overnight with a beaker containing >12 N fuming HCl for removal of trace carbonates from the SPM samples. Each filter was cut into thirds using scissors that were cleaned with ethanol. Each filter subsample was carefully rolled and encapsulated in 9x10 mm tin capsules, placed in a 48-well tray, and stored in a desiccator for stable C and N isotope analysis. Filter method blanks for Hg, MeHg, TSS, and stable isotope analysis were prepared using the procedures described above with deionized water instead of reservoir water.

3.3.3.3 Zooplankton Samples

Zooplankton samples for taxonomic analysis were preserved with a 1:100 dilution of 1% Lugol's iodine, stored in a refrigerator at 4 °C, and analyzed within 48 hours of collection (see below). Concentrated zooplankton biomass samples were triple rinsed by dilution to 2 L using deionized water, followed by filtration onto a 150-um mesh. Rinsed zooplankton biomass samples were placed onto aluminum weighing dishes and dried in an incubator at 60 °C until a constant mass was obtained. Using a clean mortar and pestle, samples were homogenized into a fine powder. Triplicate subsamples of ~1 mg were encapsulated in 5x9 mm tin capsules, placed in a 96-well tray, and stored in a desiccator for stable C and N isotope analysis. The remaining homogenate was divided in half and transferred to separate acid-washed amber glass vials for Hg and MeHg analysis. Samples were frozen until analysis.

3.3.4 Analytical Methods

3.3.4.1 Taxonomic Analysis

Algae were identified and quantified using a Zeiss Axio Imager A2 Microscope. The slides were first viewed using 100x or 200x magnification to ensure an even distribution of dominant taxa. All taxa present were identified to genus or species using various references and keys (e.g., Brook et al., 2011; Cox, 1996; Guiry and Guiry, 2016). For samples dominated by algae greater than 10-20 µm in the greatest axial or linear

dimension (GALD), a minimum of 300 cells or natural units and 15 random fields were identified and counted at 200x magnification (representing 1 mL). For samples that were dominated by algae less than 10-20 μm in GALD or containing fragile, difficult to identify taxa, a minimum of 400 natural units or cells and 25 fields were identified and counted at 400x (representing 1 mL). Algae counts were made in triplicate and averaged. Algal cell densities were calculated for each taxa as the count multiplied by 32 (cells/mL). Cell densities were converted to biovolume based on literature approximations, and biomass assuming a cell density of 1 g/cm^3 (Table C2).

Concentrated zooplankton biomass samples were diluted with tap water to 250 mL in a graduated cylinder. The sample was mixed thoroughly in the graduated cylinder with a stir bar to suspend the organisms randomly. Using a pipette, 1mL subsample was quickly removed, transferred to a Sedgwick-Rafter cell, and covered with a microscope cover slip. The cell was placed under a compound microscope under a 10x objective. All organisms were identified and counted in 5 subsamples. Zooplankton were identified to genus or species (Haney et al., 2013). Zooplankton density (count/m^3) was calculated as $(n*V_a)/V_s$ where n is the number of zooplankton counted, V_a is the analyzed sample volume (250 mL), and V_s is the volume of water sampled using the zooplankton net (m^3). Zooplankton biomass was estimated using literature measurements (Table C3).

3.3.4.2 Water Chemistry

Reservoir water samples were analyzed by Eurofins Scientific (Pleasanton, CA, USA). Total Hg was analyzed by oxidation, purge and trap, desorption, and cold-vapor atomic fluorescence spectrometry (CVAFS) (U.S. E.P.A., 2002). The method detection limit for total Hg is 0.2 ng/L. Total and FP MeHg were analyzed by distillation, aqueous ethylation, purge and trap, and CVAFS (U.S. E.P.A., 1998). The method detection limit for MeHg is 0.02 ng/L. Strict quality control standards were followed for trace-level Hg and MeHg analysis, including method blanks, matrix spikes/matrix spike duplicates (method requirement = 75–125% recovery), and check standards (method requirement = 77–123% recovery). Sulfate was analyzed by ion chromatography (U.S. E.P.A., 1993). Ammonia was analyzed by semi-automated calorimetry (U.S. E.P.A., 1993).

3.3.4.3 Hg and MeHg in Solids

Solid-phase Hg and MeHg samples were analyzed by Eurofins Scientific (Sacramento, CA, USA). Total Hg in homogenized zooplankton and SPM (filters) were analyzed using a HNO_3/H_2SO_4 digestion (3:7 ratio of 15.8 M HNO_3 to 18 M H_2SO_4), followed by oxidation, purge and trap, desorption, and CVAFS (U.S. E.P.A., 2002). Methylmercury was extracted from solid samples using 25% KOH in methanol. Digestates were analyzes using distillation, aqueous ethylation, purge and trap, and CVAFS (U.S. E.P.A., 1998). Solid phase Hg analysis followed strict quality control measures, including duplicates (acceptable relative percent difference = 30%), matrix spikes/matrix spike duplicates, and method blanks. Homogenized zooplankton were used for QA/QC samples (duplicates, matrix spikes) because extra sample was available. Adequate recovery (75–125%) was verified using certified reference material (TORT-3).

3.3.4.4 Stable Isotope Analysis

Zooplankton samples were analyzed for bulk $\delta^{15}N$ and $\delta^{13}C$ by element analysis and isotope ratio mass spectrometry (EA-IRMS) at the Stable Isotope Ecosystem Laboratory of UC Merced (SIELO) and UC Davis Stable Isotope Facility (SIF). Twenty-four zooplankton samples were analyzed at the SIELO via a Costech EA coupled to a Thermo Fisher Delta V Plus via CONFLO IV while 24 zooplankton samples were analyzed at UC Davis with a PDZ Europa ANCA-GSL elemental analyzer coupled to a DZ Europa 20-20 IRMS. One hundred forty-four SPM samples were analyzed at UC Davis using a similar method, but with an Elementar Vario EL Cube or Micro Cube elemental analyzer. Samples were analyzed in conjunction with standard reference materials (UC Davis: IAEA-600, USGS-40, USGS-41, USGS-41a, USGS-42, USGS-43, USGS-61, USGS-64, USGS-65; UC Merced: USGS-40, USGS-41) and internal standards of known isotopic composition for scale normalization, drift correction, and mass linearity correction. Isotope values were reported in permil (‰) difference relative to international standards Vienna Pee Dee Belemnite (VPDB, $\delta^{13}C$), and Earth's atmosphere (Air, $\delta^{15}N$). The standard deviation of reference materials at the SIF was 0.05 ‰ for $\delta^{13}C$ and 0.07 ‰ for $\delta^{15}N$ (n = 176). The standard deviation of reference materials analyzed at SIELO was 0.05 ‰ for $\delta^{13}C$ and 0.05 ‰ for $\delta^{15}N$ (n = 32). At both laboratories, absolute accuracy for calibrated reference materials was <0.1‰ for both $\delta^{13}C$ and $\delta^{15}N$. Zooplankton $\delta^{13}C$ values were mathematically corrected for lipid content (*Syväranta and Rautio, 2010)* to account for high carbon fractionation during lipid synthesis. Carbon isotope values in SPM were not lipid-corrected.

3.3.4.5 Statistical Analysis

All plotting and statistical analyses were performed using the R programming language. Ordination analysis performed via non-metric multidimensional scaling (NMDS) was used to examine similarities in biological communities between reservoirs and to identify potential drivers. Using a nonmetric rank-order approach, NMDS attempts to reduce large multidimensional datasets (e.g., multiple biological assemblages or sets of water quality data) into fewer dimensions to identify underlying patterns and gradients. Datasets (e.g., measured biological assemblages) that plot closely to each other are relatively similar in structure. All NMDS analyses were performed with the Vegan package in R, using the Bray-Curtis Dissimilarity Index, autotransformation (Wisconsin double standardization), and a maximum of 100 random starts (Oksanen et al., 2020). Analyses yielding stress values > 0.15 were rejected.

3.4 Results

3.4.1 Water Chemistry

Seasonal patterns in thermal stratification and water chemistry of the study reservoirs before and after HOS have been described in detail (McCord et al., 2016; Seelos et al. (2021). Briefly, each reservoir was thermally stratified beginning around March and continuing until fall turnover around October (Fig. C2). Prior to the installation of the HOSs, reservoir stratification corresponded with depletion of DO in the hypolimnia and establishment of reducing conditions. Hypolimnetic sulfate depletion coincided with elevated MeHg concentrations, which typically began to increase during the spring and peaked around August before declining with the establishment of low-

ORP conditions. During HOS operation, MeHg concentrations in the hypolimnia of all reservoirs decreased dramatically, but MeHg in surface waters remained comparable to pre-HOS levels. Primary productivity, measured as chlorophyll *a* and phycocyanin concentrations, increased in surface waters during HOS operation, possibly the result of enhanced mixing of nutrient-rich bottom waters into the photic zone.

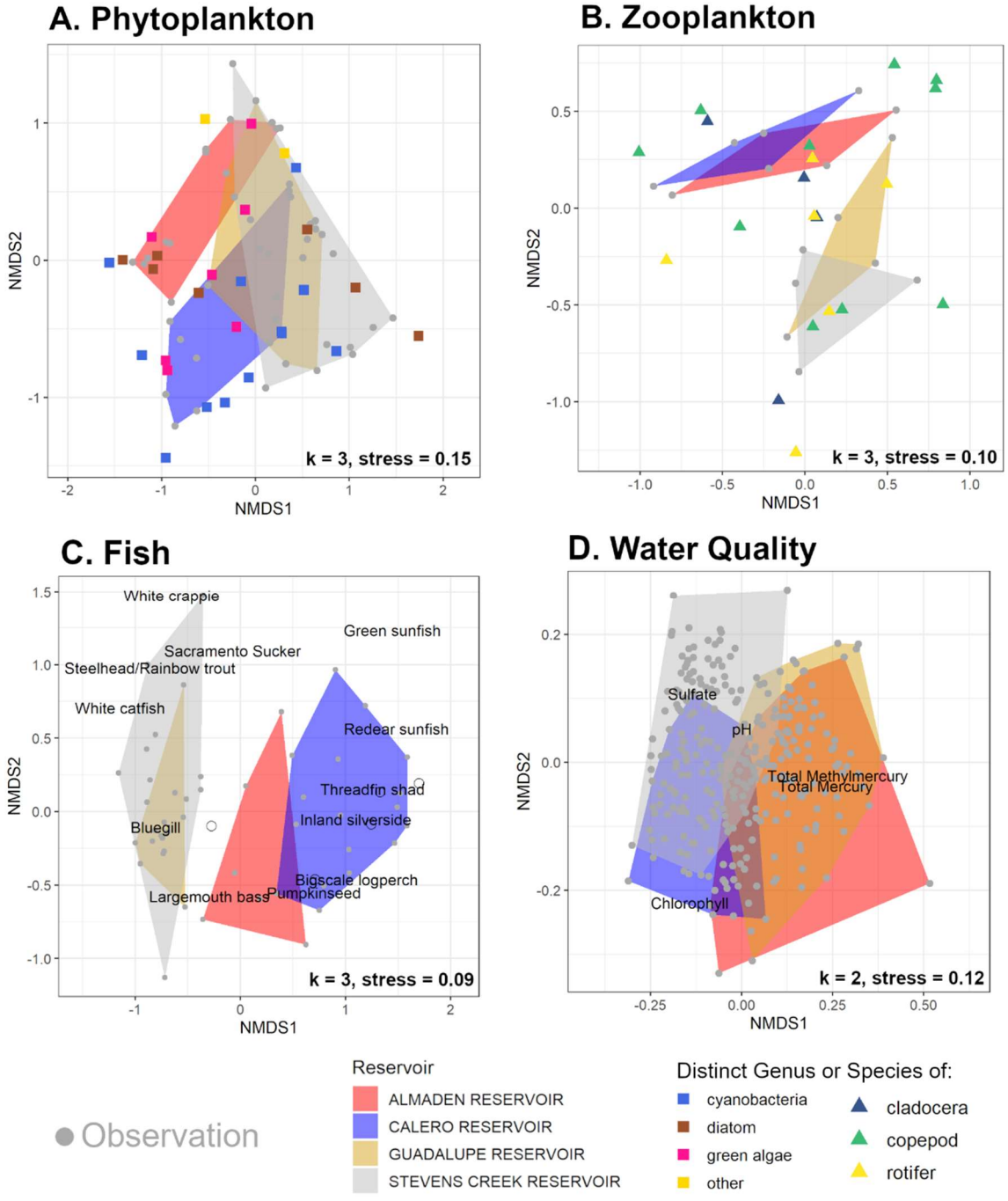

Figure 3-2: Nonmetric Multidimensional Scaling (NMDS) analysis of phytoplankton (A), zooplankton (B), fish (C), and water quality (D) data from four reservoirs. Each grey point is an individual observation containing

assemblage counts or a collection of water quality measurements in reduced dimensional space. The colored convex hulls enclose all individual observations made in each reservoir. In A and B, colored points represent a particular species or genus of the plankton group defined by the color (names not included to avoid cluttering, see legend for genus or species). In C and D, black text on plot denotes locations of relatively high values of the given species (C) or water quality parameter (D). The number of reduced dimensions (k) and Kruskal's Stress (stress) are shown in the bottom-right of each plot.

Despite similar limnological patterns and responses to HOS operation, the reservoirs had some notable differences post-HOS in the concentrations of key water quality parameters affecting MeHg production and bioaccumulation. Non-metric multidimensional scaling (NMDS) analysis of key water quality parameters collected from surface waters of the four reservoirs from 2016 to 2021 showed distinct similarities between AR and GR, and between CR and SCR (Fig. 3-2d). Mercury and MeHg concentrations were notably higher in mine-impacted AR and GR, while CR and SCR had higher sulfate concentrations. Calero Reservoir had considerably higher chlorophyll *a* than the other three reservoirs.

3.4.2 Biological Assemblages

3.4.2.1 Phytoplankton Assemblages

Each reservoir exhibited unique patterns of phytoplankton density and taxonomic distribution. Phytoplankton density was typically highest near the reservoir surface, decreasing with depth (Fig. 3-3). Calero Reservoir had notably higher phytoplankton density than the other reservoirs, peaking at 138 g/m^3 in summer 2019 (Fig. 3-3). A second peak in phytoplankton density in CR surface water was measured during the spring 2021 sampling event. Unique to the reservoirs, the phytoplankton biomass in CR was comprised almost entirely of cyanobacteria year-round, apart from a notable fraction of green algae measured mid-water column during the fall 2020 sampling event (Fig. C3). Like CR, phytoplankton density in AR peaked in summer 2019, but the measured density was about 5 times lower in AR (Fig. 3-2). The phytoplankton assemblage at AR was the most diverse of the reservoirs, with the predominant biomass shifting seasonally between cyanobacteria (summer 2019), dinoflagellates (winter 2020), and diatoms (fall 2020) (Fig. C3). Guadalupe Reservoir and SCR had peak phytoplankton densities during the fall that were similar in magnitude, consisting predominantly of cyanobacteria (Fig. 3-3, Fig. C3). Shifts from cyanobacteria to green algae and dinoflagellates occurred in summer 2019 in GR and spring 2021 in SCR.

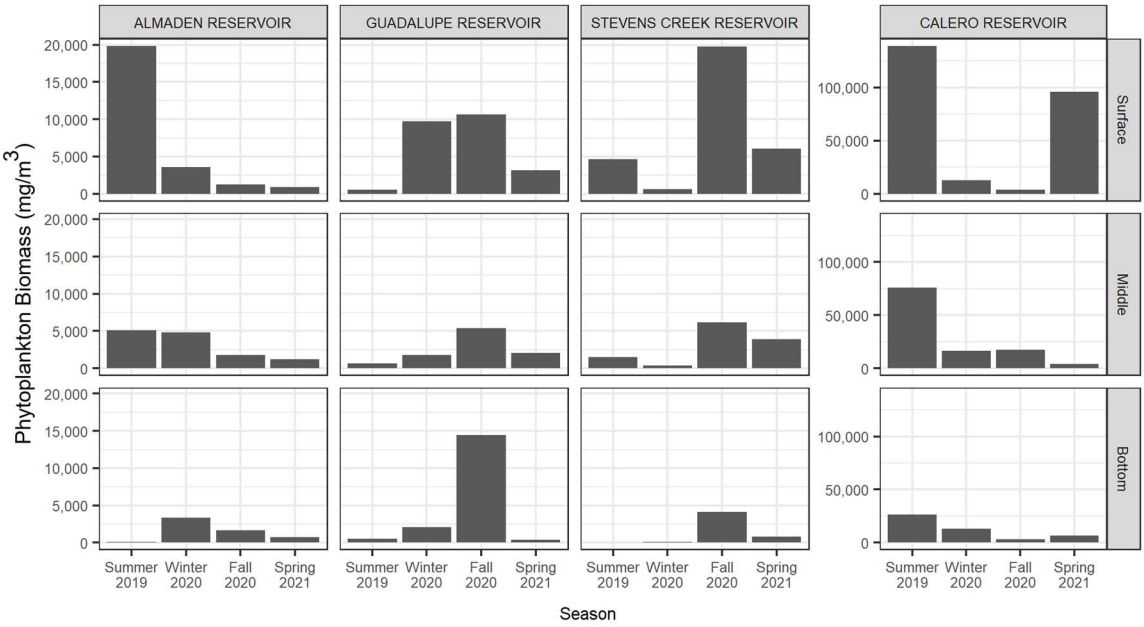

Figure 3-3: Total phytoplankton biomass concentrations measured in the surface, middle, and bottom sampling depths of each reservoir. Biomasses were calculated from algal counts using per-cell mass estimations defined in Table C2.

Ordination analysis of phytoplankton assemblages showed similarity in GR and SCR (Fig. 3-2a). Almaden Reservoir and CR had distinct assemblages with little community overlap with each other, but some overlap with GR and SCR (Fig. 3-2a). Two variables had significant associations with algal assemblages: pH ($p = 0.01$), and zooplankton concentration ($p = 0.01$) (Fig. C4). Dinoflagellate and green algae species tended to be more abundant in samples with lower pH, while golden algae species were more prevalent at higher pH. Zooplankton biomass concentration appeared to increase with green algae and cyanobacteria abundance and decrease with diatom abundance.

3.4.2.2 Zooplankton Assemblages

Seasonal patterns in zooplankton density were relatively consistent between the reservoirs. Calero Reservoir and SCR had comparable zooplankton densities, which were about twice as high as AR and GR. Zooplankton density peaked in summer 2019 and fall 2021 in all reservoirs except AR. Zooplankton density was relatively low in spring 2021 in all reservoirs. Zooplankton assemblages were comprised mainly of cladocerans, copepods, and rotifers, but copepods were dominant on a mass basis (Fig. C3, Fig. 3-4). Surprisingly, there was no correlation between zooplankton biomass and algal biomass.

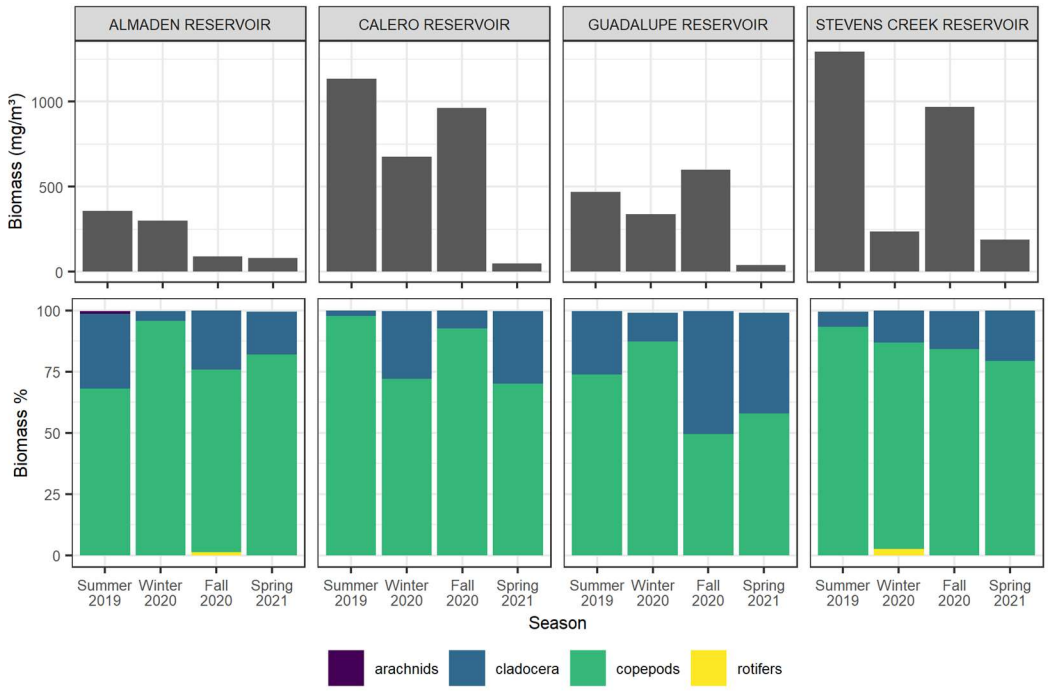

Figure 3-4: Total zooplankton biomass concentrations (top) and mass percentages per taxa (bottom) in each reservoir. Biomasses were calculated from zooplankton counts using per-organism mass estimations defined in Table C3.

Ordination analysis of zooplankton assemblages showed considerable community overlap between AR and CR, and between GR and SCR (Fig. 3-2b). Algal biomass concentration was the only environmental variable that was significantly associated ($p = 0.01$) with zooplankton community composition (Fig. C4). Copepod abundance appeared to increase with algae concentration while rotifer abundance decreased.

3.4.2.3 Fish Assemblages

Though we were unable to collect fish samples during the study period on account of the COVID-19 pandemic, historical fish assemblages offer insight into potential top-down controls on plankton populations. Using boat electrofishing with four netters, fish assemblages were estimated by capturing fish observed during 15-minute shoreline passes, then calculating the observed catch per minute (CPM) per species. Total fish CPM (all species), a relative measure of overall fish abundance, was similar at CR, GR, and SCR, with a median of around 10 (Fig. C5). Total CPM at AR was notably lower than at the other reservoirs, with a median of 3. Fish assemblages varied considerably among reservoirs. The NMDS analysis showed considerable community overlap in GR and SCR (Fig. 3-2c). Fish assemblages at GR and SCR consisted mainly of bluegill, largemouth bass, and black crappie (Fig. C6). In contrast, CR exhibited a more diverse assemblage, with 14 species observed. The fish assemblage at CR consisted of pelagic forage fish (e.g., inland silverside, threadfin shad), benthic feeders (e.g., brown bullhead, Sacramento sucker), and carnivorous gamefish (largemouth bass). Like GR and SCR, AR consisted primarily of bluegill, largemouth bass, and black crappie, but also contained a notable population of threadfin shad. Almaden Reservoir's fish assemblage represents a

"midpoint" between the low-diversity assemblages of GR and SCR, and the highly diverse assemblage of CR.

3.4.3 Suspended Particulate Matter

3.4.3.1 Stable Isotopes in SPM

Stable C and N isotopes in SPM varied with reservoir, season, and collection depth. The reservoirs of the Guadalupe River Watershed, (AR, CR, GR) had similar patterns of $\delta^{13}C$ values (Fig. 3-5). In each reservoir, SPM $\delta^{13}C$ values peaked during the summer and spring sampling events but dropped to ~ -36‰ in winter 2020. Though CR exhibited a similar seasonal pattern as AR and GR, SPM in CR was generally more enriched in ^{13}C. In SCR, SPM $\delta^{13}C$ values displayed a different pattern, with the highest values (-31.5‰) measured in winter 2020. In some samples collected during thermal stratification, SPM $\delta^{13}C$ values increased with sample depth, but the pattern was not consistent across reservoirs. Seasonal patterns in $\delta^{15}N$ values were consistent among all four reservoirs, with peaks measured in winter 2020 and lower values in the spring and summer sampling events (Fig. 3-5). Winter 2020 peaks in SPM $\delta^{15}N$ ranged from ~5‰ in AR to ~7.5‰ in CR, while summer lows ranged from ~0‰ in AR to ~2.5‰ in CR. Like $\delta^{13}C$ values, there was sometimes a vertical gradient in SPM $\delta^{15}N$ values, but the pattern was inconsistent across reservoirs. Carbon to N ratios, a measurement of food quality, were roughly constant in CR but varied seasonally in the other reservoirs (Fig. 3-5). In summer 2019, C:N ratios were generally highest, at ~6.25 in CR and ~8 in the other reservoirs. In the spring and fall sampling events, C:N ratios of SPM were more variable but generally lower.

3.4.3.2 Hg and MeHg in SPM

Mercury and MeHg were five to six orders of magnitude more concentrated in SPM than in reservoir water (Fig. 3-6). Nonetheless, MeHg was not detectable in some SPM samples collected in winter and fall 2020 from CR and SCR. Total Hg in SPM was <0.5 mg/kg year-round in CR and SCR and did not vary notably with depth. In contrast, SPM total Hg in mine-impacted AR and GR was higher and more variable. In AR, total Hg in SPM was around 0.75 mg/kg, peaking to around 1.5 mg/kg in the deepest samples in summer 2019 and spring 2021. In GR, total Hg in SPM ranged from about 0.5 to 2.5 mg/kg, with high variability by depth. Patterns in MeHg in SPM were more consistent. Methylmercury in SPM peaked in summer 2019, and to a lesser extent in spring 2021 in each reservoir. Methylmercury concentrations were consistently highest in the surface SPM samples in summer 2019 in all four reservoirs. Peak SPM MeHg concentrations in summer 2019 were similar were similar in AR, CR, and GR, but notably lower in SCR. Percent MeHg in SPM was generally highest in summer and spring, often exceeding 5%. Percent MeHg in SPM was negatively correlated with SPM $\delta^{15}N$ (Fig. C7).

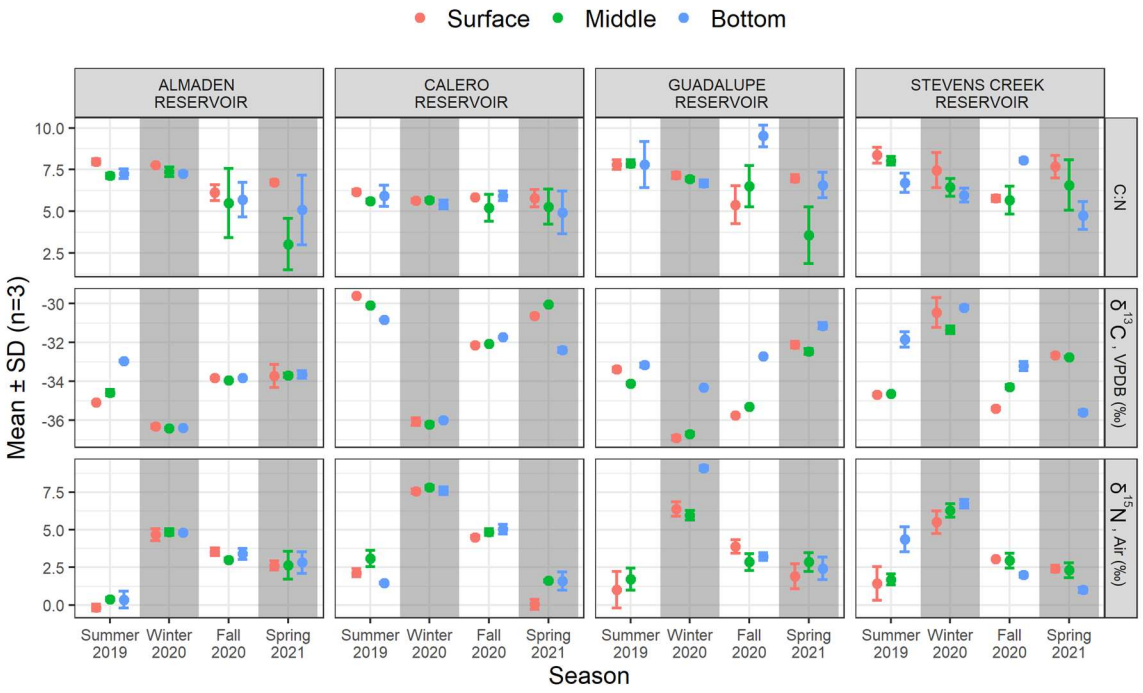

Figure 3-5: C:N ratios (top), $\delta^{13}C$ (middle), and $\delta^{15}N$ (bottom) measured in suspended particulate matter collected at three depths (colors) in each reservoir. Error bars show standard deviation of triplicate samples (some error bars are too small to be legible).

3.4.4 Zooplankton

3.4.4.1 Stable Isotopes in Zooplankton

Stable C and N isotope values of zooplankton composite samples varied by reservoir and collection season. Zooplankton $\delta^{13}C$ was elevated in CR relative to the other reservoirs except in winter (Fig. 3-7). Zooplankton $\delta^{13}C$ values were positively correlated with SPM $\delta^{13}C$ values collected near the surface and middle of the reservoirs, but not with SPM collected lower in the water column (Fig. 3-8). Zooplankton samples were enriched in ^{13}C with $\delta^{13}C$ values 1.8 ± 1.4‰ (mean ± SD) above surface SPM samples. Zooplankton $\delta^{15}N$ values appeared to have a positive association with SPM $\delta^{15}N$ values in AR and CR, but not in GR or SCR (Fig S8). In AR and CR, zooplankton were enriched in ^{15}N with $\delta^{15}N$ values of 4.9 ± 2.2‰ above surface SPM samples. There was a significant correlation between the mass percent of copepods and $\delta^{15}N$ values in the zooplankton composite samples (Fig. C9). Zooplankton C:N ratios were lower on average than C:N in SPM surface samples (4.7 ± 0.7 vs. 6.8 ± 1; mean ± SD).

3.4.4.2 Hg and MeHg in Zooplankton

Total Hg and MeHg in zooplankton varied by reservoir and by season. Total Hg concentrations in zooplankton were generally lower than total Hg in SPM, by 5 times on average. However, MeHg was generally more concentrated in zooplankton than in SPM, by 6 times on average. Differences between zooplankton and SPM MeHg were highly variable, resulting in no significant correlation between the two. The three reservoirs of

the Guadalupe River Watershed (AR, CR, GR) had peak MeHg concentrations in zooplankton during summer 2019 and spring 2021 (Fig. 3-9). Peak MeHg in zooplankton were very similar in AR and GR, around 0.5 mg/kg in summer 2019 and 0.9 mg/kg in spring 2021. Zooplankton MeHg peaked in SCR in summer 2019 and fall 2019, both at concentrations around 0.13 mg/kg. In CR, 100% of the Hg in zooplankton was MeHg during all sampling events. However, %MeHg in zooplankton varied from 2% to 100% in the other reservoirs dropping in winter 2020 in GR and SCR, and in fall 2020 in AR.

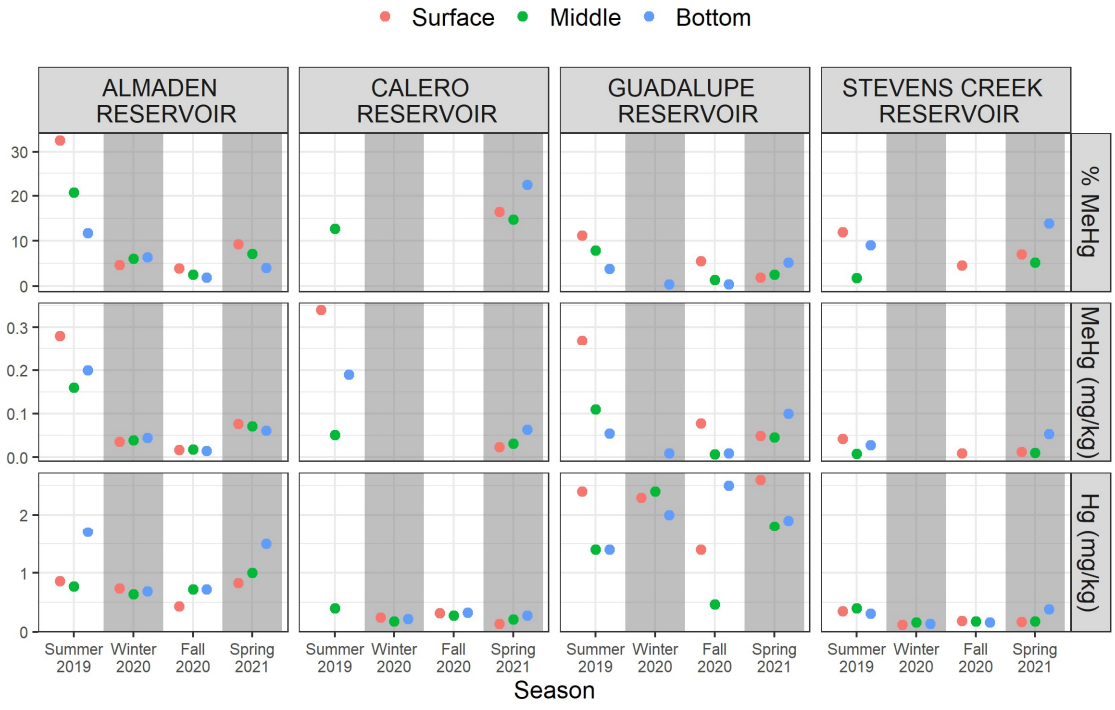

Figure 3-6: %MeHg (top), MeHg (middle), and Total Hg (bottom) measured in suspended particulate matter collected at three depths (colors) in each reservoir. Points represent single measurements. Values below detection limits are not shown. All concentrations are reported as dry weight. Percent MeHg (%MeHg) is calculated as [MeHg]/[total Hg]*100%.

3.5 Discussion

3.5.1 Key Differences Between Reservoir Water Chemistry and Food Webs

Water quality in the four reservoirs had key similarities and differences that are relevant to Hg cycling and bioaccumulation. Unsurprisingly, Hg and MeHg concentrations in water of mine-impacted AR and GR were considerably higher than in CR and SCR. However, CR and SCR contained much (2-3 times) higher concentrations of sulfate, which is known to stimulate MeHg production in aquatic sediments (Gilmour et al., 1992; Jeremiason, 1996). Additionally, eutrophic conditions observed in CR indicated by high phytoplankton density can promote high rates of MeHg production (Gray and Hines, 2009; Bravo et al., 2017). Thus, though total Hg concentrations are lower in CR and SCR, they may have more favorable conditions for MeHg production and release into the water column.

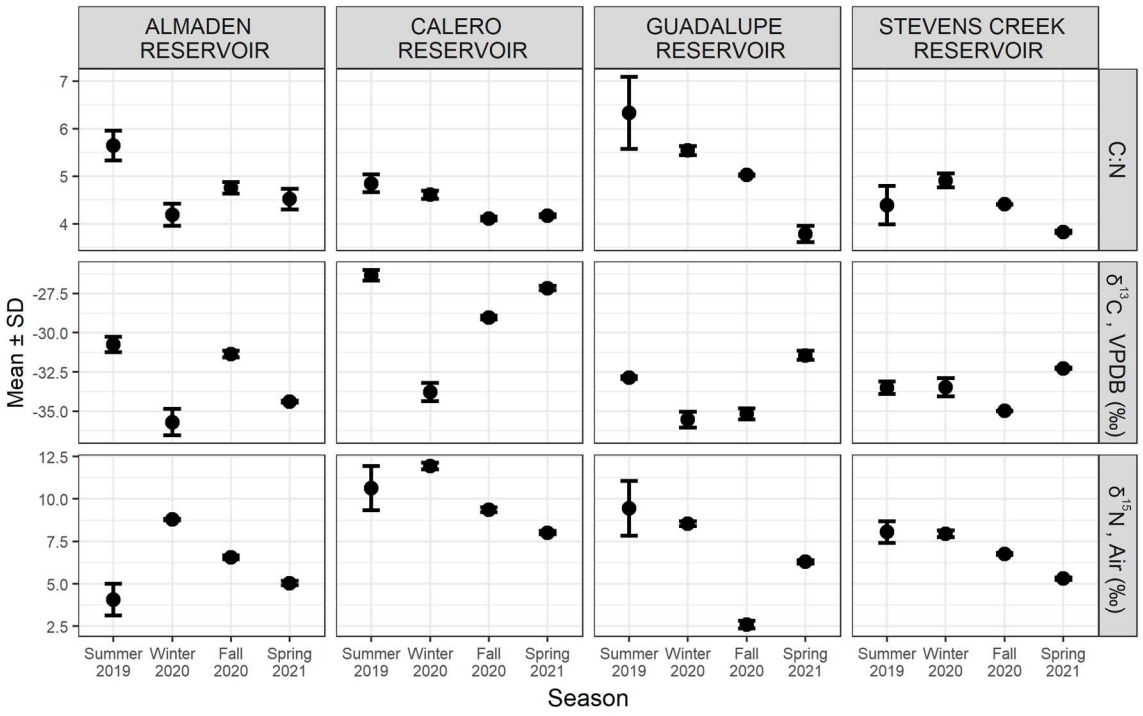

Figure 3-7: C:N ratios (top), $\delta^{13}C$ (middle), and $\delta^{15}N$ (bottom) measured in zooplankton composites from each reservoir.

Phytoplankton species distribution and biomass density are key constraints on MeHg availability to pelagic ecosystems because they affect the uptake and concentration of MeHg at the base of the food web (Pickhardt et al., 2002; Lee and Fisher, 2016). Additionally, the phytoplankton population can affect zooplankton growth and abundance, as cyanobacteria are thought to represent a low-quality and potentially toxic food source for grazers (Wilson et al., 2006; Martin-Cruezburg and von Elert, 2009). Phytoplankton assemblages in the reservoirs varied seasonally but can be roughly separated into three archetypes: lower diversity-higher abundance (CR), lower diversity-lower abundance (GR and SCR), and higher diversity-lower abundance (AR). Lower-diversity reservoirs consisted primarily of common cyanobacteria genera (e.g., Dolichospermum, Aphanizomenon, Microcystis) year-round, with minor populations of other phytoplankton groups (e.g., green algae, dinoflagellates, diatoms). In GR and SCR, these other groups increased in proportion seasonally, while cyanobacteria predominated throughout in CR. Cyanobacteria abundance and total algal density appeared to increase with residence time of water in the reservoir, likely due to nutrient accumulation and warmer, stagnant conditions that favor cyanobacteria growth (Romo et al., 2013). High concentrations of cyanobacteria are associated with enhanced MeHg production and uptake (Lázaro et al., 2013; Lee and Fisher, 2016). Additionally, high concentrations of cyanobacteria could decrease the somatic growth dilution of MeHg in zooplankton (Karimi et al., 2007). Thus, these cyanobacteria-dominant reservoirs may present elevated risk for MeHg production and bioaccumulation. In contrast, AR contained populations of green algae, golden algae, and diatoms that comprised about 25-100% of

the phytoplankton assemblage in each sampling event. Phytoplankton species often have lower surface area to volume ratios than common cyanobacteria, which could decrease passive MeHg uptake (Lee and Fisher, 2016). Green algae and diatom-dominant phytoplankton assemblages also constitute a higher quality food source for upper-level organisms, potentially increasing somatic growth dilution of MeHg in zooplankton (Wilson et al., 2006; Martin-Cruezburg and von Elert, 2009; Karimi et al., 2007).

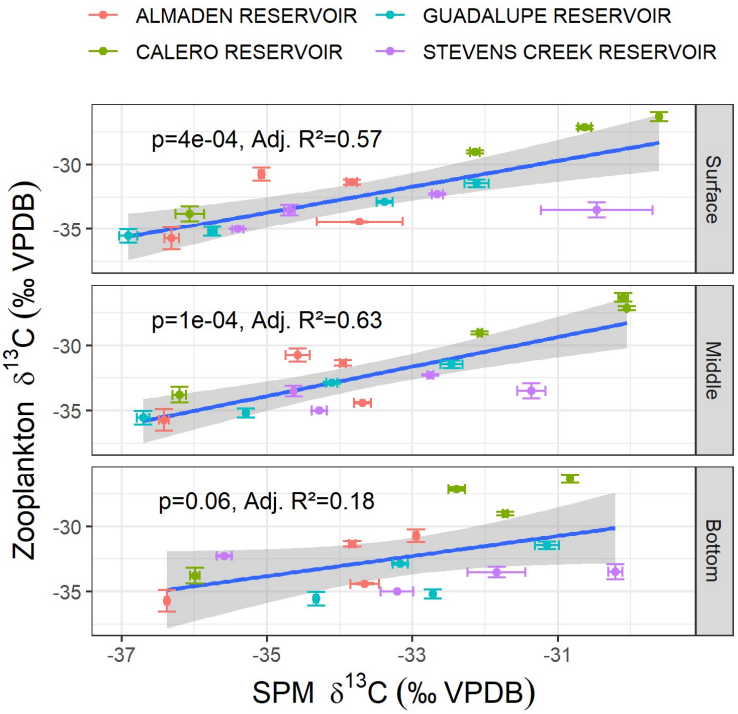

Figure 3-8: Linear correlations between $\delta^{13}C$ measured in zooplankton composites and SPM collected from the surface, middle, and bottom sampling.

Zooplankton serve as a key trophic linkage between primary producers and planktivorous fish, representing an important control on MeHg bioaccumulation in the pelagic food web (Fisher and Reinfelder, 1995). Zooplankton abundance and community composition can influence their uptake and concentration of MeHg, ultimately affecting MeHg accumulation in fish (Pickhardt et al., 2005; Stewart et al., 2008). Zooplankton biomass density was highest at CR and SCR, with the highest contribution from copepods due to their size and abundance. Like phytoplankton, zooplankton density and composition varied seasonally, but assemblages can be separated into two architypes: large-body dominant (AR, CR) and small-body dominant (GR, SCR). Zooplankton assemblages in the large-body dominant reservoirs consisted primarily of large copepods of the order Cyclopoidia and their naupli. In contrast, GR and SCR had higher percentages of rotifers and smaller copepod genera such as Microcyclops. Both archetypes contained minor (10-30%) fractions of cladocera species, primarily of the genera Bosmina and Daphnia. Rotifer abundance decreased with increasing phytoplankton density. This result disagrees with other studies that showed increased

rotifer density resulting from eutrophication (Blancher, 1984; Ejsmont-Karabin, 2012). Because rotifers are lower-order grazers that can have lower MeHg concentrations than higher-order zooplankton species, increases in algal biomass could indirectly increase MeHg concentrations in zooplankton (Stewart et al., 2008). Furthermore, increases in abundance of carnivorous copepod species under high algae density could add an additional trophic step in the food web and increase MeHg concentrations in zooplankton (Cabana et al., 1994).

Fish abundance and species distribution are important factors influencing plankton populations and MeHg bioaccumulation. The fish assemblages of GR and SCR primarily consisted of opportunistic and piscivorous feeders (e.g., bluegill, largemouth bass) that had no clear linkage to planktonic food web. In contrast, AR and CR contained planktivorous forage fish (e.g., threadfin shad, inland silverside). Unlike GR and SCR, which had small-dominant zooplankton assemblages, AR and CR contained higher abundances of large copepods and cladocera, which may explain the presence of planktivorous fish. In addition to connecting the planktonic food web to predatory fish, planktivorous fish provide a top-down control on the plankton assemblage and density in lakes (Li et al., 2020). Predation by fish could explain why zooplankton abundance is relatively low in AR and CR despite high phytoplankton diversity in AR and abundance in CR.

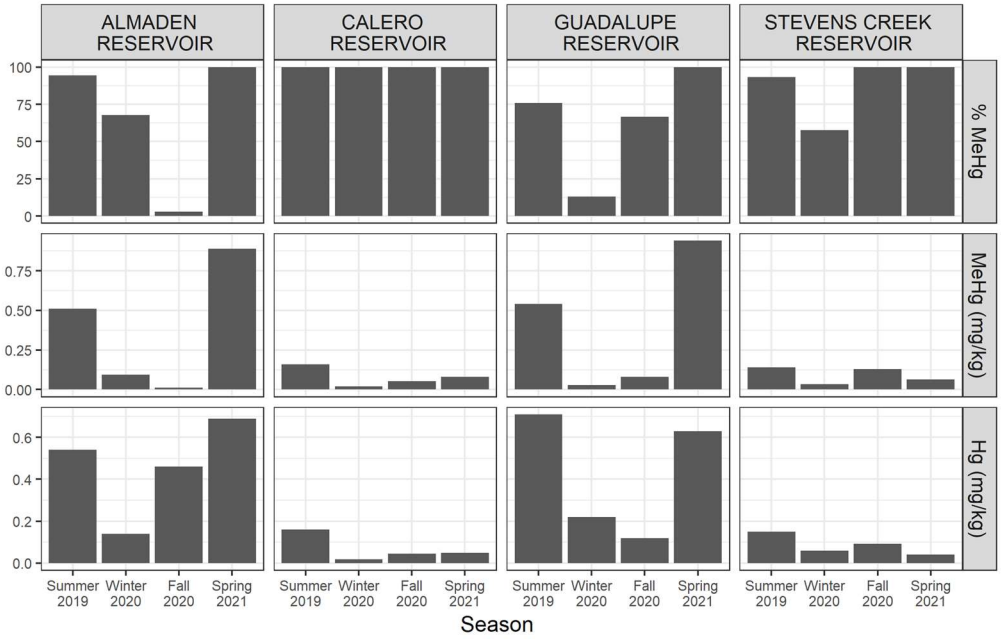

Figure 3-9: %MeHg (top), MeHg (middle), and Total Hg (bottom) measured in zooplankton composites collected in each reservoir. Bar heights represent single measurements. All concentrations are reported in dry weight.

3.5.2 Patterns in Plankton and Suspended Particulate Matter

Plankton density and community structure varied seasonally in each reservoir. There was no consistent pattern in phytoplankton productivity among the reservoirs, with peaks in phytoplankton biomass identified in summer (AR, CR), winter (GR), fall (GR,

SCR), and spring (CR). Likewise, there didn't appear to be a consistent seasonal pattern in phytoplankton assemblages. None of the water quality variables measured were correlated with phytoplankton biomass. It is likely that nutrient and/or light limitation were key factors controlling bloom events (Han et al., 2021). Patterns in zooplankton density were consistent in CR, GR, and SCR, with peaks measured during the summer and fall sampling events. However, we found no correlation between biomass densities of phytoplankton or cyanobacteria and zooplankton, suggesting that the zooplankton population is not limited by food availability. Predation by planktivorous fish and carnivorous zooplankton is likely an important top-down control on zooplankton density that obscures the relationship between the phytoplankton and zooplankton communities (Sinstro, 2010; Li et al., 2020).

Suspended particulate matter samples were depleted in ^{13}C relative to known isotope values reported in phytoplankton ($\delta^{13}C$ from -18 to -25 ‰) (Popp et al., 1998; Hayes, 2001). However, SPM $\delta^{13}C$ values fell within the range of literature values of lake SPM (Cattaneo et al., 2004; Taipale et al., 2016; Lammers et al., 2017). This difference in $\delta^{13}C$ values likely reflects contributions from allochthonous organic matter, which is expected to be relatively depleted in ^{13}C (Wang and Druffel, 2001; Hedges et al., 1997). The large decrease in SPM $\delta^{13}C$ values observed in winter 2020 likely reflects allochthonous loading of organic matter, which has lower $\delta^{13}C$ values associated with terrestrial vegetation. Conversely, $\delta^{15}N$ values in SPM was highest in winter 2020 and lower in other seasons. Differences in SPM $\delta^{15}N$ values can reflect the species of dissolved N present (NO_3^-: 3–7‰, NH_4^+: 6–8‰, and atmospheric N_2: 0‰ per Miyake and Wada, 1967) or the nitrogen source (Kendall et al., 2007). Relatively low SPM $\delta^{15}N$ values in summer and spring likely reflects the high abundance of cyanobacteria species that fix atmospheric nitrogen (Minigawa and Wada, 1986). High (>5‰) $\delta^{15}N$ values in SPM measured in winter 2020 suggests external loading of particulate organic nitrogen, and/ or phytoplankton reliance on dissolved N species.

Stable C and N isotope values in zooplankton reflected their food source and community structure. Zooplankton $\delta^{13}C$ values were significantly associated with SPM $\delta^{13}C$ values collected from the surface and mid-water column. This correspondence indicates that zooplankton primarily feed in the pelagic zone. However, there appeared to be no association between zooplankton $\delta^{15}N$ and SPM $\delta^{15}N$ values in GR and SCR. Instead, zooplankton $\delta^{15}N$ values were related to the zooplankton community structure, with $\delta^{15}N$ values increasing with the mass percentage of copepods present. Carnivory of other zooplankton species by copepods could increase the trophic fractionation of N disproportionally to C, causing a misalignment of $\delta^{15}N$ and $\delta^{13}C$ values (Post, 2002). It is likely that variations in zooplankton $\delta^{15}N$ values in GR and SCR reflect seasonal variability in N source and carnivory by zooplankton. Zooplankton carnivory effectively adds a trophic step to the pelagic food web, which could increase MeHg bioaccumulation (Cabana et al., 1994).

3.5.3 Patterns in Hg Bioaccumulation

Suspended particulate matter accumulated Hg and MeHg at much higher concentrations (~1 million times) than were present in reservoir water. However, we did

not observe predictive relationships between Hg or MeHg measured in SPM and water at the time of collection. This was especially true when considering FP MeHg as representative of the pool of MeHg in water because FP MeHg was highly variable and often not detectable. The concentration of Hg species in SPM represents a time-averaged snapshot of Hg exposure influenced by factors such as Hg concentration and speciation in water, SPM origin and age, and phytoplankton density and composition. Each of these factors can vary on timescales from days to months. Thus, a single water measurement of Hg or MeHg taken during the collection of SPM will not represent the Hg time history associated with the SPM sample and cannot accurately explain fine-timescale changes in Hg uptake by SPM. Increasing sampling frequency to monthly or less could help constrain water-SPM biomagnification.

Consistent total Hg concentrations in SPM (~0.25 mg/kg) measured year-round in CR and SCR suggests that a relatively unchanging input (e.g., atmospheric deposition) dominates Hg loading to these reservoirs. In contrast, the higher (0.5-2.5 mg/kg) and more variable Hg concentrations measured in SPM collected from AR and GR suggests that Hg loading varies with inflow and reservoir conditions. Methylmercury concentrations in SPM peaked during the summer and spring sampling events in each reservoir. This is consistent with studies that have noted enhanced MeHg production in stratified reservoirs during the spring and early summer prior to the establishment of highly reducing conditions (Beutel et al., 2020; Fuhrmann et al., 2021). We did not measure elevated Hg or MeHg in biota following fall turnover, as has been noted in other studies (Herrin et al., 1998; Slotton et al., 1995). It is likely that bottom discharge from the reservoirs and hypolimnetic oxygenation kept MeHg concentrations relatively low in bottom waters, such that MeHg bioaccumulation was more dependent on MeHg production occurring in the littoral zone and/or water column than on seasonal inputs from the hypolimnion during reservoir mixing (McCord et al., 2016; Seelos et al., 2021). This hypothesis is supported by higher MeHg concentrations measured in surface SPM samples in summer 2019 compared to those measured closer to the bottom. Percent MeHg in SPM was negatively associated with $\delta^{15}N$ values in SPM, likely due to enhanced MeHg production at times when SPM was autochthonous in origin, or preferential MeHg uptake relative to inorganic Hg. Phytoplankton-derived dissolved organic matter is known to support relatively high rates of Hg methylation (Bravo et al., 2017).

Zooplankton assimilated MeHg much more efficiently than inorganic Hg. Whereas total Hg concentrations in zooplankton were about 5 times lower than in SPM, MeHg concentrations averaged 5-6x times higher. This result agrees with other studies showing high rates of MeHg assimilation by zooplankton compared to inorganic Hg (Lee and Fisher, 2016; Gosnell et al., 2021). The fraction of total Hg in zooplankton as MeHg was typically >50% with lower fractions generally occurring during the winter when MeHg production was low. Despite similar concentrations of MeHg in surface SPM of AR, CR, and GR during summer 2019, zooplankton MeHg concentrations were much lower in

CR. Zooplankton may have selectively fed in the mid-water column where phytoplankton density was ~50% lower and MeHg concentrations were ~0.05 mg/kg. Zooplankton in AR and GR contained the highest MeHg concentrations during spring 2021 when MeHg in SPM was relatively low. This result corresponded with decreased zooplankton density and lower C:N in zooplankton composites. It is possible that low zooplankton densities decreased grazer competition and allowed for more selective feeding on "fresh" phytoplankton that likely contained higher concentrations of MeHg. Conversely, high zooplankton densities measured in summer 2019 could have led to lower selectivity by zooplankton, including feeding on older detritus that may have had lower MeHg concentrations compared to fresh algal biomass. Zooplankton feed selectively on the best available resources, perhaps making bulk SPM and phytoplankton counts poor proxies for zooplankton diet (Sailley et al., 2015; Meunier et al., 2015). This was evident in the poor correlations between MeHg or $\delta^{15}N$ in SPM and zooplankton composites.

3.6 Conclusion

Building understanding of the factors that contribute to MeHg bioaccumulation in reservoirs is crucial to developing management strategies aimed at lowering Hg bioaccumulation, particularly because MeHg concentrations in surface waters are often poorly correlated with MeHg concentrations in biota. This study presents one approach for assessing the drivers of MeHg bioaccumulation in reservoir systems using a diverse set of chemical and ecological data. Nonmetric multidimensional scaling analysis revealed key similarities and differences between four monomictic reservoirs that could affect MeHg production and bioaccumulation. Mine-impacted AR and GR had high Hg and MeHg concentrations, but likely less favorable conditions for MeHg production than CR and SCR, which had higher sulfate concentrations and phytoplankton productivity. Significant overlaps in the plankton and fish assemblages of GR and SCR suggest ecological similarities that could affect MeHg bioaccumulation in these reservoirs. Almaden and Calero reservoirs likewise had similar plankton and fish assemblages, with the notable presence of pelagic forage fish that could efficiently connect the planktonic food web with upper trophic level fish. Stable isotope results indicated that zooplankton likely fed primarily in the upper water column of the reservoirs, but zooplankton biomass did not seem to be limited by food availability. Instead, fish and carnivorous zooplankton may present a top-down control on the zooplankton population. Percent MeHg in SPM was negatively associated with $\delta^{15}N$ values, suggesting that "fresh" algal biomass could support preferential MeHg uptake (relative to total Hg) or enhanced MeHg production. Methylmercury accumulated in SPM during the spring and summer seasons in each reservoir, when conditions were most favorable to MeHg production. Though MeHg concentrations in SPM were highest during the summer, zooplankton MeHg was highest in the spring in AR and GR. This may have been due to low zooplankton density, which could decrease feeding competition and allow for more ingestion of MeHg per organism. Methylmercury and stable isotope data in biota suggest that bulk SPM may not represent dietary inputs to zooplankton, which feed selectively and adjust their diet based on the

best available food source. Overall, our results demonstrate the seasonal patterns in MeHg introduction into the pelagic food web, and ecological similarities in AR and CR, and in GR and SCR.

3.7 References

Beutel, M., Fuhrmann, B., Herbon, G., Chow, A., Brower, S. and Pasek, J. (2020). Cycling of methylmercury and other redox-sensitive compounds in the profundal zone of a hypereutrophic water supply reservoir. Hydrobiologia, 847(21), pp.4425-4446.

Bigham, G. N., Murray, K. J., Masue-Slowey, Y., & Henry, E. A. (2017). Biogeochemical controls on methylmercury in soils and sediments: Implications for site management. *Integrated Environmental Assessment and Management*, *13*(2), 249–263. https://doi.org/10.1002/ieam.1822

Blancher, E. C. (1984). Zooplankton-trophic state relationships in some north and central Florida lakes. *Hydrobiologia*, *109*(3), 251–263. https://doi.org/10.1007/BF00007743

Branfireun, B. A., Cosio, C., Poulain, A. J., Riise, G., & Bravo, A. G. (2020). Mercury cycling in freshwater systems - An updated conceptual model. *Science of The Total Environment*, *745*, 140906. https://doi.org/10.1016/j.scitotenv.2020.140906

Bravo, A. G., Bouchet, S., Tolu, J., Björn, E., Mateos-Rivera, A., & Bertilsson, S. (2017). Molecular composition of organic matter controls methylmercury formation in boreal lakes. *Nature Communications*, *8*(1), 14255. https://doi.org/10.1038/ncomms14255

Cabana, G., Tremblay, A., Kalff, J., & Rasmussen, J. B. (1994). Pelagic Food Chain Structure in Ontario Lakes: A Determinant of Mercury Levels in Lake Trout (*Salvelinus namaycush*). *Canadian Journal of Fisheries and Aquatic Sciences*, *51*(2), 381–389. https://doi.org/10.1139/f94-039

Cattaneo, A., Manca, M., & Rasmussen, J. B. (2004). Peculiarities in the stable isotope composition of organisms from an alpine lake. *Aquatic Sciences*, *66*(4), 440–445. https://doi.org/10.1007/s00027-004-0730-9

Chiasson-Gould, S. A., Blais, J. M., & Poulain, A. J. (2014). Dissolved Organic Matter Kinetically Controls Mercury Bioavailability to Bacteria. *Environmental Science & Technology*, *48*(6), 3153–3161. https://doi.org/10.1021/es4038484

Cox, Eileen J. Identification of Freshwater Diatoms from Live Material. (2006) London: Chapman & Hall. Print.

Driscoll, C. T., Mason, R. P., Chan, H. M., Jacob, D. J., & Pirrone, N. (2013). Mercury as a Global Pollutant: Sources, Pathways, and Effects. *Environmental Science & Technology*, *47*(10), 4967–4983. https://doi.org/10.1021/es305071v

Eagles-Smith, C. A., Ackerman, J. T., Willacker, J. J., Tate, M. T., Lutz, M. A., Fleck, J. A., … Pritz, C. F. (2016). Spatial and temporal patterns of mercury concentrations in freshwater fish across the Western United States and Canada. *Science of The Total Environment*, *568*, 1171–1184. https://doi.org/10.1016/j.scitotenv.2016.03.229

Eagles-Smith, C. A., Suchanek, T. H., Colwell, A. E., Anderson, N. L., & Moyle, P. B. (2008). CHANGES IN FISH DIETS AND FOOD WEB MERCURY BIOACCUMULATION INDUCED BY AN INVASIVE PLANKTIVOROUS FISH. *Ecological Applications*, *18*(sp8), A213–A226. https://doi.org/10.1890/06-1415.1

Eckley, C. S., Luxton, T. P., Goetz, J., & McKernan, J. (2017). Water-level fluctuations influence sediment porewater chemistry and methylmercury production in a flood-control reservoir. *Environmental Pollution*, *222*, 32–41. https://doi.org/10.1016/j.envpol.2017.01.010

Ejsmont-Karabin, Jolanta. (2012). The usefulness of zooplankton as lake ecosystem indicators: Rotifer trophic state index. Polish Journal of Ecology. 60. 339-350.

Fisher NS, Reinfelder JR. (1995). The trophic transfer of metals in marine systems. In: Tessier A, Turner DR, editors. Metal speciation and bioavailability in aquatic systems. Chichester: John Wiley, 363-406.

Fuhrmann, B., Beutel, M., Ganguli, P., Zhao, L., Brower, S., Funk, A., & Pasek, J. (2021). Seasonal patterns of methylmercury production, release, and degradation in profundal sediment of a hypereutrophic reservoir. *Lake and Reservoir Management*, *37*(4), 360–377. https://doi.org/10.1080/10402381.2021.1940397

Gilmour, C. C., Henry, E. A., & Mitchell, R. (1992). Sulfate stimulation of mercury methylation in freshwater sediments. *Environmental Science & Technology*, *26*(11), 2281–2287. https://doi.org/10.1021/es00035a029

Gosnell, K. J., Dam, H. G., & Mason, R. P. (2021). Mercury and methylmercury uptake and trophic transfer from marine diatoms to copepods and field collected zooplankton. *Marine Environmental Research*, *170*, 105446. https://doi.org/10.1016/j.marenvres.2021.105446

Graham, A. M., Aiken, G. R., & Gilmour, C. C. (2013). Effect of Dissolved Organic Matter Source and Character on Microbial Hg Methylation in Hg–S–DOM Solutions. *Environmental Science & Technology*, *47*(11), 5746–5754. https://doi.org/10.1021/es400414a

Gray, J. E., & Hines, M. E. (2009). Biogeochemical mercury methylation influenced by reservoir eutrophication, Salmon Falls Creek Reservoir, Idaho, USA. *Chemical Geology*, *258*(3–4), 157–167. https://doi.org/10.1016/j.chemgeo.2008.09.023

Guiry, M.D. & Guiry, G.M. (2022). AlgaeBase. World-wide electronic publication, National University of Ireland, Galway. https://www.algaebase.org; searched on March 18, 2022.

Han, Y., Aziz, T. N., Del Giudice, D., Hall, N. S., & Obenour, D. R. (2021). Exploring nutrient and light limitation of algal production in a shallow turbid reservoir. *Environmental Pollution*, *269*, 116210. https://doi.org/10.1016/j.envpol.2020.116210

Hannides, C. C. S., Popp, B. N., Choy, C. A., & Drazen, J. C. (2013). Midwater zooplankton and suspended particle dynamics in the North Pacific Subtropical Gyre: A stable isotope perspective. *Limnology and Oceanography*, *58*(6), 1931–1946. https://doi.org/10.4319/lo.2013.58.6.1931

Hayes, J. M. (2001). Fractionation of Carbon and Hydrogen Isotopes in Biosynthetic Processes. *Reviews in Mineralogy and Geochemistry*, *43*(1), 225–277. https://doi.org/10.2138/gsrmg.43.1.225

Hedges, J. I., Keil, R. G., & Benner, R. (1997). What happens to terrestrial organic matter in the ocean? *Organic Geochemistry*, *27*(5–6), 195–212. https://doi.org/10.1016/S0146-6380(97)00066-1

Herrero Ortega, S., Catalán, N., Björn, E., Gröntoft, H., Hilmarsson, T. G., Bertilsson, S., … Bravo, A. G. (2018). High methylmercury formation in ponds fueled by fresh humic and algal derived organic matter. *Limnology and Oceanography*, *63*(S1), S44–S53. https://doi.org/10.1002/lno.10722

Herrin, R. T., Lathrop, R. C., Gorski, P. R., & Andren, A. W. (1998). Hypolimnetic methylmercury and its uptake by plankton during fall destratification: A key entry point of mercury into lake food chains? *Limnology and Oceanography*, *43*(7), 1476–1486. https://doi.org/10.4319/lo.1998.43.7.1476

Hong, Y.-S., Kim, Y.-M., & Lee, K.-E. (2012). Methylmercury Exposure and Health Effects. *Journal of Preventive Medicine & Public Health*, *45*(6), 353–363. https://doi.org/10.3961/jpmph.2012.45.6.353

Hsu-Kim, H., Eckley, C. S., Achá, D., Feng, X., Gilmour, C. C., Jonsson, S., & Mitchell, C. P. J. (2018). Challenges and opportunities for managing aquatic mercury pollution in altered landscapes. *Ambio*, *47*(2), 141–169. https://doi.org/10.1007/s13280-017-1006-7

Jeremiason, J. D., Engstrom, D. R., Swain, E. B., Nater, E. A., Johnson, B. M., Almendinger, J. E., … Kolka, R. K. (2006). Sulfate Addition Increases Methylmercury Production in an Experimental Wetland. *Environmental Science & Technology*, *40*(12), 3800–3806. https://doi.org/10.1021/es0524144

Kainz, M., & Mazumder, A. (2005). Effect of Algal and Bacterial Diet on Methyl Mercury Concentrations in Zooplankton. *Environmental Science & Technology*, *39*(6), 1666–1672. https://doi.org/10.1021/es049119o

Karimi, R., Chen, C. Y., Pickhardt, P. C., Fisher, N. S., & Folt, C. L. (2007). Stoichiometric controls of mercury dilution by growth. *Proceedings of the National Academy of Sciences*, *104*(18), 7477–7482. https://doi.org/10.1073/pnas.0611261104

Kendall, C., Silva, S. R., & Kelly, V. J. (2001). Carbon and nitrogen isotopic compositions of particulate organic matter in four large river systems across the United States. *Hydrological Processes*, *15*(7), 1301–1346. https://doi.org/10.1002/hyp.216

Lammers, J. M., Reichart, G. J., & Middelburg, J. J. (2017). Seasonal variability in phytoplankton stable carbon isotope ratios and bacterial carbon sources in a shallow Dutch lake. *Limnology and Oceanography*, *62*(6), 2773–2787. https://doi.org/10.1002/lno.10605

Lázaro, W. L., Guimarães, J. R. D., Ignácio, A. R. A., Da Silva, C. J., & Díez, S. (2013). Cyanobacteria enhance methylmercury production: A hypothesis tested in the periphyton of two lakes in the Pantanal floodplain, Brazil. *Science of The Total Environment*, *456–457*, 231–238. https://doi.org/10.1016/j.scitotenv.2013.03.022

Lee, C.-S., & Fisher, N. S. (2016). Methylmercury uptake by diverse marine phytoplankton. *Limnology and Oceanography*, *61*(5), 1626–1639. https://doi.org/10.1002/lno.10318

Lehnherr, I. (2014). Methylmercury biogeochemistry: a review with special reference to Arctic aquatic ecosystems. *Environmental Reviews*, *22*(3), 229–243. https://doi.org/10.1139/er-2013-0059

Li, Y., Meng, J., Zhang, C., Ji, S., Kong, Q., Wang, R., & Liu, J. (2020). Bottom-up and top-down effects on phytoplankton communities in two freshwater lakes. *PLOS ONE*, *15*(4), e0231357. https://doi.org/10.1371/journal.pone.0231357

Luengen, A. C., Fisher, N. S., & Bergamaschi, B. A. (2012). Dissolved organic matter reduces algal accumulation of methylmercury. *Environmental Toxicology and Chemistry*, *31*(8), 1712–1719. https://doi.org/10.1002/etc.1885

Martin-Creuzburg, D., Sperfeld, E., & Wacker, A. (2009). Colimitation of a freshwater herbivore by sterols and polyunsaturated fatty acids. *Proceedings of the Royal Society B: Biological Sciences*, *276*(1663), 1805–1814. https://doi.org/10.1098/rspb.2008.1540

MATTHEWS, B., & MAZUMDER, A. (2005). Temporal variation in body composition (C : N) helps explain seasonal patterns of zooplankton delta13C. *Freshwater Biology*, *50*(3), 502–515. https://doi.org/10.1111/j.1365-2427.2005.01336.x

McCord, S. A., M. W. Beutel, S. R. Dent, and S. G. Schladow (2016), Evaluation of mercury cycling and hypolimnetic oxygenation in mercury-impacted seasonally stratified reservoirs in the Guadalupe River watershed, California, Water Resour. Res., 52, 7726–7743, doi:10.1002/2016WR019061.

McKee, L. J., Bonnema, A., David, N., Davis, J. A., Franz, A., Grace, R., … Yee, D. (2017). Long-term variation in concentrations and mass loads in a semi-arid watershed influenced by historic mercury mining and urban pollutant sources. *Science of The Total Environment*, *605–606*, 482–497. https://doi.org/10.1016/j.scitotenv.2017.04.203

Meunier, C. L., Boersma, M., Wiltshire, K. H., & Malzahn, A. M. (2016). Zooplankton eat what they need: copepod selective feeding and potential consequences for marine systems. *Oikos*, *125*(1), 50–58. https://doi.org/10.1111/oik.02072

Minagawa, M., & Wada, E. (1984). Stepwise enrichment of 15N along food chains: Further evidence and the relation between δ15N and animal age. *Geochimica et Cosmochimica Acta*, *48*(5), 1135–1140. https://doi.org/10.1016/0016-7037(84)90204-7

Ogorek, J. M., Lepak, R. F., Hoffman, J. C., DeWild, J. F., Rosera, T. J., Tate, M. T., … Krabbenhoft, D. P. (2021). Enhanced Susceptibility of Methylmercury Bioaccumulation into Seston of the Laurentian Great Lakes. *Environmental Science & Technology*, *55*(18), 12714–12723. https://doi.org/10.1021/acs.est.1c02319

Oksanen, F.J., et al. (2017) Vegan: Community Ecology Package. R package Version 2.4-3. https://CRAN.R-project.org/package=vegan

Ouédraogo, O., Chételat, J., & Amyot, M. (2015). Bioaccumulation and Trophic Transfer of Mercury and Selenium in African Sub-Tropical Fluvial Reservoirs Food Webs (Burkina Faso). *PLOS ONE*, *10*(4), e0123048. https://doi.org/10.1371/journal.pone.0123048

Pickhardt, P. C., Folt, C. L., Chen, C. Y., Klaue, B., & Blum, J. D. (2005). Impacts of zooplankton composition and algal enrichment on the accumulation of mercury in an experimental freshwater food web. *Science of The Total Environment*, *339*(1–3), 89–101. https://doi.org/10.1016/j.scitotenv.2004.07.025

Pickhardt, P. C., Folt, C. L., Chen, C. Y., Klaue, B., & Blum, J. D. (2002). Algal blooms reduce the uptake of toxic methylmercury in freshwater food webs. *Proceedings of the National Academy of Sciences*, *99*(7), 4419–4423. https://doi.org/10.1073/pnas.072531099

Popp, B. N., Laws, E. A., Bidigare, R. R., Dore, J. E., Hanson, K. L., & Wakeham, S. G. (1998). Effect of Phytoplankton Cell Geometry on Carbon Isotopic Fractionation. *Geochimica et Cosmochimica Acta*, *62*(1), 69–77. https://doi.org/10.1016/S0016-7037(97)00333-5

Post, D.M. (2002), USING STABLE ISOTOPES TO ESTIMATE TROPHIC POSITION: MODELS, METHODS, AND ASSUMPTIONS. Ecology, 83: 703-718. https://doi.org/10.1890/0012-9658(2002)083[0703:USITET]2.0.CO;2

Qian, Y., Yin, X., Lin, H., Rao, B., Brooks, S. C., Liang, L., & Gu, B. (2014). Why Dissolved Organic Matter Enhances Photodegradation of Methylmercury. *Environmental Science & Technology Letters*, *1*(10), 426–431. https://doi.org/10.1021/ez500254z

Ravichandran, M. (2004). Interactions between mercury and dissolved organic matter—a review. *Chemosphere*, *55*(3), 319–331. https://doi.org/10.1016/j.chemosphere.2003.11.011

ROMO, S., SORIA, J., FERNÁNDEZ, F., OUAHID, Y., & BARÓN-SOLÁ, Á. (2013). Water residence time and the dynamics of toxic cyanobacteria. *Freshwater Biology*, *58*(3), 513–522. https://doi.org/10.1111/j.1365-2427.2012.02734.x

Sailley, S. F., Polimene, L., Mitra, A., Atkinson, A., & Allen, J. I. (2015). Impact of zooplankton food selectivity on plankton dynamics and nutrient cycling. *Journal of Plankton Research*, *37*(3), 519–529. https://doi.org/10.1093/plankt/fbv020

San Francisco Bay Regional Water Quality Control Board. (2008). *Guadalupe River Watershed Mercury Total Maximum Daily Load (TMDL) Project STAFF REPORT*.

Scheuhammer AM, Meyer MW, Sandheinrich MB, Murray MW (2007) Effects of environmental methylmercury on the health of wild birds, mammals, and fish. AMBIO J Hum Environ 36:12–19

Seelos, M., Beutel, M., Austin, C. M., Wilkinson, E., & Leal, C. (2021). Effects of hypolimnetic oxygenation on fish tissue mercury in reservoirs near the new Almaden Mining District, California, USA. *Environmental Pollution*, *268*, 115759. https://doi.org/10.1016/j.envpol.2020.115759

Sime, I. (2004). The freshwater algal flora of the British Isles: An identification guide to freshwater and terrestrial algae, edited by David M. John, Brian A. Whitton and Alan J. Brook. Cambridge University Press, Cambridge, 2002, 702pp. ISBN 0-521-77051-3. *Aquatic Conservation: Marine and Freshwater Ecosystems*, *14*(1), 105–105. https://doi.org/10.1002/aqc.579

Sinistro, R. (2010). Top-down and bottom-up regulation of planktonic communities in a warm temperate wetland. *Journal of Plankton Research*, *32*(2), 209–220. https://doi.org/10.1093/plankt/fbp114

Slotton, D. G., Reuter, J. E., & Goldman, C. R. (1995). Mercury uptake patterns of biota in a seasonally anoxic northern California Reservoir. *Water, Air, & Soil Pollution*, *80*(1–4), 841–850. https://doi.org/10.1007/BF01189735

Stewart, A. R., Saiki, M. K., Kuwabara, J. S., Alpers, C. N., Marvin-DiPasquale, M., & Krabbenhoft, D. P. (2008). Influence of plankton mercury dynamics and trophic pathways on mercury concentrations of top predator fish of a mining-impacted reservoir. *Canadian Journal of Fisheries and Aquatic Sciences*, *65*(11), 2351–2366. https://doi.org/10.1139/F08-140

Syväranta, J., & Rautio, M. (2010). Zooplankton, lipids and stable isotopes: importance of seasonal, latitudinal, and taxonomic differences. *Canadian Journal of Fisheries and Aquatic Sciences*, *67*(11), 1721–1729. https://doi.org/10.1139/F10-091

Taipale, S. J., Vuorio, K., Brett, M. T., Peltomaa, E., Hiltunen, M., & Kankaala, P. (2016). Lake zooplankton δ^{13}C values are strongly correlated with the δ^{13}C values of distinct phytoplankton taxa. *Ecosphere*, *7*(8). https://doi.org/10.1002/ecs2.1392

Thomas, S. M., Kiljunen, M., Malinen, T., Eloranta, A. P., Amundsen, P.-A., Lodenius, M., & Kahilainen, K. K. (2016). Food-web structure and mercury dynamics in a large subarctic lake following multiple species introductions. *Freshwater Biology*, *61*(4), 500–517. https://doi.org/10.1111/fwb.12723

U.S. E.P.A. (1993). US EPA Method 300.0, Revision 2.1: Determination of Inorganic Anions By Ion Chromatography. *Standard Methods*, (August), 28.

U.S. E.P.A. (1993). *Method 350.1 Determination of Ammonia Nitrogen By Semi-Automated Colorimetry*.

U.S. E.P.A. (1998). *Method 1630. Methyl mercury in water by distillation, aqueous ethylation, purge and trap, and CVAFS. US Environmental Protection Agency, Washington, DC*.

U.S. E.P.A. (1996). *Method 1669 Sampling Ambient Water for Trace Metals at EPA Water Quality Criteria Levels*.

U.S. E.P.A. (2002). *Method 1631, Revision E: Mercury in Water by Oxidation, Purge and Trap, and Cold Vapor Atomic Fluorescence Spectrometry*. *United States Environmental Protection Agency*.

Wang, X.-C., & Druffel, E. R. . (2001). Radiocarbon and stable carbon isotope compositions of organic compound classes in sediments from the NE Pacific and Southern Oceans. *Marine Chemistry*, *73*(1), 65–81. https://doi.org/10.1016/S0304-4203(00)00090-6

Ward, D. M., Nislow, K. H., Chen, C. Y., & Folt, C. L. (2010). Rapid, Efficient Growth Reduces Mercury Concentrations in Stream-Dwelling Atlantic Salmon. *Transactions of the American Fisheries Society*, *139*(1), 1–10. https://doi.org/10.1577/T09-032.1

Wilson, A. E., Sarnelle, O., & Tillmanns, A. R. (2006). Effects of cyanobacterial toxicity and morphology on the population growth of freshwater zooplankton: Meta-analyses of laboratory experiments. *Limnology and Oceanography*, *51*(4), 1915–1924. https://doi.org/10.4319/lo.2006.51.4.1915

Wu, P., Kainz, M. J., Bravo, A. G., Åkerblom, S., Sonesten, L., & Bishop, K. (2019). The importance of bioconcentration into the pelagic food web base for methylmercury bioaccumulation: A meta-analysis. *Science of The Total Environment*, *646*, 357–367. https://doi.org/10.1016/j.scitotenv.2018.07.328

Supporting Information: Appendices A, B, and C available for download in supplemental file.